Dissertation
submitted to the
Combined Faculties for the Natural Sciences and for Mathematics
of the Ruperto-Carola University of Heidelberg, Germany
for the degree of
Doctor of Natural Sciences

put forward by
M.Sc. Elena Kozlikin
born in Arkalyk, Kazakhstan

Oral examination: 27.06.2018

Structure formation under different interaction laws

Referees:
Prof. Dr. Matthias Bartelmann
Prof. Dr. Manfred Salmhofer

Abstract

We use a novel kinetic field theory approach to investigate structure formation [1] in vastly different classical systems ranging from cosmic large-scale structures to many-body systems of Rydberg atoms or spins. The interaction laws governing the dynamics of these systems greatly differ from one another.
In the application of the formalism to the formation of cosmic large-scale structures, we address the question whether the shape of the gravitational potential has any influence on the shape of the non-linear density-fluctuation power spectrum on small scales. Since the non-linear power spectrum is a convolution of the NFW halo density profile with the mass function according to the halo model, we are interested in finding out whether the NFW profile depends on the potential shape. However, we find that the balance between the attractive force due to particle interactions and the damping due to momentum-diffusion is very finely tuned and is broken easily when Newtonian gravity is replaced by any different power-law interaction potential. This prevents us from drawing definitive conclusions and requires further analysis.
The applications of the kinetic field theory formalism to classical laboratory systems such as Rydberg gases and spin-system is a much less evolved field. We therefore present first results as a test of the applicability of KFT to such systems which, so far, are encouraging.

Zusammenfassung

Wir verwenden einen neuen Ansatz auf der Grundlage einer Kinetischen Feldtheorie zur Untersuchung von Strukturbildung [1] in sehr verschiedenen klassischen Systemen. Diese reichen von großskaligen, kosmischen Strukturen, über Systeme bestehend aus Rydberg-Atomen bis hin zu Spin-Systemen. Die Wechselwirkungen, die die Dynamik dieser Systeme bestimmen, unterscheiden sich stark.
In der Anwendung des Formalismus auf kosmische Strukturbildung, beschäftigen wir uns mit der Fragestellung, ob die Form des Gravitationspotentials Einfluss auf die Form des nicht-linearen Leistungspektrums von Dichtefluktuationen auf kleinen Skalen hat. Da das nicht-lineare Leistungsspektrum, dem Halo-Model zufolge, lediglich eine Faltung des NFW-Dichteprofils von Halos mit der Massenfunktion darstellt, möchten wir herausfinden, ob das NFW-Dichteprofil von der Potentialform abhängt. Wir stellen jedoch fest, dass das Gleichgewicht zwischen den anziehenden Kräften aufgrund von

Teilchenwechselwirkungen und der Dämpfung aufgrund von Impulsdiffusion sehr fein eingestellt ist. Ersetzt man das Newtonsche Gravitationspotential durch ein anderes Wechselwirkungspotential, das durch ein Potenzgesetz gegeben ist, so kann dieses Gleichgewicht leicht gebrochen werden. Daher bedarf es weiterer Untersuchungen um definitive Aussagen über Dichteprofile treffen zu können.
Die Anwendung des kinetischen Feldtheorie-Formalismus auf Laborsysteme, wie zum Beispiel Rydberg-Gase oder Spin-Systeme, befindet sich derzeit noch in der Entwicklungsphase. Wir stellen daher lediglich erste Ergebnisse in diesem Zusammenhang vor, um die Anwendbarkeit von KFT auf solche Systeme zu überprüfen. Die Ergebnisse sind soweit viel versprechend.

"The story so far:
In the beginning the Universe was created.
This has made a lot of people very angry and been widely regarded as a bad move."

– Douglas Adams,
The Restaurant at the End of the Universe

Contents

1. Introduction **1**

I. Kinetic Field Theory **3**

2. Theoretical background **5**

2.1. Quantum Field Theory Methods 5

2.1.1. Path Integrals and Functional Derivatives 5

2.1.2. The Generating Functional 6

2.1.3. Analogy Between QFT and Statistical Mechanics 6

2.1.4. Remark on the notation 7

3. The kinetic field theory formalism **9**

3.1. Transition probability for classical fields 10

3.1.1. Generating functional of the theory 12

3.2. Microscopic and collective fields 14

3.2.1. Microscopic degrees of freedom 14

3.2.2. Collective fields 15

3.2.3. General expressions for density correlators 17

3.3. Initial probability distribution 18

3.3.1. Initial conditions for correlated particles 18

3.3.2. Approximation of initial density correlations 20

3.3.3. Full hierarchy of initial momentum correlations 21

3.4. Evaluation of particle trajectories 23
3.4.1. Born's approximation 24
3.4.2. Perturbative approach 25

II. Cosmology **29**

4. Theoretical background on cosmology **31**
4.1. ΛCDM cosmology 31
4.2. Power spectrum and correlation function 34
4.3. Dark matter halos 35
4.3.1. Press-Schechter mass function 36
4.3.2. The Navarro-Frenk-White density profile 36
4.4. Conventional approaches to cosmic structure formation 37
4.4.1. Eulerian perturbation theory 37
4.4.2. Lagrangian perturbation theory 39
4.4.3. The Halo Model 39
4.4.4. Numerical N-body simulation 41
4.5. Advantages of the KFT approach to cosmic structure formation 42

5. Influence of gravitational potential on structure formation on small scales **45**
5.1. Overview 45
5.2. The scale dependent linear growth factor 46
5.3. Power spectrum and NFW density profile 47
5.4. Analysis in perturbative expansion 48
5.5. Analysis in the Born approximation 52
5.6. Discussion of results 59
5.7. Conclusions 61

III. Classical many-body systems **63**

6. Theoretical background on Rydberg systems **65**
6.1. Rydberg atoms 65
6.1.1. Interaction between Rydberg atoms 65
6.1.2. Rydberg blockade 66
6.2. Rydberg systems and KFT 68
6.2.1. Initial conditions 68

6.2.2. Propagator 69

7. Structure formation in a Rydberg gas **71**
7.1. Density-fluctuation power spectrum 71
7.1.1. Resummed propagator 71
7.1.2. Analytical result 72
7.2. Numerical reference model 73
7.2.1. Molecular dynamics simulation 73
7.2.2. Shot noise 74
7.2.3. Initial power spectrum 74
7.3. Results 75
7.3.1. Free evolution 76
7.3.2. Evolution with Gaussian potential 77
7.3.3. Evolution with van der Waals potential 81
7.4. Conclusions 82

8. Extension of the KFT formalism to spin systems **85**
8.1. Motivation 85
8.2. Many-body spin systems in KFT 86
8.3. Hamiltonian of the spin-system 87
8.4. Initial conditions and correlation functions 88
8.5. Conclusions and outlook 92

9. Conclusions **95**

10. Acknowledgements **97**

11. Publications **99**

1

Introduction

This thesis is split into three parts. In the first part a novel analytical approach to structure formation in classical many-body systems based on a microscopic, non-equilibrium, statistical field theory (or kinetic field theory) is recapped. This theory is then applied to the formation of large-scale structure in cosmology in the second part. The third part of this thesis is dedicated to applications in laboratory many-body systems, such as Rydberg atoms and spins, on much smaller scales.
The broad range of applications is a consequence of the wide range of applicability of our kinetic field theory (KFT). The main focus of our work is on the different interaction laws that govern the formation of structure in these systems.
The formation of structure is a global phenomenon in physics that can be found on all scales. The forces driving structure formation, however, can be quite different. Understanding the mechanisms behind this phenomenon on a fundamental level requires a theory that is abstract enough to be applicable to a great variety of systems. In this context, structure does not have to mean an accumulation of particles but has a broader meaning in terms of n-point correlation functions. Due to the non-linearities generally involved in the formation and evolution of structures, the description of such correlations and their evolution has proven a formidable task not only in cosmology but also for laboratory systems. Many approaches – several of which we will discuss later – have been developed to tackle this problem, but only few have succeeded in producing viable results. The most successful techniques are based on numerical many-body simulations. This holds for cosmology as well as for classical or quantum many-body systems. While numerical simulations are able to provide results that agree

well with observations and/or experimental data, they provide little basis for gaining an understanding of the fundamental principles governing structure formation. In some cases this is due to the vast amount of adjustable parameters involved and in other cases the computational capabilities are exceeded so that, yet again, approximations have to be made.
The analytical framework of KFT is not tuned to any one system, cosmology or other, and offers a great amount of freedom in choosing the fundamental laws that enter into the description of structure formation, like the equations of free motion, the particle interaction potential and the initial conditions. It is this freedom of choice that has allowed us to apply this approach to cosmology as well as to correlated classical spin-systems in this thesis. Furthermore, the theory offers no free parameters that can be tuned or calibrated externally in any way. So far, the results for cosmic structure formation have been very encouraging.
In this thesis we apply the KFT formalism to three very different systems: cosmic structures, many-body systems of Rydberg atoms and many-body classical spin-systems. In all of these systems we investigate how interactions affect the formation and evolution of structure. For many-body systems of Rydberg atoms or spins, we present first results and show how to set up the theory in order to treat systems of this kind. In the cosmological application, which is by far more advanced, we aim at understanding how the interaction potential affects structures at small scales, i.e. the scales of dark matter halos, by replacing the Newtonian gravitational potential between particles by a different power-law potential. With this, we aim at understanding the origin of the universal Navarro-Frenk-White density profile of dark matter halos.

This thesis is structured as follows: In part one, we give a brief overview of the theoretical and mathematical tools needed in order to understand the theoretical framework of our approach in chapter 2. We then introduce the reader to the kinetic field theory formalism in chapter 3.
In part two, we discuss our cosmological application of KFT to structure formation on halo-scales and provide the reader with a background on cosmology in general and approaches to large-scale structure formation, in particular, in chapter 4. We then present and discuss the results in chapter 5.
Part three harbours the application of KFT to Rydberg systems in chapters 6 and 7, as well as to classical spin-systems in chapter 8. We give a brief introduction to both, preceding the discussion of each system respectively.
Finally, we summarise our conclusions in chapter 9.

Part I.

Kinetic Field Theory

2

Theoretical background

2.1 Quantum Field Theory Methods

2.1.1 Path Integrals and Functional Derivatives

In classical mechanics the ordinary integral is used where a function is integrated over its domain.Thus a sum over all values the function takes at each point of the domain of the integrand is performed. The path integral on the other hand is a means to integrate a functional, which is a function of a function, over its domain which itself is a space or subspace of functions.
In quantum field theory (QFT) the path integral is introduced as a generalisation of the action principle according to the quantum nature of the systems. The notion of a single particle with a deterministic trajectory which is to be integrated over is replaced by an integral over all possible trajectories the particle may take. In the framework of QFT the particles and their trajectories are replaced by fields and their evolution in time. The integration over all possible particle trajectories or evolutionary tracks of the fields allows the computation of a complete transition probability or transition amplitude between an initial and a final state of the system.
The path integral of a functional F of the function φ is denoted by

$$\int \mathcal{D}\varphi \, F[\varphi] \tag{2.1}$$

where the integration measure $\mathcal{D}\varphi$ signifies that the integral has to be taken over all possible paths, or field configurations.

A functional derivative is an operation inverse of the path integral. It relates the change in a functional in response to a change in a function that the functional depends on and is familiar from variational principles. It will be useful later to consider that the functional derivative of a function $\varphi(x)$ with respect to a function $\varphi(x')$ is given by

$$\frac{\delta\varphi(x)}{\delta\varphi(x')} = \delta_{\mathrm{D}}(x - x') \tag{2.2}$$

with the Dirac delta distribution $\delta_{\mathrm{D}}[\,\cdot\,]$.
Just as the ordinary derivative, the functional derivative satisfies linearity, the product rule and the chain rule.

2.1.2 The Generating Functional

In quantum field theory, the generating functional is the generator of all correlation functions and a generalisation of the partition sum known from statistical mechanics. The generating functional for a scalar field theory $Z[J]$ is defined as

$$Z[J] \coloneqq \int \mathcal{D}\varphi \, \exp\left[\mathrm{i}\int \mathrm{d}^4x \, (\mathcal{L} + J(x)\varphi(x))\right] \tag{2.3}$$

with the Lagrangian $\mathcal{L}$ and the so-called source field $J(x)$.
Correlation functions can then be computed by simply taking functional derivatives of the generating functional with respect to the source field. The n-point function is then given by

$$\langle 0|T\varphi(x_1)\varphi(x_2)...\varphi(x_n)|0\rangle = \frac{1}{Z_0}\left(\frac{\delta}{\mathrm{i}\delta J(x_1)}\right)\left(\frac{\delta}{\mathrm{i}\delta J(x_2)}\right)...\left(\frac{\delta}{\mathrm{i}\delta J(x_n)}\right) Z[J]\Big|_{J=0} \tag{2.4}$$

where $Z_0 \coloneqq Z[J=0]$. After taking all necessary derivatives, the source field can be set to zero since it is only an auxiliary field. Each functional derivative brings down a factor of φ.
This generating functional method can also be used for an interacting theory in the same manner. The expression given in (2.4) does not depend on whether the theory is free or interacting.

2.1.3 Analogy Between QFT and Statistical Mechanics

The generating functional (2.3) is an integral over all possible configurations of an exponential statistical weight and thus has the same structure as a partition function. The source field $J(x)$ plays the role of an external field. The method presented in

2.1.2 of taking derivatives with respect to the source field to compute correlations is analogous to the approach often used in statistical mechanics for the computation of correlation functions by differentiating with respect to variables like the pressure or the magnetic field.
By performing a Wick rotation – a rotation into the complex plane – for the time component one can show that the Wick-rotated generating functional $Z[J]$ becomes

$$Z[J] = \int \mathcal{D}\varphi \, \exp\left[- \int \mathrm{d}^4 x_E \, (\mathcal{L}_E + J\varphi) \right] \tag{2.5}$$

where the functional $\mathcal{L}_E$ has the form of an energy (for a complete derivation see [2]). Furthermore $\mathcal{L}_E$ is bounded from below and becomes large when φ has a large amplitude or large gradients. It is therefore a reasonable statistical weight for the fluctuations of φ. In this form $Z[J]$ is now precisely the partition function that describes the statistical mechanics of a macroscopic system, described approximately by treating the fluctuating variable as a continuum field.
This correspondence will lay the groundwork for our further analysis.

2.1.4 Remark on the notation

To streamline the notation, we will often use the abbreviations

$$\int_x := \int \mathrm{d}^d x \mathrm{d}t \quad \text{and} \quad \int_k := \int \frac{\mathrm{d}^d k}{(2\pi)^d} \, , \tag{2.6}$$

throughout this thesis, where d is the number of spatial dimensions.

3

The kinetic field theory formalism

In order to give the reader a complete picture of the theory this work is based on, we will go through the steps leading to the central object of our analysis. In the following chapters we will show how a generating functional is derived from which n-point correlation functions of collective fields can be computed by applying functional derivatives.
In this chapter we will be closely following the derivations presented in [1] with a few minor modifications.
The Kinetic Field Theory (KFT) approach [1] is based on the Martin-Siggia-Rose formalism [3] and was developed to describe the formation and evolution of cosmic structures, following the ideas of Mazenko [4, 5] and Das and Mazenko [6, 7]. The theory is based on a generating functional for classical particles subject to Hamiltonian dynamics, whose positions and momenta are initially correlated in phase space. Structurally, it resembles a non-equilibrium quantum field theory but simplifies considerably due to the symplectic structure of the Hamiltonian equations and the deterministic trajectories of classical particles. Cumulants of collective fields such as the macroscopic mass density can be obtained by repeatedly applying suitable functional derivatives to the generating functional. Particle interactions can either be taken into account by applying an interaction operator to the free generating functional or by evaluating particle trajectories in the Born approximation.

3.1 Transition probability for classical fields

In this section we show how a path-integral formulation of classical Hamiltonian dynamics can be derived by giving a functional-integral representation of classical transition probabilities. This is done by setting the weight for classical paths to unity and all other possible paths to zero.
We start from a classical field $\varphi_a(t, \vec{q})$ with n components, $1 \leq a \leq n$, at time t and position $\vec{q}$, in d space-time dimensions. The dynamics of this field is given by some equation of motion, symbolically denoted as

$$E\left(\varphi_a\right) = 0 \,. \tag{3.1}$$

Any classical field $\varphi_a(t, \vec{q})$ must satisfy (3.1) everywhere in the space-time domain considered.
We then specify initial conditions, $\varphi_a(t_\mathrm{i}, \vec{q}) =: \varphi_a^{(\mathrm{i})}(\vec{q})$, which are defined at some instant of time t_i that we set to $t_\mathrm{i} = 0$ without loss of generality. By doing so, we pick out one particular field configuration from all the classical field configurations that satisfy (3.1). The initial field configuration is mapped to a later field configuration by the classical flow $\Phi_t^{(\mathrm{cl})}$,

$$\varphi_a^{(\mathrm{i})}(\vec{q}) \mapsto \varphi_a(t, \vec{q}) = \Phi_t^{(\mathrm{cl})}\left(\varphi_a^{(\mathrm{i})}(\vec{q})\right) \,, \quad \text{with} \quad \Phi_0^{(\mathrm{cl})} = \mathrm{id} \,. \tag{3.2}$$

Since we are considering classical fields, it is clear that their evolution is deterministic. Therefore, a field configuration $\varphi_a(t, \vec{q})$ can be reached at $t \geq 0$ beginning with an initial field configuration $\varphi_a^{(\mathrm{i})}(\vec{q})$ if and only if

$$\varphi_a(t, \vec{q}) = \Phi_t^{(\mathrm{cl})}\left(\varphi_a^{(\mathrm{i})}(\vec{q})\right) \,. \tag{3.3}$$

In analogy to quantum field theory, we now construct the probability for the transition of an initial field configuration $\varphi_a^{(\mathrm{i})}(\vec{q})$ to a field configuration $\varphi_a(t, \vec{q})$ at a later time t. This probability must be unity if and only if the evolution from $\varphi_a^{(\mathrm{i})}(\vec{q})$ to $\varphi_a(t, \vec{q})$ follows the classical flow $\Phi_t^{(\mathrm{cl})}$. This can be expressed by a path integral using the Dirac delta distribution $\delta_\mathrm{D}[\,\cdot\,]$

$$P\left[\varphi_a, \varphi_a^{(\mathrm{i})}\right] = \int \mathcal{D}\Phi_t \, \delta_\mathrm{D}\left[\Phi_t\left(\varphi_a^{(\mathrm{i})}\right) - \Phi_t^{(\mathrm{cl})}\left(\varphi_a^{(\mathrm{i})}\right)\right] \,. \tag{3.4}$$

If we assume that the equations of motion have a symplectic structure, which is the case for Hamiltonian equations of motion, it can be directly shown that the functional determinant for a transformation of the sort

$$\delta_\mathrm{D}[\varphi_a - \varphi_a^{(0)}] = \delta_\mathrm{D}[R(\varphi_a)] \det\left[\frac{\partial R(\varphi_a)}{\partial \varphi_b}|_{\varphi_a = \varphi_a^0}\right] \,, \tag{3.5}$$

where φ_a are some vector valued field components and R is some functional mapping these field components onto the real numbers, equals unity if

$$R(\varphi_a^{(0)}) = 0 \tag{3.6}$$

holds (see [8]).
Using this functional identity where R is identified as $E(\varphi_a)$, we can write the transition probability as

$$P\left[\varphi_a, \varphi_a^{(\mathrm{i})}\right] = \int \mathcal{D}\varphi_a \, \delta_{\mathrm{D}}\left[E\left(\varphi_a\right)\right] \ . \tag{3.7}$$

The meaning of this expression is quite intuitive: while we are integrating over all possible field configurations φ_a that start with the initial field configuration $\varphi_a^{(\mathrm{i})}$, the functional delta distribution makes sure that only that particular path contributes which satisfies the equation of motion.
We now re-write the delta distribution by its functional Fourier transform with the help of a conjugate field χ_a,

$$\delta_{\mathrm{D}}\left[E\left(\varphi_a\right)\right] = \int \mathcal{D}\chi_a \, \exp\left\{\mathrm{i}\int_x \chi_a E\left(\varphi_a\right)\right\} \ , \tag{3.8}$$

where the integration within the exponential function is taken over all d space-time coordinates that the fields φ_a and χ_a depend on. In addition, a summation over a is implied. The transition probability (3.7) is then given by

$$P\left[\varphi_a, \varphi_a^{(\mathrm{i})}\right] = \int \mathcal{D}\varphi_a \int \mathcal{D}\chi_a \, \exp\left\{\mathrm{i}\int_x \chi_a E\left(\varphi_a\right)\right\} \ . \tag{3.9}$$

We now identify the action S with the integral in the exponential

$$S\left[\varphi_a, \chi_a\right] := \int_x \mathcal{L}(x) \ , \tag{3.10}$$

with the Lagrange density $\mathcal{L}$ given by

$$\mathcal{L}(x) := \chi_a(x) E\left(\varphi_a(x)\right) \ . \tag{3.11}$$

If we now take the functional derivative of the action with respect to the conjugate field χ_a and evaluate at $\chi_a = 0$,

$$\left.\frac{\delta S\left[\varphi_a, \chi_a\right]}{\delta \chi_a(x)}\right|_{\chi_a = 0} = E\left(\varphi_a(x)\right) = 0 \ , \tag{3.12}$$

the equation of motion (3.1) is recovered.

3.1.1 Generating functional of the theory

Now that we have an expression for the transition probability from initial to final field configurations $P[\varphi_a, \varphi_a^{(\mathrm{i})}]$, we can construct a generating functional for our non-equilibrium field theory. Since we are working with classical fields, the path from an initial field configuration $\varphi_a^{(\mathrm{i})}(\vec{q})$ to a final field configuration $\varphi_a^{(\mathrm{i})}(t, \vec{q})$ at a later time t is, of course, deterministic. The only possible random element in such a theory is therefore the configuration of initial states. Hence, the configuration space that we have to integrate or sum over when constructing our generating functional must be the space of initial field configurations.
We therefore integrate over all possible configurations of initial states, weighted by an initial probability distribution $P_0\left[\varphi_a^{(\mathrm{i})}\right]$. This path integral over the initial field configurations is abbreviated by

$$\int \mathcal{D}\varphi_a^{(\mathrm{i})} P_0\left[\varphi_a^{(\mathrm{i})}\right] =: \int \mathcal{D}\Gamma_{\mathrm{i}} \,. \tag{3.13}$$

As a final step, we introduce an auxiliary source field J_a coupling to φ_a into the Lagrangian and arrive at the generating functional

$$\begin{aligned} Z[J_a] &= \int \mathcal{D}\Gamma_{\mathrm{i}}\, P\left[\varphi_a, \varphi_a^{(\mathrm{i})}\right] \\ &= \int \mathcal{D}\Gamma_{\mathrm{i}} \int \mathcal{D}\varphi_a \int \mathcal{D}\chi_a \exp\left[\mathrm{i}\int_x \left(\mathcal{L} + J_a\varphi_a\right)\right] \,. \end{aligned} \tag{3.14}$$

Taking functional derivatives of Z with respect to the source field J_a, evaluated at $J_a = 0$, yields

$$\begin{aligned} \frac{1}{\mathrm{i}}\frac{\delta Z}{\delta J_a}\bigg|_{J=0=K} &= \int \mathcal{D}\Gamma_{\mathrm{i}} \int \mathcal{D}\varphi_a \int \mathcal{D}\chi_a\, \varphi_a \mathrm{e}^{\mathrm{i}S[\varphi_a,\chi_a]} \\ &= \int \mathcal{D}\Gamma_{\mathrm{i}} \int \mathcal{D}\varphi_a\, \varphi_a \delta_{\mathrm{D}}\left[E(\varphi_a)\right] = \langle\varphi_a\rangle_{P_0} \,. \end{aligned} \tag{3.15}$$

This is simply the classical solution to the equation of motion, averaged over all possible initial field configurations $\varphi_a^{(\mathrm{i})}$ drawn from the probability distribution $P_0\left[\varphi_a^{(\mathrm{i})}\right]$. Field correlators can now be obtained in the same manner by taking consecutive functional derivatives with respect to the source field J_a and evaluating at $J_a = 0$,

$$\langle\varphi_{a_1}(x_1)\varphi_{a_2}(x_2)\ldots\varphi_{a_n}(x_n)\rangle = \frac{\delta}{\mathrm{i}\delta J_{a_1}(x_1)} \cdots \frac{\delta}{\mathrm{i}\delta J_{a_n}(x_n)} Z[J_a]|_{J=0} \,, \tag{3.16}$$

as is familiar from quantum field theory. Since we have constructed Z by integration over a functional delta distribution, we have made sure that Z is normalised, i.e.

$Z[0,0] = 1$.
We can now write down the generating functional again in the form

$$Z[J_a] = \int \mathcal{D}\Gamma_\mathrm{i} \int \mathcal{D}\varphi_a \delta_\mathrm{D}\left[E(\varphi_a)\right] \exp\left\{\mathrm{i}\int_x J_a\varphi_a\right\} , \tag{3.17}$$

where the delta functional singles out the solution φ_a^s of the equation of motion for any given initial field configuration $\varphi_a^{(\mathrm{i})}$.
We now suppose that we can split the equation of motion into a free part described by E_0 and a part containing some interaction given by E_I. We can then write the equation of motion as

$$E\left(\varphi_a\right) = \dot{\varphi}_a + E_0\left(\varphi_a\right) + E_\mathrm{I}\left(\varphi_a\right) = 0 . \tag{3.18}$$

Introducing the propagator (or Green's function) $G_{ab}(x,x')$ of the free equation of motion, we can formally write the solution to the full equation of motion as

$$\varphi_a^\mathrm{s}(x) = G_{ab}(x,x_\mathrm{i})\varphi_b^{(\mathrm{i})}(x_\mathrm{i}) - \int_{x'} G_{ab}(x,x')F_b(x') , \tag{3.19}$$

with a force $F_b(x')$ that is given by a gradient of an interaction potential V according to Hamilton's equations. Since the equations of motion are a set of linear differential equations such a Green's function must exist.
The delta distribution in (3.17) can now be replaced by

$$\delta_\mathrm{D}\left[E(\varphi_a)\right] \to \delta_\mathrm{D}\left[\varphi_a - \varphi_a^\mathrm{s}\right] \tag{3.20}$$

where φ_a^s denotes the solution to the full equation of motion and a constant functional determinant was absorbed into the normalisation of the generating functional.
This allows us to write the generating functional in terms of the solution φ_a^s

$$Z[J_a] = \int \mathcal{D}\Gamma_\mathrm{i} \exp\left\{\mathrm{i}\int_x J_a\varphi_a^\mathrm{s}\right\} , \tag{3.21}$$

by integrating over the delta distribution.
It is however clear that the particle trajectories (3.26) cannot be evaluated exactly because the actual particle coordinates would need to be known to evaluate the interaction potential V or its gradient between particle positions. Therefore, it will become necessary to introduce expansion or approximation schemes to evaluate the interaction term later on.

3.2 Microscopic and collective fields

3.2.1 Microscopic degrees of freedom

Instead of using macroscopic fields, we will make the transition to point particles and describe their kinematics under the influence of Hamiltonian dynamics in three spatial dimensions. The fields φ_a are therefore replaced by delta distributions at the phase-space coordinates $\vec{x}_j^{\,\top} := (\vec{q}_j, \vec{p}_j)$ for all particles $1 \leq j \leq N$. The equations of motion of the phase-space points $\vec{x}_j$ are Hamilton's equations,

$$\partial_t \vec{x}_j = \mathcal{J} \partial_j \mathcal{H} \,, \tag{3.22}$$

with the Hamiltonian $\mathcal{H}$ and the symplectic matrix

$$\mathcal{J} = \begin{pmatrix} 0 & \mathcal{I}_3 \\ -\mathcal{I}_3 & 0 \end{pmatrix} \,, \tag{3.23}$$

where $\mathcal{I}_d$ is the unit matrix in d dimensions.The partial derivative ∂_j acts upon all six phase-space coordinates x_j of the j-th particle. The action S in (3.10) is reduced to a time integral, due to the fields being represented by delta distributions, as is the case for classical mechanics. The Green's function will then also depend on time only.
For a compact notation we will organise the positions $\{\vec{q}_j\}$ and the momenta $\{\vec{p}_j\}$ of N microscopic particles by means of the tensor product into phase-space coordinate tensors. The phase-space coordinates of the complete particle ensemble,

$$\vec{x}_j \coloneqq \begin{pmatrix} \vec{q}_j \\ \vec{p}_j \end{pmatrix} \,, \quad \mathbf{x} \coloneqq \vec{x}_j \otimes \vec{e}_j \,, \tag{3.24}$$

are bundled into a tensorial structure where the Einstein convention is used to sum over repeated indices and where $\vec{e}_j$ is the N-dimensional column vector whose only non-vanishing entry is 1 at component j.
The scalar product between such tensorial objects is defined as

$$\langle \mathbf{a}, \mathbf{b} \rangle = \langle \vec{a}_j \otimes \vec{e}_j, \vec{b}_l \otimes \vec{e}_l \rangle = \vec{a}_j \cdot \vec{b}_j \tag{3.25}$$

where again Einstein's summation convention is implied.
With this notation, the solution to the full equations of motion (3.19) is given by

$$\mathbf{x}(t) = \mathcal{G}(t,0)\mathbf{x}^{(\mathrm{i})} - \int_{t_\mathrm{i}}^{t} \mathrm{d}t' \, \mathcal{G}(t,t') \begin{pmatrix} 0 \\ \nabla V \end{pmatrix} \,, \tag{3.26}$$

where

$$\mathcal{G} = G \otimes \mathcal{I}_N \tag{3.27}$$

is defined with a 6×6 dimensional matrix-valued Green's function G describing the free propagation of an individual phase-space point

$$G = \begin{pmatrix} g_{qq}(t,t') & g_{qp}(t,t') \\ 0 & g_{pp}(t,t') \end{pmatrix} . \tag{3.28}$$

The phase-space trajectories (3.26) explicitly contain the interaction potential V between particles that is responsible for any deviation from a free evolution of particle trajectories.
Just as the phase-space coordinates, the source field $\mathbf{J}$ is bundled as

$$\mathbf{J}_q = \vec{J}_{q_j} \otimes \vec{e}_j \ , \quad \mathbf{J}_p = \vec{J}_{p_j} \otimes \vec{e}_j \ , \quad \mathbf{J} = \begin{pmatrix} \vec{J}_{q_j} \\ \vec{J}_{p_j} \end{pmatrix} \otimes \vec{e}_j \ . \tag{3.29}$$

The phase-space measure is given by

$$\mathrm{d}\Gamma = P(\mathbf{q},\mathbf{p})\, \mathrm{d}\mathbf{q}\, \mathrm{d}\mathbf{p} \tag{3.30}$$

with an appropriate probability distribution P that is chosen according to the initial conditions at hand and which will be specified later. The integral over the initial phase-space configurations is now an ordinary rather than a path integral. This, again, is a consequence of the fields being represented by delta distributions.
The generating functional then assumes the simple form

$$Z[\mathbf{J}] = \int \mathrm{d}\Gamma_{\mathrm{i}} \exp\left\{ \mathrm{i} \int \mathrm{d}t \ \langle \mathbf{J}(t), \mathbf{x}(t) \rangle \right\} . \tag{3.31}$$

3.2.2 Collective fields

Although the generating functional is formulated in terms of microscopic degrees of freedom which brings an enormous advantage in the description of N-particle ensembles, we now need to introduce collective fields that will allow us to compute collective properties, like the n-point functions, of the ensemble from the generating functional. The most obvious example of such a collective field for our applications is the number density $\rho(t,\vec{q})$,

$$\rho(t,\vec{q}) = \sum_{j=1}^{N} \delta_{\mathrm{D}} \left(\vec{q} - \vec{q}_j(t) \right) \ , \tag{3.32}$$

here assumed to be composed of N point-particle contributions.
The potential $V(t, \vec{q})$ experienced by any particle at time t and at position $\vec{q}$ is the sum over all point-particle potentials v,

$$V(t, \vec{q}) = \sum_{j=1}^{N} v\left(\vec{q} - \vec{q}_j(t)\right) \ , \tag{3.33}$$

and can be written as

$$V(t, \vec{q}) = \int \mathrm{d}^3 y \, v\left(\vec{q} - \vec{y}\right) \sum_{j=1}^{N} \delta_{\mathrm{D}}\left(\vec{y} - \vec{q}_j(t)\right) = \int \mathrm{d}^3 y \, v\left(\vec{q} - \vec{y}\right) \rho(t, \vec{y}\,) \tag{3.34}$$

in terms of an integral over the density (3.32).
For most cases, computations in Fourier space will prove to be much simpler later on. We therefore express the density ρ as well as the interaction potential v by their Fourier transforms assuming that the potential v in (3.33) is translation invariant and thus depends on the difference $\vec{q} - \vec{y}$ only.
The next step is to promote the density field to an operator, such that applying this operator on the generating functional will yield n-point density correlation functions. As assumed in (3.32), the density ρ is composed of delta contributions. In Fourier space, the one-particle contribution of particle j to the density at the space-time position $1 = (t_1, \vec{k}_1)$ is

$$\rho_j(1) = \exp\left(-\mathrm{i}\vec{k}_1 \cdot \vec{q}_j(t_1)\right) \ , \tag{3.35}$$

where $\vec{q}_j(t_1)$ is the position of particle number j in configuration space at time t_1. In this expression for the density, we replace the particle position $\vec{q}_j$ by a functional derivative with respect to $\vec{J}_{q_j}(1)$, obtaining the one-particle density operator

$$\hat{\rho}_j(1) = \exp\left(-\mathrm{i}\vec{k}_1^{\top} \cdot \frac{\delta}{\mathrm{i}\delta \vec{J}_{q_j}(1)}\right) \ . \tag{3.36}$$

The action of the density operator (3.36) on $Z[\mathbf{J}]$ becomes clear if we re-write the exponential as a series,

$$\hat{\rho}_j(1) Z[\mathbf{J}] = \sum_{n=0}^{\infty} \frac{1}{n!} \left(-\vec{k}_1^{\top} \cdot \frac{\delta}{\mathrm{i}\delta \vec{J}_{q_j}(1)}\right)^n Z[\mathbf{J}] \ . \tag{3.37}$$

Since acting once with $\frac{\delta}{\mathrm{i}\delta \vec{J}_{q_j}(1)}$ on $Z[\mathbf{J}]$ yields

$$\left[-\vec{k}_1^{\top} \cdot \frac{\delta}{\delta \vec{J}_{q_j}(1)}\right] Z[\mathbf{J}] = Z[\mathbf{J}] \left(-\vec{k}_1 \int \mathrm{d}t \left\langle \frac{\delta \mathbf{J}(t)}{\delta \vec{J}_{q_j}(1)}, \mathbf{x}(t) \right\rangle\right) \ , \tag{3.38}$$

we immediately see that

$$\hat{\rho}_j(1) Z[\mathbf{J}] = Z[\mathbf{J} + \mathbf{L}_j(1)] \,, \tag{3.39}$$

where the tensor $\mathbf{L}_j(1)$ is defined by

$$\mathbf{L}_j(1) := -\vec{k}_1 \cdot \frac{\delta \mathbf{J}(t)}{\delta \vec{J}_{q_j}(1)} = -\delta_{\mathrm{D}}\,(t - t_1) \begin{pmatrix} \vec{k}_1 \\ 0 \end{pmatrix} \otimes \vec{e}_j \,. \tag{3.40}$$

The application of the density operator $\hat{\rho}_j(1)$ thus results in a shift of the source field $\mathbf{J}$ in the free generating functional by the tensor $\mathbf{L}_j(1)$. This is not surprising due to the fact that spatial derivatives generate translations, and so exponentials of spatial derivatives must be finite translations.

3.2.3 General expressions for density correlators

We now derive a general expression for an m-point density correlator. First m density operators will have to be applied to the free generating functional. Since no further derivatives with respect to $\mathbf{J}$ will be required afterwards, the source field $\mathbf{J}$ can then be set to zero.
The operator for the density contributions by N particles is simply the sum over the one-particle density operators,

$$\hat{\rho}(1) = \sum_{j=1}^{N} \hat{\rho}_j(1) \,. \tag{3.41}$$

As we have shown in (3.39) for a single one-particle density operator, the result of applying m one-particle density operators to the free generating functional is

$$\hat{\rho}_{j_m}(m) \cdots \hat{\rho}_{j_1}(1) Z[\mathbf{J}]|_{\mathbf{J}=0} = Z[\mathbf{L}] \tag{3.42}$$

with

$$\mathbf{L} = -\sum_{s=1}^{m} \delta_{\mathrm{D}}(t - t_s) \begin{pmatrix} \vec{k}_s \\ 0 \end{pmatrix} \otimes \vec{e}_{j_s} \,. \tag{3.43}$$

Using (3.41) together with (3.42), we get the m-point density correlator $G_{\rho\ldots\rho}(1\ldots m)$ by summing over all particle indices,

$$G_{\rho\ldots\rho}(1\ldots m) = \sum_{j_1\ldots j_m=1}^{N} \hat{\rho}_{j_1} \cdots \hat{\rho}_{j_m} Z[\mathbf{J}]|_{\mathbf{J}=0} = \sum_{j_1\ldots j_m=1}^{N} Z[\mathbf{L}] \,. \tag{3.44}$$

We see now that all we have to evaluate for m-point density correlators is the generating functional taken at $\mathbf{J} = \mathbf{L}$,

$$Z[\mathbf{L}] = \int \mathrm{d}\Gamma \exp\left\{ \mathrm{i} \int \mathrm{d}t \ \langle \mathbf{L}, \mathbf{x} \rangle \right\} \ . \tag{3.45}$$

With the shift tensors

$$\mathbf{L}_q := -\vec{k}_1 \otimes (\vec{e}_1 - \vec{e}_2) \ , \quad \mathbf{L}_p(t) := g_{qp}(t,0)\, \mathbf{L}_q \ , \tag{3.46}$$

we can write the generating functional evaluated at $\mathbf{J} = \mathbf{L}$ as

$$Z[\mathbf{L}] = \int \mathrm{d}\Gamma \ \exp^{\mathrm{i}\langle \mathbf{L}_q, \mathbf{q} \rangle + \mathrm{i}\langle \mathbf{L}_p(t), \mathbf{p} \rangle - \bar{F}(t)} \ , \tag{3.47}$$

with the time-integrated interaction term

$$\bar{F}(t) = \mathrm{i} \int_0^t \mathrm{d}t' \langle \mathbf{L}_p(t'), \nabla \mathbf{V}(t') \rangle =: \int_0^t \mathrm{d}t' F(t,t') \tag{3.48}$$

containing the interaction potential between particles $\mathbf{V}$.
The shift tensors $\mathbf{L}_q$ and $\mathbf{L}_p$ have non-vanishing components only for the particles specified by the indices j_s set by the one-particle density operators applied to the generating functional. In accordance with (3.44), we can now briefly write

$$Z[\mathbf{L}] = G_{\rho_{j_1} \dots \rho_{j_m}} \ , \quad G_{\rho \dots \rho}(1 \dots m) = \sum_{j_1 \dots j_m = 1}^{N} G_{\rho_{j_1} \dots \rho_{j_m}} \ , \tag{3.49}$$

for any shift tensor specified by a complete set of m particle indices $j_1 \dots j_m$. The integral over the initial phase-space configuration that remains in the generating functional $Z[\mathbf{L}]$ still has to be carried out. Up to this point the generating functional is exact.
For later convenience we will introduce what we will call the free generating functional $Z_0[\mathbf{J}]$ as the part of the generating functional that does not include the interaction term,

$$Z_0[\mathbf{L}] = \int \mathrm{d}\Gamma \ \exp^{\mathrm{i}\langle \mathbf{L}_q, \mathbf{q} \rangle + \mathrm{i}\langle \mathbf{L}_p(t), \mathbf{p} \rangle} \ . \tag{3.50}$$

3.3 Initial probability distribution

3.3.1 Initial conditions for correlated particles

As one of the main results of [1] it was shown that the initial phase-space probability distribution $P(\mathbf{q}, \mathbf{p})$ is given by a multivariate Gaussian distribution. For our derivation,

we have assumed that a statistically homogeneous and isotropic, Gaussian random velocity potential ψ exists such that the momentum $\vec{p}$ at an arbitrary position is given by its gradient

$$\vec{p} = \vec{\nabla}\psi \ . \tag{3.51}$$

Due to the continuity equation, the density contrast

$$\delta = \frac{\rho - \rho_0}{\rho_0} \tag{3.52}$$

must then satisfy

$$\delta = -\vec{\nabla}^2\psi \ . \tag{3.53}$$

This allows us to connect the initial velocity and the initial density fluctuation power spectra, P_ψ and P_δ, via

$$P_\psi(k) = k^{-4} P_\delta(k) \ . \tag{3.54}$$

It is therefore sufficient to specify the initial density fluctuation power spectrum $P_\delta(k)$ to fully specify the initial probability distribution. As shown in [1], it is given by the multivariate Gaussian of the form

$$P(\mathbf{q},\mathbf{p}) = \frac{V^{-N}}{\sqrt{(2\pi)^{3N}\det C_{pp}}}\,\mathcal{C}(\mathbf{p}\,)\exp\left(-\frac{1}{2}\mathbf{p}^\top C_{pp}^{-1}\mathbf{p}\right) \tag{3.55}$$

where $\mathbf{p} = \vec{p}_j \otimes \vec{e}_j$ with the correlation operator

$$\begin{aligned}\mathcal{C}(\mathbf{p}) =& (-1)^N \prod_{j=1}^{N}\left(1 + \left(C_{\delta p}\frac{\partial}{\partial \mathbf{p}}\right)_j\right) + (-1)^N \sum_{(j,k)}(C_{\delta\delta})_{jk}\prod_{\{l\}'}\left(1 + \left(C_{\delta p}\frac{\partial}{\partial \mathbf{p}}\right)_l\right) \\ &+ (-1)^N \sum_{(j,k)}(C_{\delta\delta})_{jk}\sum_{(a,b)'}(C_{\delta\delta})_{ab}\prod_{\{l\}''}\left(1 + \left(C_{\delta p}\frac{\partial}{\partial \mathbf{p}}\right)_l\right) + \dots\end{aligned} \tag{3.56}$$

where $j \neq k$ as well as $a \neq b$ and $\{\,\}'$ indicates that l runs over all indices except (j,k) and $\{\,\}''$ indicates that l runs over all indices except (j,k,a,b).
The correlation matrices in (3.56) are defined as follows

$$\begin{aligned}&C_{\delta\delta} := \sigma_2^2 \otimes \mathcal{I}_N + \langle\delta_j\delta_k\rangle \otimes E_{jk} \ , \quad C_{\delta p} := \langle\delta_j\vec{p}_k\rangle \otimes E_{jk} \quad \text{and} \\ &C_{pp} := \frac{\sigma_1^2}{3}\mathcal{I}_3 \otimes \mathcal{I}_N + \langle\vec{p}_j \otimes \vec{p}_k\rangle \otimes E_{jk}\end{aligned} \tag{3.57}$$

with the matrix

$$E_{jk} := \vec{e}_j \otimes \vec{e}_k \tag{3.58}$$

and the correlators

$$\begin{aligned}\langle\delta_j\delta_k\rangle &= \int \frac{\mathrm{d}^3k}{(2\pi)^3}\, P_\delta(k)\, \mathrm{e}^{-\mathrm{i}\vec{k}\cdot(\vec{q}_j-\vec{q}_k)}\ ,\\ \langle\delta_j\vec{p}_k\rangle &= \mathrm{i}\int \frac{\mathrm{d}^3k}{(2\pi)^3}\, k^2\,\vec{k}\, P_\psi(k)\, \mathrm{e}^{-\mathrm{i}\vec{k}\cdot(\vec{q}_j-\vec{q}_k)}\ ,\\ \langle\vec{p}_j\otimes\vec{p}_k\rangle &= \int \frac{\mathrm{d}^3k}{(2\pi)^3}\, \vec{k}\otimes\vec{k}\, P_\psi(k)\, \mathrm{e}^{-\mathrm{i}\vec{k}\cdot(\vec{q}_j-\vec{q}_k)}\ .\end{aligned} \tag{3.59}$$

The moments σ_n^2 are defined by

$$\sigma_n^2 := \int_k k^{2n}\, P_\psi(k)\ . \tag{3.60}$$

3.3.2 Approximation of initial density correlations

If we assume that initially the density correlations $C_{\delta\delta}$ and density-momentum correlations $C_{\delta p}$ are weak, as we expect for cosmology, the probability distribution can be approximated up to first order in $C_{\delta\delta}$ and $C_{\delta p}$,

$$P(\boldsymbol{q},\boldsymbol{p}) \approx \frac{V^{-N}}{\sqrt{(2\pi)^{3N}\det\bar{C}_{pp}}}\exp\left(-\frac{1}{2}\boldsymbol{p}^\top\bar{C}_{pp}^{-1}\boldsymbol{p}\right)\left(1+\sum_{j=1}^{N}M_{\delta_j p_k}\vec{p}_k+\frac{1}{2}\sum_{j\neq k}C_{\delta_j\delta_k}\right) \tag{3.61}$$

with

$$M_{\delta_j p_k} := C^\top_{\delta_j p_a}\bar{C}^{-1}_{p_a p_k}\ . \tag{3.62}$$

If we evaluate density correlators at times much later than the initial time, we can even approximate

$$\mathcal{C}(\mathbf{p}) \approx 1\ . \tag{3.63}$$

For our cosmological applications this case is realised.
Using this approximation for the initial density correlations, we can write down the free part of the generating functional after having applied arbitrarily many density operators and set the source field $\mathbf{J}$ to zero, as

$$Z_0[\mathbf{L}] = V^{-N}\int \mathrm{d}\mathbf{q}\exp\left(-\frac{1}{2}\mathbf{L}_p^\top C_{pp}\mathbf{L}_p+\mathrm{i}\,\langle\mathbf{L}_q,\mathbf{q}\rangle\right)\ . \tag{3.64}$$

The quadratic form

$$Q := \mathbf{L}_p^\top C_{pp}\mathbf{L}_p \tag{3.65}$$

remaining in (3.64) splits into two terms if we use the definition of C_{pp} from (3.57),

$$Q = \frac{\sigma_1^2}{3}\sum_j \vec{L}_{p_j}^{\,2}+\sum_{j\neq i}\vec{L}^\top_{p_i}C_{p_ip_j}\vec{L}_{p_j}\ . \tag{3.66}$$

Replacing the sum of squares by a squared sum, we can instead write

$$Q = Q_0 - Q_\mathrm{D} + \sum_{j \neq i} \vec{L}_{p_i}^\top C_{p_i p_j} \vec{L}_{p_j} \tag{3.67}$$

with the damping terms

$$Q_0 := \frac{\sigma_1^2}{3} \left(\sum_j \vec{L}_{p_j} \right)^2 \quad , \quad Q_\mathrm{D} := \frac{\sigma_1^2}{3} \sum_{j \neq k} \vec{L}_{p_j} \cdot \vec{L}_{p_k} \ . \tag{3.68}$$

We will refer to the Q_0 and Q_D as dispersion and diffusion terms, respectively. It turns out that Q_0 will vanish identically in important cases (see [9] for a complete discussion). The diffusion term Q_D on the other hand does generally not vanish and has an intuitive and important effect on the time evolution of the density-fluctuation power spectrum, as will be explained in section 3.3.3.
Although expression (3.64) looks fairly simple, the final integral over particle positions cannot be evaluated without some additional labor.

3.3.3 Full hierarchy of initial momentum correlations

The most obvious course of action is to expand the exponential in (3.64) in a Taylor-series in orders of the damping factor Q_D and thus to include the damping term order by order in the generating functional. While this is easily done, deciding at which order to truncate the series is not evident. This difficulty has been met with in [1] and the damping term was included up to second order in momentum correlations at most. But being able to truncate the series was, in some sense, not completely arbitrary due to the fact that for our cosmological application we have the advantage of knowing (from numerical N-body simulations or even observations) what the end result, i.e. the non-linear density-fluctuation power spectrum, should look like today.
It was then shown in [9] that, in fact, the full hierarchy of momentum correlations can be included in the free generating functional by a factorisation of the latter. The derivation of the factorised generating functional can be found in [9] and shall not be repeated in this work. We will merely state the result of the procedure and discuss its implications.
The main ideas are that, in a statistically homogeneous field, only relative particle coordinates $\vec{q}_j - \vec{q}_i$ must matter, and that all these coordinate differences must be statistically indistinguishable. The central result is then the form of the generating

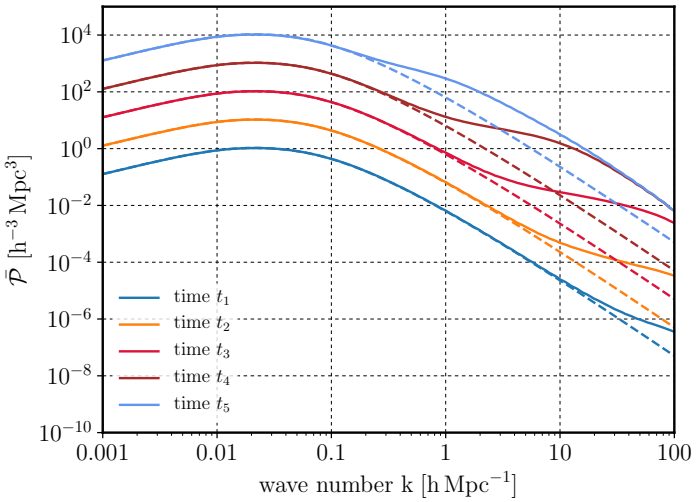

Figure 3.1.: We show the non-linearly evolved power spectrum $\bar{\mathcal{P}}$ where late-time diffusion is suppressed as specified in [9] Eq. (50) for different times t_i (t_1 is earliest and t_5 is latest). If free streaming is thus neglected, we can see how structure formation proceeds from small to large scales. The shape of the non-linear density-fluctuation power spectrum is already recovered to a large degree. (This figure has been published in [9] as Fig.2.)

functional for a two-point function containing the full hierarchy of initial momentum correlations that is given in [9] (Eq. 42),

$$Z_0[\mathbf{L}] = \mathcal{N} \mathrm{e}^{Q_\mathrm{D}(\kappa,t)} \left[(2\pi)^3 \delta_\mathrm{D}(\vec{\kappa}\,) + \mathcal{P}(\kappa,t)\right] \tag{3.69}$$

with

$$\mathcal{P}(\kappa,t) = \int_q \left\{ \mathrm{e}^{-g_{qp}^2(t,0)\kappa^2 a_\parallel(q)} - 1 \right\} \mathrm{e}^{\mathrm{i}\vec{\kappa}\cdot\vec{q}} \tag{3.70}$$

and the shift tensors

$$\mathbf{L}_q := -\vec{\kappa} \otimes (\vec{e}_1 - \vec{e}_2) \ , \quad \mathbf{L}_p(t) := g_{qp}(t,0)\mathbf{L}_q \tag{3.71}$$

where $\vec{\kappa} := \vec{k}_1 - \vec{k}$ is defined as the difference between an internal wave vector k that is integrated over and an external wave vector k_1.

We have introduced $\mathcal{N}$ to abbreviate the normalisation factor, because its particular form will not be needed throughout the derivations in this work.

The momentum-diffusion term Q_D appearing in (3.89) is

$$Q_\mathrm{D}(\kappa,t) = -\frac{\sigma_1^2}{3} g_{qp}^2(t,0)\kappa^2 \ . \tag{3.72}$$

The function $a_{\parallel}(q)$ that appears in (3.87) is the correlation function of the momentum components parallel to the line connecting the correlated particles (see [9], Eq. B.28),

$$a_{\parallel}(q) = \mu^2 \xi''_{\psi}(q) + (1-\mu^2)\frac{\xi'_{\psi}(q)}{q} \,, \tag{3.73}$$

where $\xi_{\psi}(q)$ is the correlation function of the initial velocity potential and μ is the angle cosine between the vectors $\vec{\kappa}$ and $\vec{q}$.
For sufficiently small arguments of the exponential in (3.70) we can approximate the evolved power spectrum $\mathcal{P}(\kappa, t)$ by the linearly evolved density-fluctuation power spectrum,

$$\mathcal{P}(\kappa, t') \approx g^2_{qp}(t', 0) P_{\delta}(\kappa) \,, \tag{3.74}$$

as was shown in [9] Eq. (B.41).
We now have a closed analytic expression for the free part of the generating functional which includes the full hierarchy of momentum correlations. We will neglect density and density-momentum correlations as they have been shown to be negligible for late cosmic times. It has been further shown in [9] that including the full hierarchy of momentum correlations causes a charachteristic deformation of the non-linear density-fluctuation power spectrum on intermediate scales. This can be observed if, in addition, free streaming is neglected (see discussion following [9], Eq. (49)). We can then see how structure formation proceeds from small to large scales and even recover the shape of the non-linear density-fluctuation power spectrum to a large degree. We show this in Fig. 3.1.
All that remains to be done now is to find a way of including particle interactions.

3.4 Evaluation of particle trajectories

We have already mentioned in section 3.1.1 that in general we are not able to evaluate particle trajectories exactly because we do not know the actual coordinates belonging to each particle. Although we will show a toy example in chapter 8 where we can write down the full trajectories exactly and can use the generating functional without any approximation or expansion schemes. But while we are dealing with kinematics of particles we will need to introduce a workaround for this issue. We choose two approaches here; one in which the interaction term is evaluated in Born's approximation, and one in which particle interactions are evaluated perturbatively.
In the first approach, that is presented in detail in [10], we compute an averaged interaction term that we evaluate in the Born approximation for particle trajectories.

This means that we replace the actual particle trajectories by inertial trajectories. This procedure may be familiar to the reader, if they happen to have a background in cosmology, from weak gravitational lensing and was originally developed by Max Born for scattering theory in quantum mechanics. The interaction term we obtain in this way describes the net force exerted on each particle by all other particles of the ensemble, whereby contributions from particle interactions to the force term are weighted by the correlation function. This approach gives us a simple, closed expression for the non-linear density-fluctuation power spectrum containing the full momentum correlations.
For the second, perturbative approach, we first split off the interaction term and apply it as the exponential of an interaction operator acting on the generating functional now containing the free Hamiltonian particle trajectories only, as discussed in full detail in [1]. To evaluate the resulting expression, the exponential operator is then Taylor-expanded into a perturbation series. This allows us to compute the non-linear density-fluctuation power spectrum perturbatively since we must then apply the interaction operator order by order in the interaction potential.

3.4.1 Born's approximation

Let us return to the still exact expression for the generating functional in (3.47). In [10] it was demonstrated how the interaction term can be evaluated in the Born approximation for particle trajectories and then averaged over particle positions to provide an effective force that is experienced by each particle due to the interaction with all the other particles in the ensemble.
The averaged force term in the Born approximation is given by

$$\langle F(t,t')\rangle = 2g_{qp}(t,t')A(t')\vec{k}_1 \int_k \vec{k}\,\tilde{v}\left(k,t'\right)\bar{P}_\delta\left(\kappa,t'\right) \ , \tag{3.75}$$

with the damped, evolved density-fluctuation power spectrum

$$\bar{P}_\delta(\kappa,t') := \mathrm{e}^{Q_\mathrm{D}(\kappa,t')}\, g_{qp}^2(t',0)\, P_\delta(\kappa) \tag{3.76}$$

and the Fourier transform of the two-particle interaction potential $\tilde{v}\left(k,t'\right)$ that we will specify later.
The time dependence of the potential amplitude $A(t')$ is attributed to cosmic expansion. The expression for the amplitude is specified in [10] (Eq. 33).
We can now integrate (3.90) over time and replace the interaction term $\bar{F}(k_1,\, t)$ in

(3.47) by the result of

$$\langle \bar{F}(k_1,\, t)\rangle = \int_0^t \mathrm{d}t' \langle F(k_1; t, t')\rangle \; . \tag{3.77}$$

This allows us to give to give a closed, analytic expression for the evolved, non-linear density-fluctuation power spectrum including the interaction between particles,

$$\bar{\mathcal{P}}(k_1, t) = \mathrm{e}^{Q_\mathrm{D}(k_1,t) - \langle \bar{F}(k_1,\, t)\rangle} \int_q \left\{ \mathrm{e}^{-g_{qp}^2(t) a_\parallel(q) k_1^2} - 1 \right\} \mathrm{e}^{\mathrm{i}\vec{q}\cdot\vec{k}_1} \; . \tag{3.78}$$

In the exponential we have the momentum-diffusion term Q_D that is being counteracted by the interaction term $\langle \bar{F}(k_1,\, t)\rangle$. The exponential is multiplied by the evolved density-fluctuation power spectrum $\mathcal{P}(k_1, t)$ given in (3.70).

3.4.2 Perturbative approach

A different way to evaluate the trajectories of interacting particles is through perturbation theory which was presented in detail in [1]. Here we replace the solution of the equations of motion to the actual particle trajectories by the solution to the *free* equations of motion denoted by $\bar{\mathbf{x}}$. In terms of the Green's function $\mathcal{G}$ of the free equations of motion, the particle trajectories $\bar{\mathbf{x}}$ in phase space are

$$\bar{\mathbf{x}}(t) = \mathcal{G}(t, 0)\mathbf{x}^{(\mathrm{i})} - \int_0^t \mathrm{d}t' \, \mathcal{G}(t, t')\mathbf{K}(t') \; , \tag{3.79}$$

where we have introduced an additional source field $\mathbf{K}$ that is going to mediate the effect of particle interactions on the inertial particle trajectories. $\mathbf{K}$ has the same tensorial structure as the source field $\mathbf{J}$ in (3.29).
The free part of the generating functional then reads

$$Z_0[\mathbf{J}, \mathbf{K}] = \int \mathrm{d}\Gamma \, \exp\left(\mathrm{i} \int_0^\infty \mathrm{d}t \, \langle \mathbf{J}, \bar{\mathbf{x}}\rangle \right) \; . \tag{3.80}$$

Particle interactions are included by applying an interaction operator $\hat{S}_\mathrm{I}$ to the free generating functional. The full generating functional can then be written as

$$Z[\mathbf{J}, \mathbf{K}] = \mathrm{e}^{\mathrm{i}\hat{S}_\mathrm{I}} \, Z_0[\mathbf{J}, \mathbf{K}] \; , \tag{3.81}$$

with

$$\hat{S}_\mathrm{I} = - \int \mathrm{d}1 \, \hat{B}(-1)\tilde{v}(1)\hat{\rho}(1) \; . \tag{3.82}$$

The newly introduced field operator $\hat{B}$ will be called the response-field operator. The many-particle response field B describes how a particle ensemble responds to a change

in the phase-space coordinates of one of its particles. In a Fourier-space representation, these operators are sums over one-particle operators,

$$\hat{B}_j(1) = \left(\mathrm{i}\vec{k}_1 \cdot \frac{\delta}{\mathrm{i}\delta \vec{K}_{p_j}(1)} \right) \hat{\rho}_j(1) =: \hat{b}_j(1)\hat{\rho}_j(1) \,, \tag{3.83}$$

and $\hat{\rho}_j(1)$ retains its form given in (3.36). The response-field operator $\hat{B}$ thus contains a density operator $\hat{\rho}$.

The perturbative evaluation of (3.81) begins with expanding the exponential interaction operator $\exp(\mathrm{i}\hat{S}_\mathrm{I})$ into a power series, introducing two density operators $\hat{\rho}$ and one response-field operator $\hat{b}$ per power of $\hat{S}_\mathrm{I}$. For an n-th order correlator with m-th order particle interaction, we therefore need to evaluate one-particle expressions of the form

$$\hat{\rho}_{j_1}(1) \cdots \hat{\rho}_{j_r}(r) \;\; Z_0[\mathbf{J}, \mathbf{K}]|_{\mathbf{J}=0} = Z_0[\mathbf{L}, \mathbf{K}] \tag{3.84}$$

with $r = n + 2m$, and with the particle indices $j_s = 1 \dots N$. As we have already seen in section 3.2.2, the density operators then replace the generator field $\mathbf{J}$ by the shift tensor

$$\mathbf{L} = - \sum_{s=1}^{r=n+2m} \begin{pmatrix} \vec{k}_s \\ 0 \end{pmatrix} \delta_\mathrm{D}(t - t_s) \otimes \vec{e}_{j_s} \,. \tag{3.85}$$

The position and momentum components of the shift tensor $\mathbf{L}$ are again given by the projections

$$\begin{aligned} \vec{L}_{q_j}(c) &= \textstyle\int_0^\infty \mathrm{d}t \left\langle \mathbf{L}(t), G(t, t_c) \begin{pmatrix} \mathcal{I}_3 \\ 0 \end{pmatrix} \otimes \vec{e}_j \right\rangle \,, \\ \vec{L}_{p_j}(c) &= \textstyle\int_0^\infty \mathrm{d}t \left\langle \mathbf{L}(t), G(t, t_c) \begin{pmatrix} 0 \\ \mathcal{I}_3 \end{pmatrix} \otimes \vec{e}_j \right\rangle \,. \end{aligned} \tag{3.86}$$

In a second step, we have to apply all response-field operators $\hat{b}_{j_c}(c)$ to $Z_0[\mathbf{L}, \mathbf{K}]$. But the subsequent application of a single, one-particle response-field operator $\hat{b}_{j_c}(c)$ to $Z_0[\mathbf{L}, \mathbf{K}]$, taken at $\mathbf{K} = 0$, simply returns a response-field pre-factor $b_{j_c}(c)$,

$$\hat{b}_{j_c}(c) \;\; Z_0[\mathbf{L}, \mathbf{K}]|_{\mathbf{K}=0} = b_{j_c}(c) \, Z_0[\mathbf{L}, 0] \,, \tag{3.87}$$

given in terms of $\vec{L}_{p_{j_c}}$ as defined in (3.86) by

$$b_{j_c}(c) = -\mathrm{i}\vec{k}_c \cdot \vec{L}_{p_{j_c}}(c) \,. \tag{3.88}$$

Inserting (3.86) results in

$$b_{j_c}(c) = \mathrm{i} \sum_{s=1}^{r} \left(\vec{k}_c \cdot \vec{k}_s \right) \, g_{qp}(t_s, t_c) \, \delta_{j_c j_s} \; . \tag{3.89}$$

Note that causality ensures that the particle ensemble can only respond to causes preceding the response, i.e. $g_{qp}(t_s, t_c) = 0$ for $t_c \geq t_s$. Therefore, only response-field factors with $t_c < t_s$ contribute.
As usual, correlators of order n in the density are obtained by applying n density operators to $Z[\mathbf{J}, \mathbf{K}]$,

$$G_{\rho \ldots \rho}(1 \ldots n) = \hat{\rho}(1) \cdots \hat{\rho}(n) \, Z[\mathbf{J}, \mathbf{K}] \; . \tag{3.90}$$

and setting each of the generator fields $\mathbf{J}$ and $\mathbf{K}$ to zero once all functional derivatives with respect to $\mathbf{J}$ or $\mathbf{K}$ have been applied.
It should be mentioned at this point that while the factorisation of the functional presented in section 3.3.3 that allowed us to include the full hierarchy of initial momentum correlations is in principle possible for the generating functional expanded in this manner, the actual procedure is quite involved and is still work in progress.

Part II.

Cosmology

4

Theoretical background on cosmology

4.1 ΛCDM cosmology

In this section, we will discuss the standard ΛCDM model of cosmology which today is widely accepted as a valid description of our Universe. This will also be the cosmological model that we will use in all our calculations later on.
In this model, the Universe is presumed to follow the dynamics of the Friedmann equations that are derived from Einstein's field equations under symmetry assumptions which are the two fundamental assumptions of cosmology:

1. Isotropy: meaning that when averaged over sufficiently large scales, the observable properties of the Universe must be isotropic i.e. independent of direction.
2. The Cosmological Principle: stating that our position in the Universe is by no means special or preferred to any other.

By the second assumption, isotropy must hold for any observer. If the Universe is isotropic around each point, then it must be homogeneous. Isotropy and homogeneity induce symmetries that simplify the metric greatly. The first assumption implies that, when averaged over sufficiently large scales, there exists a mean motion of matter and energy in the Universe with respect to which all observable properties are isotropic. Together with the second assumption, this means that all fundamental observers, i.e. imagined observers following this mean motion, experience the same history of the Universe, i.e. the same averaged observable properties, provided they synchronize their

clocks suitably. The line element

$$\mathrm{d}s^2 = g_{\mu\nu}\mathrm{d}x^\mu \mathrm{d}x^\nu \tag{4.1}$$

in comoving coordinates, i.e. coordinates attached to fundamental observers, simplifies to

$$\mathrm{d}s^2 = g_{00}\mathrm{d}t^2 \ , \tag{4.2}$$

because in such coordinates $\mathrm{d}x^i = 0$ for fundamental observers. Requiring further that the fundamental observer's proper time be equal to the coordinate time, we must have

$$\mathrm{d}s^2 = -c^2\mathrm{d}t^2 \ \Rightarrow \ g_{00} = -c^2 \ . \tag{4.3}$$

Isotropy further requires that there must be a coordinate frame in which

$$g_{0i} = 0 \ . \tag{4.4}$$

If this was not possible, it would single out a preferred direction which, in turn, would violate the isotropy assumption.
The line element, thus, simplifies to

$$\mathrm{d}s^2 = -c^2\mathrm{d}t^2 + g_{ij}\mathrm{d}x^i\mathrm{d}x^j \ . \tag{4.5}$$

Spacetime can now be decomposed into spatial hyper-surfaces of constant time that can be scaled by a function $a(t)$ that depends on time only

$$\mathrm{d}s^2 = -c^2\mathrm{d}t^2 + a(t)\mathrm{d}l^2 \ , \tag{4.6}$$

with the line element of isotropic and homogeneous three-space $\mathrm{d}l$. Isotropy requires three-space to be spherically symmetric. We can thus re-write the line element as

$$\mathrm{d}s^2 = -c^2\mathrm{d}t^2 + a(t)\left[\frac{\mathrm{d}r^2}{1-Kr^2} + r^2\mathrm{d}\Omega^2\right] \tag{4.7}$$

in terms of polar coordinates, where r is a radial coordinate, chosen such that spheres of constant r have the surface area $4\pi r^2$, and K is a constant parametrising the curvature of spatial hyper-surfaces. The solid angle $\mathrm{d}\Omega^2$ is given by

$$\mathrm{d}\Omega^2 = \mathrm{d}\theta^2 + \sin^2\theta \ \mathrm{d}\varphi^2 \tag{4.8}$$

with polar angles θ and φ. The line element specified in (4.7) is known as the Friedmann-Lemaître-Robertson-Walker (FLRW) metric.

The dynamics of the metric (4.7) thus reduces to the dynamics of the scale factor $a(t)$. Two differential equations for $a(t)$ are obtained from Einstein's field equations

$$G_{\mu\nu} = \frac{8\,\pi\,G}{c^4} T_{\mu\nu} + \Lambda g_{\mu\nu} \tag{4.9}$$

where Λ is the cosmological constant, $G_{\mu\nu}$ is the Einstein field tensor that can be directly computed from the first and second derivatives of the metric tensor and $T_{\mu\nu}$ is the energy-momentum tensor of the cosmic fluid. $T_{\mu\nu}$ must be of the form of the stress-energy tensor of a perfect fluid, which is characterised by pressure p and (energy) density ρ. Due to homogeneity, $p = p(t)$ and $\rho = \rho(t)$ can only be functions of time.

Using the metric (4.7) in Einstein's field equations we obtain the two Friedmann equations

$$\left(\frac{\dot{a}}{a}\right)^2 = \frac{8\,\pi\,G}{3}\rho - \frac{K\,c^2}{a^2} + \frac{\Lambda\,c^2}{3}\ , \tag{4.10}$$

$$\frac{\ddot{a}}{a} = -\frac{4\,\pi\,G}{3}\left(\rho - \frac{3\,p}{c^2}\right) + \frac{\Lambda\,c^2}{3}\ . \tag{4.11}$$

With the adiabatic equation that follows from combining (4.10) and (4.11)

$$\frac{\mathrm{d}}{\mathrm{d}t}(a^3\,\rho\,c^2) + p\frac{\mathrm{d}}{\mathrm{d}t}(a^3) = 0\ , \tag{4.12}$$

we can derive the scaling behaviour of relativistic and non-relativistic matter. With the Hubble function

$$H \coloneqq \frac{\dot{a}}{a}\ , \tag{4.13}$$

and the critical density

$$\rho_{\mathrm{cr}}(t) \coloneqq \frac{3\,H^2(t)}{8\,\pi\,G}\ , \tag{4.14}$$

we can define the dimensionless density parameters expressed in units of the critical density

$$\Omega_i(t) \coloneqq \frac{\rho(t)}{\rho_{\mathrm{cr}}(t)}\ , \quad \Omega_{i\,0} \coloneqq \frac{\rho(t_0)}{\rho_{\mathrm{cr}}(t_0)} \tag{4.15}$$

with i denoting the type of matter (e.g. radiation, Dark Matter, baryonic matter) and t_0 meaning today. This allows us to bring the remaining single Friedmann equation into the familiar and widely used form

$$H^2(a) = H_0^2\left[\Omega_{\mathrm{r}0}a^{-4} + \Omega_{\mathrm{m}0}a^{-3} + \Omega_{\mathrm{K}0}a^{-2} + \Omega_{\Lambda 0}\right] \tag{4.16}$$

with $H_0 := H(a = 1)$ and a = 1 expressing today.
$\Omega_{\mathrm{r}0}$ is the radiation density and $\Omega_{\mathrm{m}0}$ the matter density including ordinary matter

(in cosmology often called "baryonic"[1]) and dark matter, which does not interact electromagnetically. $\Omega_{\mathrm{K}0}$ denotes spatial curvature and $\Omega_{\Lambda 0}$ signifies the dark energy content.

The standard cosmological model specifies a universe obeying the Friedmann equation (4.16). It is further assumed that two forms of matter exist. Ordinary matter is usually referred to as "baryonic" and the other, and by far larger amount, of matter is called dark matter due to the fact that it does not seem to interact electromagnetically and is thus invisible. One usually makes the distinction between "Cold Dark Matter" and "Warm Dark Matter". Hereby, the terms "cold" and "warm" do not refer to a temperature but indicate whether we have non-relativistic (cold) or relativistic (warm) particles as dark matter candidates. In standard cosmology, cold dark matter is empirically preferred over warm dark matter. In addition to the existence of dark matter, standard cosmology assumes a form of energy that leads to the observed accelerated expansion of the Universe. Within the current limits of observation, this so-called "dark energy", whatever it may be, behaves like a cosmological constant Λ. This cosmological model is often denoted as "ΛCDM" (Λ Cold Dark Matter) cosmology.

4.2 Power spectrum and correlation function

So far, we have described the dynamics of a homogeneous and isotropic Universe in section 4.1. But of course this cannot be the end of the story, because otherwise our own existence would not be possible. It is obvious that while the Universe is homogeneous and isotropic *on average*, inhomogeneities exist on comparably small scales. We will now move towards quantifying these inhomogeneities in the Universe which, most likely, were already present during and after inflation and were amplified and morphed into the large-scale structures that we observe today.
The correlation function and its Fourier transform, the power spectrum, are useful tools to quantify structures in the universe. We have defined the density contrast and its Fourier transform in (4.28) already. The density contrast is a random field, which must be isotropic and homogeneous in order to agree with the cosmological principle that the Universe is isotropic and homogeneous on large scales so that its statistical properties have to be invariant under rotations. The mean of the density contrast is

$$\langle \delta \rangle = 0 \tag{4.17}$$

[1] This jargon may be confusing, because by "baryonic" we actually mean: all particles of the Standard Model that interact electromagnetically.

by definition.
In real space, the correlation function of δ is defined as

$$\xi(y) \coloneqq \langle \delta(\vec{x})\delta(\vec{x}+\vec{y})\rangle \ , \tag{4.18}$$

where the average is taken over all positions $\vec{x}$ and all orientations of $\vec{y}$. ξ cannot depend on the direction of $\vec{y}$ because that would violate isotropy. The correlation function measures the coherence of the density field between all points separated by a distance $|\vec{y}|$.
The variance of the density contrast in Fourier space defines the power spectrum $P_\delta(k)$

$$\langle \hat{\delta}(\vec{k})\,\hat{\delta}^*(\vec{k}')\rangle =: (2\pi)^3\,P_\delta(k)\,\delta_{\mathrm{D}}(\vec{k}-\vec{k}') \ . \tag{4.19}$$

The power spectrum cannot depend on the direction of $\vec{k}$ because that would violate isotropy. To ensure homogeneity, the Dirac delta function makes sure that modes of different wave vectors $\vec{k}$ are uncorrelated in Fourier space. It can be shown that the power spectrum is simply the Fourier transform of the correlation function.
We will often compute the variance of the filtered density field, expressed by the power spectrum $P_\delta(k)$, which is given by

$$\sigma_R^2(a) = D_+^2(a)\,4\,\pi\int_0^\infty \frac{k^2\mathrm{d}k}{(2\,\pi)^3}P(k)\hat{W}^2(k\,R) \ , \tag{4.20}$$

with the power spectrum $P(k)$, a window function $\hat{W}(k\,R)$ and the linear growth factor $D_+^2(a)$. Often, the growth factor $D_+^2(a)$ is excluded from the definition and later multiplied, because for Newtonian gravity it is simply a function of the scale factor a. The variance on a scale of $8h^{-1}$Mpc today, $\sigma_8(a=1)$, is often used for characterising the amplitude of the power spectrum at $a=1$.

4.3 Dark matter halos

Gravitationally bound, dark matter structures in the Universe can be seen as composed of individual so-called halos. These are approximately spherical overdense clouds of dark matter which can reach highly non-linear densities in their centres. It is assumed that halos are formed through spherical collapse of overdense regions in the Universe. Thereby halos of different masses and sizes are produced. The distribution of halos over mass, the so-called mass function, typically gives the comoving number density of halos at redshift z within the mass range between M and $M+dM$. There are different, more or less sophisticated, ways to model the halo mass function. One of the simpler

ones, that still yields qualitatively good results, is the Press-Schechter mass function which we will discuss below.

4.3.1 Press-Schechter mass function

Press-Schechter theory assumes the spherical collapse of dark matter structures into halos of different mass on an otherwise smooth background density field. We skip the derivation which can be found in any good introductory textbook to cosmology and just state the result here.
The fraction of the cosmic volume filled with halos of masses within $[M,\, M + dM]$ is given by a comoving number density

$$n(M,z)\mathrm{d}M = \sqrt{\frac{2}{\pi}}\frac{\rho_0}{M}\frac{\delta_\mathrm{c}}{\sigma_R\, D_+(a)}\frac{\mathrm{d}\ln\sigma_R}{\mathrm{d}M}\exp\left(-\frac{\delta_\mathrm{c}^2}{2\sigma_R^2\, D_+^2(a)}\right)\mathrm{d}M\ . \tag{4.21}$$

ρ_0 is the mean density of the background, δ_c is the linear density contrast for spherical collapse at which structures can be assumed as collapsed. $D_+(a)$ is the linear growth factor and σ_R is the variance given by

$$\sigma_R^2 = 4\,\pi\int_0^\infty \frac{k^2\mathrm{d}k}{(2\,\pi)^3}P(k)\hat{W}^2(k\,R)\ , \tag{4.22}$$

with the power spectrum $P(k)$ and a window function $\hat{W}(k\,R)$.
The Press-Schechter mass function has turned out to fit the mass distribution of dark-matter halos in cosmological N-body simulations astonishingly well. The theory has recently acquired some modifications in order to improve its agreement with large, high-resolution simulations, or to take into account that halo collapse is not expected to proceed spherically in general, but elliptically.

4.3.2 The Navarro-Frenk-White density profile

An interesting and at the same time puzzling feature of dark matter halos is the universality of their density profile. Universality in this context means that the density profiles of mark matter halos on all scales, from dwarf galaxies to massive galaxy clusters, can be fitted by the same function. The general form of this function is given by

$$\rho(r|m) = \frac{\rho_s}{\left(\frac{r}{r_s}\right)^\alpha\left[1+\left(\frac{r}{r_s}\right)^\beta\right]}\ , \tag{4.23}$$

with the scale radius r_s and the density at that radius ρ_s.
The preferred choice today is to set $(\alpha, \beta) = (1, 2)$ which gives the Navarro-Frenk-White (NFW) density profile [11, 12]. The NFW profile provides a very good fit to the radial density distribution of dark matter halos in numerical simulations.
All the profiles used today to fit the density distribution within dark matter halos are heuristic fits to numerical simulations and/or observational data. It is unclear why halos of all sizes and masses acquire the same density profile or what determines its particular shape.

4.4 Conventional approaches to cosmic structure formation

4.4.1 Eulerian perturbation theory

Conventionally, structure growth and evolution are described within the scope of hydrodynamics where a perturbation ansatz is made. The description is thus based on the continuity equation, Euler's equation and the Poisson equation,

$$\begin{aligned} \frac{\partial \rho}{\partial t} + \vec{\nabla} \cdot (\rho \vec{v}) &= 0 \\ \frac{\partial \vec{v}}{\partial t} + \left(\vec{v} \cdot \vec{\nabla}\right) \vec{v} &= -\frac{\vec{\nabla} p}{\rho} + \vec{\nabla}\Phi \\ \nabla^2 \Phi &= 4\pi G \rho \,, \end{aligned} \tag{4.24}$$

where $\rho(\vec{x}, t)$ is the density, $\vec{v}(\vec{x}, t)$ the velocity of the cosmic fluid and Φ the gravitational potential. The density and the velocity are then decomposed into their homogeneous background parts $\rho_0(t)$ and $\vec{v}_0(t)$ and small perturbations $\delta\rho$ and $\delta\vec{v}$,

$$\begin{aligned} \rho(\vec{x}, t) &= \rho_0(t) + \delta\rho(\vec{x}, t) \\ \vec{v}(\vec{x}, t) &= \vec{v}_0(t) + \delta\vec{v}(\vec{x}, t) \,. \end{aligned} \tag{4.25}$$

Introducing physical coordinates $\vec{r}$ such that they relate to the co-moving coordinates $\vec{x}$ as $\vec{r} = a\,\vec{x}$ with the scale factor a, the velocity in physical coordinates is given by

$$\vec{v} = \dot{\vec{r}} = \dot{a}\vec{x} + a\dot{\vec{x}} = \vec{v}_0 + \delta\vec{v} \tag{4.26}$$

with the Hubble velocity $\vec{v}_0 = H\,\vec{r}$ and the peculiar velocity $\delta\vec{v} = a\,\dot{\vec{x}}$[2]. Together with,

$$\delta p = c_s^2 \rho_0 \delta \,, \tag{4.27}$$

[2]Often, $\dot{\vec{x}} =: \vec{u}$ is also called the peculiar velocity.

relating the pressure fluctuations to the density fluctuations by the sound speed c_s, and the definition of the density contrast,

$$\delta \coloneqq \frac{\rho - \rho_0}{\rho_0} = \frac{\delta\rho}{\rho_0} \,, \tag{4.28}$$

we can write down an equation for the evolution of the density contrast

$$\ddot{\delta} + 2\,H\,\dot{\delta} = 4\pi G\rho_0\delta + \frac{c_s^2\nabla^2\delta}{a^2} \,. \tag{4.29}$$

Since (4.29) is a homogeneous and linear differential equation, it is useful to decompose δ into plane waves,

$$\delta(\vec{x},t) = \int \frac{\mathrm{d}^3k}{(2\pi)^3}\hat{\delta}(\vec{k},t)\,\mathrm{e}^{-\mathrm{i}\vec{k}\cdot\vec{x}}, \quad \hat{\delta}(\vec{k},t) = \int \mathrm{d}^3x\,\delta(\vec{x},t)\,\mathrm{e}^{\mathrm{i}\vec{k}\cdot\vec{x}} \,, \tag{4.30}$$

and write (4.29) in Fourier space

$$\ddot{\hat{\delta}} + H\,\dot{\hat{\delta}} = \hat{\delta}\left(4\pi G\rho_0 - \frac{c_s^2k^2}{a^2}\right) \,, \tag{4.31}$$

decoupling time evolution from the spatial dependence.
The linear evolution of the density contrast during the matter-dominated era in models with $\Omega_{m,0} \neq 1$ and a cosmological constant, the linear evolution of the density contrast is given by

$$\delta(a) = \delta_0 D_+(a) \tag{4.32}$$

with the linear growth factor $D_+(a)$ that contains cosmological density parameters. For a ΛCDM-Universe it is well described by the fit-formula given in [13],

$$D_+(a) = \frac{5\,a\,\Omega_m(a)}{2}\left[\Omega_m^{4/7}(a) - \Omega_\Lambda(a) + \left(1 + \frac{\Omega_m(a)}{2}\right) + \left(1 + \frac{\Omega_\Lambda(a)}{70}\right)\right]^{-1} \,. \tag{4.33}$$

To proceed beyond linear growth, higher order perturbation terms have to be included and solved. This is a cumbersome and non-trivial task (for an extensive review see [14]).

This approach faces major conceptual difficulties:
First of all, dark matter is assumed to be collision-less, and yet Eulerian perturbation theory treats it as a fluid. This is flawed on a fundamental level.
Second of all, at the latest when the density contrast reaches unity, perturbation theory in the density contrast must break down.
And last, shell crossing (the formation of multiple streams) is a notorious problem for Eulerian perturbation theory. Whenever shell crossing occurs the description by

unique and smooth density and velocity fields breaks down.
Despite these difficulties, Eulerian perturbation theory remains the favoured analytical approach to cosmic structure formation in the community. Much effort has been put into extending its reach into the non-linear regime (see [15–36] for a selection of works).

4.4.2 Lagrangian perturbation theory

For completeness, we also mention Lagrangian perturbation theory. An extended review on Eulerian and Lagrangian perturbation theory can be found in [14].
Instead of solving the equations of motion for density and velocity fields, the Lagrangian approach follows the trajectories of particles or fluid elements. A displacement field $\vec{\Psi}(q)$ is introduced which maps the initial Lagrangian coordinate $\vec{q}^{(\mathrm{i})}$ onto its final position $\vec{x}$ in Eulerian space at a later time t,

$$\vec{x}(t) = \vec{q}^{(\mathrm{i})} + \vec{\Psi}(\vec{q}^{(\mathrm{i})}, t) \; . \tag{4.34}$$

While solving the equation of motion for the particle trajectories $\vec{x}(t)$ the inverse of the Jacobian of the transformation between Eulerian and Lagrangian space needs to be computed and therein lies the again the conceptual problem:
If there is shell crossing, i.e. particles with different initial Lagrangian positions $\vec{q}^{(\mathrm{i})}$ that end up at the same Eulerian coordinates $\vec{x}$, the Jacobian of the transformation vanishes and the density field becomes singular at these points. Thus, the description of dynamics in terms of a mapping breaks down.
One can, as for Eulerian perturbation theory, set up a Lagrangian perturbation theory in terms of the displacement field $\vec{\Psi}(q)$ and expand around its linear solution. It can be shown that, in linear order, the displacement field has the solution

$$\nabla_q \cdot \vec{\Psi}^{(1)} = D_+(t)\delta(\vec{q}^{(\mathrm{i})}) \tag{4.35}$$

where $\delta(\vec{q}^{(\mathrm{i})})$ is the initial density field satisfying $\delta(\vec{q}^{(\mathrm{i})}) \ll 1$. Thus, in this approximation, particles simply move on straight lines with the time dependence given by the linear growth factor $D_+(t)$. The Zel'dovich approximation now extrapolates these trajectories to the present time.

4.4.3 The Halo Model

A very crude but surprisingly effective approach to describing large scale structure formation is given by the Halo Model (for a detailed review see for example [37]).

The approach assumes that all the mass in the Universe is composed of distinct units, i.e. halos. If halos are distinct objects, then they are likely small compared to the typical distances between them. This would suggest that the statistics of the mass density field on small scales is determined by the spatial distribution within the halos. At these scales the precise way how the halos themselves are organized into large scale structures is irrelevant. But then, the details of the internal structure of the halos cannot be relevant on scales larger than a typical halo. Thus, on large scales, the important ingredient is the spatial distribution of the halos. This assumption allows us to decompose the non-linear density-fluctuation power spectrum into contributions from correlations between any two different dark matter halos and a contribution from correlations within each single halo.
The two contributions are called the two-halo $P^{2\mathrm{h}}(k)$ and the one-halo $P^{1\mathrm{h}}(k)$ terms, respectively, and are given by

$$P^{1\mathrm{h}}(k) = \int \mathrm{d}m\, n(m) \left(\frac{m}{\bar{\rho}}\right)^2 |u(k|m)|^2 \tag{4.36}$$

$$P^{2\mathrm{h}}(k) = \int \mathrm{d}m_1\, n(m_1) \left(\frac{m_1}{\bar{\rho}}\right) u(k|m_1) \int \mathrm{d}m_2\, n(m_2) \left(\frac{m_2}{\bar{\rho}}\right) u(k|m_2) P_{hh}(k|m_1, m_2)\ ,$$

which are convolutions of the Fourier transform of the dark matter density profile $u(k|m)$ and the number density of halos $n(m)$ for halos of given mass m and the mean density $\bar{\rho}$. In the two-halo term, $P_{hh}(k|m_1, m_2)$ represents the power spectrum of halos of mass m_1 and m_2 and can, for convenience, be approximated by the linear power spectrum weighted by some factor correcting for a bias that is usually determined empirically from observations or simulations.
Since we are not interested in an accurate quantitative comparison between the Halo Model and N-body simulations, we compute $n(m)$ from the Press-Schechter mass function [38] for simplicity.
For the halo density profile we will assume the Navarro-Frenk-White profile

$$\rho(r|m) = \frac{\rho_s}{\left(\frac{r}{r_s}\right)\left[1 + \left(\frac{r}{r_s}\right)^2\right]}\ . \tag{4.37}$$

In Fourier space it is given by

$$\begin{aligned} u(k|m) =& \frac{4\pi\rho_s r_s^3}{m} \Big\{ \sin(kr_s)\left[\mathrm{Si}([1+c]kr_s) - \mathrm{Si}(kr_s)\right] - \frac{\sin(ckr_s)}{(1+c)kr_s} \\ &+ \cos(kr_s)\left[\mathrm{Ci}([1+c]kr_s) - \mathrm{Ci}(kr_s)\right] \Big\} \end{aligned} \tag{4.38}$$

with the scale radius r_s, the density at that radius ρ_s and the concentration parameter $c = r_{vir}/r_s$ with virial radius r_{vir}. Numerical simulations show that there is, in fact, a

distribution of concentrations for halos of the same mass which is well described by a log-normal distribution

$$p(c|m,a) = \frac{\mathrm{d}\ln c}{\sqrt{2\pi\sigma_c^2}} \exp\left\{ -\frac{\ln^2\left(\frac{c}{\bar{c}(m,a)}\right)}{2\sigma^2_{\ln c}} \right\} \tag{4.39}$$

where

$$\bar{c}(m,a) = C_0\, a \left(\frac{m}{m_*}\right)^{\gamma} \tag{4.40}$$

is the mean concentration with the mass normalisation taken to be $m_* = 2 \cdot 10^{13} M_\odot$. Thus, the Halo Model actually requires input from numerical simulations to make sensible predictions for the non-linear power spectrum. There have been further attempts to expand the model to make predictions match results from numerical simulations more accurately by, for example, including sub-structures of halos. Including sub-structures in the Halo Model has been shown to raise the predicted power on scales $k > 1\,h\,\mathrm{Mpc}^{-1}$ by up to several 10%. However, an excess in power around $k \approx 1\,h\,\mathrm{Mpc}^{-1}$ has been observed in numerical simulations when compared to results of the Halo Model which could not be explained by including halo sub-structures[39].

4.4.4 Numerical N-body simulation

Numerical N-body simulation are believed to provide the best model for cosmic structure formation and thus to produce the most accurate predictions of the non-linear power spectra.

Numerical simulations follow a quite simple idea: N particles are randomly placed into a box of volume V according to some initial distribution. The particles move within the box according to the Hamiltonian equations of motion and interact with each other via the Newtonian gravitational potential. At some final time the final positions (and momenta) of particles are sampled and a density (and momentum) correlation function or power spectrum can be computed. In reality, the whole process is, of course, far more involved. Clever algorithms, for instance, allow to shorten the runtime of the simulations considerably while still retaining the required level of resolution.

However, numerical simulations are computationally very expensive. They are, therefore, not an ideal tool to explore a wide range of cosmological parameters or deviations from the usual physics that governs large scale structure formation. In addition, higher order statistics (meaning n-point correlators) are increasingly harder to extract with increasing n.

It is therefore advantageous to develop an analytic approach that allows us to easily

access higher order spectra and that is at the same time computationally inexpensive. In the last years, so-called emulators have been heavily in use to predict the non-linear power spectrum for different cosmologies without having to run a simulation for every parameter set. These emulators use results from simulation runs with certain sets of cosmological parameters and then interpolate between those to get predictions for parameter sets for which no simulations exist. One example of such an emulator is the Cosmic Emulator [40–43] from which we obtain our reference power spectra.

4.5 Advantages of the KFT approach to cosmic structure formation

In Part I we have shown how to develop a kinetic field theory that allows us to describe the formation of structure in an initially correlated many-body system. In the following, we will give a short description of how the KFT approach avoids the difficulties known from other, conventional, approaches and point out its conceptual and methodical advantages.

The most important advantage of KFT over Eulerian or Lagrangian theory is that, since KFT is based on the Hamiltonian flow in phase space, the problem of shell crossing does not occur. Instead, the flow in phase space is diffeomorphic and, due to the symplectic structure of the Hamiltonian equations, even volume-conserving. The notorious problem with multiple streams, as they occur in standard perturbation theories based on either the Boltzmann equation or the hydrodynamic equations which assume the existence of uniquely valued velocity fields, is absent from KFT by construction since phase-space trajectories cannot cross. Similar difficulties that arise in Lagrangian perturbation theories due to functional determinants developing singularities in convergent flows do not occur in KFT because the functional determinant of the phase-space flow is unity at all times.

Another conceptual advantage of KFT is that it, in principle, contains the complete hierarchy of moments and of the particle correlations in configuration and momentum space because it neither assumes the existence of smooth density or velocity fields nor their uniqueness and avoids taking moments over momentum space. Since we do not assume the existence of smooth and uniquely-valued velocity field, the particle motions in phase space also trace the formation of vorticity on small scales and at late times.

An important methodical advantage of the KFT approach lies in the linearity of Hamilton's equations. It guarantees the existence of a Green's function. We can thus split the Hamiltonian into parts which are interpreted as an unperturbed and a

perturbed contribution. How we split the Hamiltonian is to a large degree arbitrary and thus the Green's function can be chosen such that the interaction Hamiltonian becomes small. This is also one of the main reasons why our first-order perturbation theory is already highly successful in KFT, as demonstrated in [1].

5

Influence of gravitational potential on structure formation on small scales

5.1 Overview

In this chapter, we present the main cosmological results of this thesis.
We investigate the influence of the shape of the particle interaction potential on the slope of the non-linear density-fluctuation power spectrum on scales $k \geq 1\,h\,\mathrm{Mpc}^{-1}$. These scales are considered small in the context of large-scale structure formation. It is at these small scales that contributions to the non-linear power spectrum from inner structures of dark matter halos begin to dominate. This will allow us to draw conclusions on the density profiles of dark matter halos from our analysis.
Our only goal here is to see whether, with the interaction amplitude suitably adapted, the potential shape is responsible for the shape of the non-linear power spectrum. We thus allow ourselves to change the interaction amplitude to maximise the agreement with observations or simulations.
We start our analysis using the perturbative approach described in 3.4.2 for the evaluation of particle trajectories. Doing so, we show that the slope of the non-linear contributions to the density-fluctuation power spectrum at $k \geq 1\,h\,\mathrm{Mpc}^{-1}$ is seemingly unaffected by the shape of the interaction potential between particles.
We then check these results using the more recent Born approximation for the evaluation of particle trajectories. We show that we cannot reproduce the results obtained with the perturbative approach and discuss the implications of this discrepancy.

5.2 The scale dependent linear growth factor

One of the consequences of changing the shape of the particle interaction potential away from Newtonian gravity will be that the linear growth factor (4.32) will be no longer a function of time only, but will depend on the wave number k in addition. In this section, we will show how we can modify Poisson's equation to compute the appropriate growth factor for a general power-law potential.

We start with the continuity and Euler equations in comoving coordinates,

$$\dot{\delta} + (1+\delta)\vec{\nabla}\cdot\vec{u} + \vec{u}\cdot\vec{\nabla}\delta = 0 \tag{5.1}$$

$$\dot{\vec{u}} + 2H(t)\vec{u} + \left(\vec{u}\cdot\vec{\nabla}\right)\vec{u} = -\frac{1}{a^2}\vec{\nabla}\Phi \; . \tag{5.2}$$

We combine these two equations, set up a perturbation ansatz for δ, $\vec{u}$ and Φ and linearise the resulting equation. For convenience, we can rename the perturbation $\delta\vec{u}$ by $\vec{u}$ and do the same for the gravitational potential. Using the continuity equation once more

$$\vec{\nabla}\cdot\vec{u} = -\dot{\delta} \; , \tag{5.3}$$

we end up with the following equation for the dynamics of the density perturbations

$$\ddot{\delta} + 2H(a)\dot{\delta} - \frac{1}{a^2}\vec{\nabla}^2\Phi = 0 \; . \tag{5.4}$$

In Fourier space the equation reads

$$\ddot{\tilde{\delta}} + 2H(a)\dot{\tilde{\delta}} + \frac{k^2}{a^2}\tilde{\Phi} = 0 \; . \tag{5.5}$$

Since we are dealing with a general form of power-law potentials, we cannot simply use Poisson's equation to substitute the Laplacian of the gravitational potential. Therefore, we consider an algebraic modification of Poisson's equation in Fourier space. It now reads

$$-f(k)\,\tilde{\Phi} = 4\pi G\bar{\rho}a^2\tilde{\delta} \tag{5.6}$$

with G the gravitational constant and $\bar{\rho}$ the mean density. The modifying function $f(k)$ is the inverse of the Fourier-transformed particle interaction potential and is, in that sense, fixed. For the Newtonian gravitational interaction it is simply k^2.
With this modification, (5.5) can be brought into the form

$$\tilde{\delta}'' + \left(\frac{3}{a} + \frac{H'(a)}{H(a)}\right)\tilde{\delta}' + \frac{k^2}{f(k)}\frac{3\,\Omega_m(a)}{2\,a^2}\tilde{\delta} = 0 \; , \tag{5.7}$$

where we have transformed to a new time variable a, which is the scale factor, and used

$$\bar{\rho} = \frac{3\,H^2(a)}{8\,\pi\,G}\Omega_m(a). \tag{5.8}$$

This differential equation can then be solved numerically. The growing mode of the solution is then the linear growth factor $D_+(k,a)$ which now in general can depend on the wave number k. For the Newtonian gravitational potential, the linear growth factor reduces to the usual, scale-factor dependent function $D_+(a)$.

5.3 Power spectrum and NFW density profile

From the halo model (4.36), we know that the non-linear power spectrum is a convolution of Fourier-transformed NFW profiles, weighted with the mass function. Since we reproduce the non-linear power spectrum at least up to $k = 10\,h\,\mathrm{Mpc}^{-1}$ with KFT, both perturbatively and with the Born approximation, un-weighting with the mass function would lead to the NFW profile. Thus, leaving the relative abundances of haloes with different mass unchanged, we can conclude from our results how different choices for the gravitational potential would affect the density-profile shape.
We point out that, while the halo model must be provided with the explicit form of the halo density profile in (4.36), the KFT approach does not need any input of this kind. The halo density profile that is produced in the KFT approach is thus the result of particle interactions and correlations.

For our analysis, we will assume that the non-linear contributions to the power spectrum obtained from KFT approximately correspond to the one-halo term of the halo model (4.36). The validity of this assumption is quantified in Fig. 5.1 where we have computed $P^{\mathrm{1h}}(k)$ using an NFW-density profile (4.38) with $C_0 = 9$, $\sigma_{\ln c} = 0.25$ and $\gamma = -0.13$, as commonly found in simulations [37, 44], and the Press-Schechter mass function. The comparison with the Fourier transform of NFW is a consistency check for us. We find reasonable agreement with our KFT results, although we see a clear deviation at $k > 10$. We also show the result for $\gamma = -0.5$ which is seemingly preferred by KFT. Slopes this steep have only been found in analyses conducted with X-ray surveys [45, 46] so far, whereas simulations yield values around $\gamma \approx -0.1$. A steeper slope would suggest a stronger trend for high-mass halos to have lower concentrations, and a larger scatter of concentrations for a given mass. It is however unclear how much significance should be attributed to this finding; after all, we are using a crude implementation of the halo model without including any sub-structures here. In addition, an excess in power around $k \approx 1\,h\,\mathrm{Mpc}^{-1}$ as we see for KFT has been

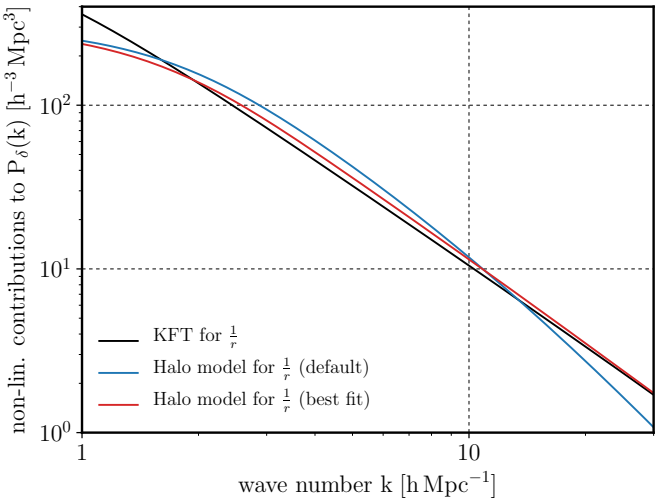

Figure 5.1.: The non-linear contributions from KFT are shown with the one-halo term for $\gamma = -0.13$ (default) and $\gamma = -0.5$ (best fit) for $k > 1\,h\,\mathrm{Mpc}^{-1}$. The one-halo term includes the NFW density profile with commonly used parameters ($C_0 = 9$, $\sigma_{\ln c} = 0.25$ [37]). For $\gamma = -0.13$ a deviation at $k > 15\,h\,\mathrm{Mpc}^{-1}$ becomes evident. Setting $\gamma = -0.5$ instead provides better agreement with KFT.

observed in numerical simulations as well when compared to results of the halo model. It should also be noted that we are only at the first-order level of perturbation theory here, although we do expect corrections from higher-order perturbations to be small if the perturbation series converges. Because of that and the uncertainties present in the halo model itself, we would like to refrain from speculations about the meaning of this high value for γ.

5.4 Analysis in perturbative expansion

We use the perturbative approach (see section 3.4.2) to analyse the small-scale behaviour of the non-linear contributions to the power spectrum under different gravitational laws. We include particle interactions up to first order in the interaction operator only, since we have seen in our previous work [1] that already at this order our result for the non-linear density-fluctuation power spectrum agrees well with non-linear power

spectra from Cosmic Emulator [40–43] that uses state of the art N-body simulations. In our KFT approach, initial correlations appear in a quadratic form in an exponential. We use a Taylor expansion in order to perform the integration over initial particle positions and momenta in (3.31). Initial correlations are included up to second order only. Including the full hierarchy of initial momentum correlations proves to be much more cumbersome in the perturbative approach compared to the Born approximation (see comment in section 3.4.2). It is also unnecessary for our purposes here to include the full hierarchy of initial momentum correlations since they only affect the shape of the power spectrum on intermediate scales ($k \approx 0.3\,h\,\mathrm{Mpc}^{-1}$) as we have shown in [9]. Initial density and density-momentum correlations only contribute at very high redshifts and can be neglected in our analysis.

We compare the non-linear contributions to the density-fluctuation power spectrum for interaction potentials of the form

$$v(r) = \frac{A}{(r^2+\varepsilon^2)^{\frac{n}{2}}}\ . \tag{5.9}$$

with particle distance r, smoothing scale ε and amplitude A. For the actual computations, we will require the respective Fourier transforms of $v(r)$, which are given by

$$\tilde{v}(k) = \bar{A}\,k^{\frac{n-3}{2}}\,\mathrm{K}_{\left|\frac{3-n}{2}\right|}(k\,\varepsilon)\ . \tag{5.10}$$

Here $\bar{A}$ is again an amplitude and $\mathrm{K}_a(k\,\varepsilon)$ is the modified Bessel function of the second kind of order a.

We present our results in Fig.5.2, where we show the non-linear contributions to the density-fluctuation power spectrum for various slopes of the interaction potential. Note that the linear power spectrum in this plot belongs to the Newtonian case only and is shown for reference only. Linear power spectra consistent with non-linear contributions for interaction potentials that are not Newtonian will look different. This can be seen if we derive the appropriate linear growth factors $D_+(a,k)$ for non-Newtonian potentials as discussed in 5.2.

We normalise the linear growth such that $\sigma_8 = 0.8$ for any interaction potential on large scales, i.e. $k \ll 1\,h\,\mathrm{Mpc}^{-1}$, is reproduced today. We choose the amplitude of the interaction potential (5.10) and the amplitude of the initial density-fluctuation power spectrum such that the amplitudes of the non-linear contributions to the power spectrum for any potential match that of the Newtonian case and the above normalisation criterion is satisfied.

The linear power spectrum can be obtained by multiplying the initial power spectrum

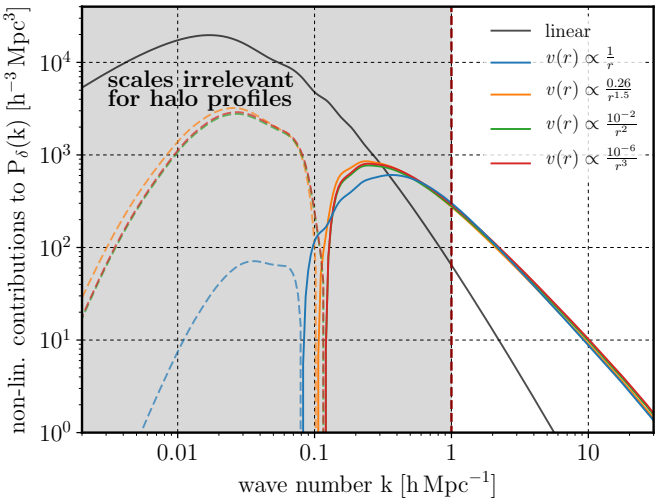

Figure 5.2.: The non-linear contributions to the power spectrum today ($a = 1$) are shown together with the linear power spectrum for Newtonian gravity which serves here as a reference only. The power spectrum in the gray-shaded area, to a large degree, does not depend on the inner correlations on dark matter halos and is therefore neglected in our analysis. Starting from $k = 1\,h\,\mathrm{Mpc}^{-1}$ we assume that inner-halo structures begin to affect the shape of the non-linear power spectrum. On scales $k > 1\,h\,\mathrm{Mpc}^{-1}$ we see a very good agreement of the non-linear corrections independent of the shape of the interaction potential.

$P_\delta^{(\mathrm{i})}$ with the appropriate linear growth factor corresponding to the interaction potential being used,

$$P_\delta(k) = D_+^2(a,k) P_\delta^{(\mathrm{i})}(k)\ . \tag{5.11}$$

It is clear from this expression that the linear growth for non-Newtonian potentials will be different from the Newtonian case. Therefore, the linear growth together with the non-linear growth for non-Newtonian gravity will produce power spectra that look quite different from the Newtonian case. However, this is unimportant for our analysis, because we are only interested in those contributions to the density-fluctuation power spectrum which are due to the inner structure, i.e. density profile, of dark matter halos. If we think about this in the picture of the halo model the argument becomes clearer: While the linear power spectrum, corresponding to the two-halo term, describes the correlations between two different dark matter halos, the one-halo term describes the

contributions from the inner structures of halos, which are highly non-linear. Therefore, also in KFT the information on the density profile of dark matter halos will be hidden solely in the non-linear contributions.

The conclusion that we then draw from our analysis is that, for smaller scales, i.e. $k > 1\,h\,\mathrm{Mpc}^{-1}$, the non-linear contributions show almost no sensitivity to the slope of the interaction potential. In the gray-shaded area in Fig. 5.2 we see some sensitivity to the potential slope, however these scales are too large to be relevant for the density profiles of even the largest dark matter halos.
Since we find that the slopes of the non-linear contributions remain the same even for strongly varying interactions laws, following the discussion in 5.3 we must conclude that different choices for the gravitational potential would not affect the density-profile shape of dark matter halos.

Let us recall, at this point, that the results from the perturbative KFT approach for the non-linear power spectrum under Newtonian gravity are in good agreement with predictions from numerical simulations. This agreement was already found when the perturbation series in terms of the order of the particle interaction potential was truncated after the first order. If the perturbation series is convergent, which should be ideally the case, then higher order terms should yield ever smaller corrections to the non-linear power spectrum that we have so far.
If, however, we use short-ranged interaction potentials most of the structure will be accumulated on very small scales and higher-order interaction terms will become more dominant. Hence, the perturbative ansatz is expected to perform worse and may eventually break down. To see whether this is the case we would need to compute higher-order terms and check the convergence of the perturbation series.

We would further like to stress that the interpretation of the above results was done under the assumption that the relative abundances of haloes with different mass remains unchanged. This assumption was made because we considered the non-linear contributions corresponding to the one-halo term only. If we had considered the full non-linear density-fluctuation power spectrum which corresponds to the one-halo term and two-halo term combined, the mass function in the halo model would have had to be adjusted accordingly, i.e. more low-mass halos and less high-mass halos for short ranged interaction potentials. This point will be important for the analysis in the next section.

5.5 Analysis in the Born approximation

We have described in 3.4 that it is also possible to include particle interactions in terms of the Born approximation. Naively, we would expect to find the same results as for the perturbative ansatz. But it turns out that even comparing what we call "non-linear contributions" in the perturbative ansatz and in the Born approximation scheme is not straightforward. As general rule, the non-linear contributions must be the difference between the full non-linear density-fluctuation power spectrum and the linear density-fluctuation power spectrum. Let us first compare the non-linear contributions defined in this way in the perturbative ansatz and in the Born approximation for Newtonian gravity only. In Fig. 5.2, the blue line shows the non-linear contributions from the pertubative ansatz and in Fig. 5.3 we see (supposedly) the same quantity in red. While the non-linear contributions in Fig. 5.2 are composed of a negative part and a positive part, depicting a mode transport from large to small scales, such a phenomenon is not observed in Fig. 5.3 for the non-linear contributions. Instead we see a throughout positive contribution to the linear power spectrum. It is therefore yet unclear how the terms leading to the non-linear contributions in the perturbative approach could be directly compared to those from the Born ansatz.

To gain better understanding of the physical processes involved in the non-linear power spectrum in Fig. 5.3, let us take a closer look at the simple analytic expression (3.78) for the non-linear density-fluctuation power spectrum,

$$\bar{\mathcal{P}}(k_1,t) = \mathrm{e}^{Q_{\mathrm{D}}(k_1,t)-\langle\bar{F}(k_1,t)\rangle}\mathcal{P}(k_1,t)\ . \tag{5.12}$$

In the leading exponential factor, we have the momentum-diffusion term Q_{D} that is being counter-acted by the Born-approximated interaction term $\langle\bar{F}(k_1,\,t)\rangle$. This factor is multiplied by the evolved density-fluctuation power spectrum $\mathcal{P}(k_1,t)$ given by (3.70).

The orange curve in Fig. 5.3 shows the factor $\mathrm{e}^{Q_{\mathrm{D}}(k_1,t)}\mathcal{P}(k_1,t)$. We can see that the later shape of the non-linear density-fluctuation power spectrum is already visible there (see also Fig. 3.1 in 3.3.3). This is a consequence of the full hierarchy of initial momentum correlations contained in $\mathcal{P}(k_1,t)$ as was shown in [9].

In the way the interaction term $\langle\bar{F}(k_1,\,t)\rangle$ is included in (5.12), it directly reduces damping. Neglecting the damping term in (5.12) leads to the behaviour depicted in 5.4 where we see that the interaction term alone would lead to a diverging power spectrum on small scales. This illustrates the delicate balance between the interaction and the damping term for Newtonian gravity that leads to the non-linear density-fluctuation

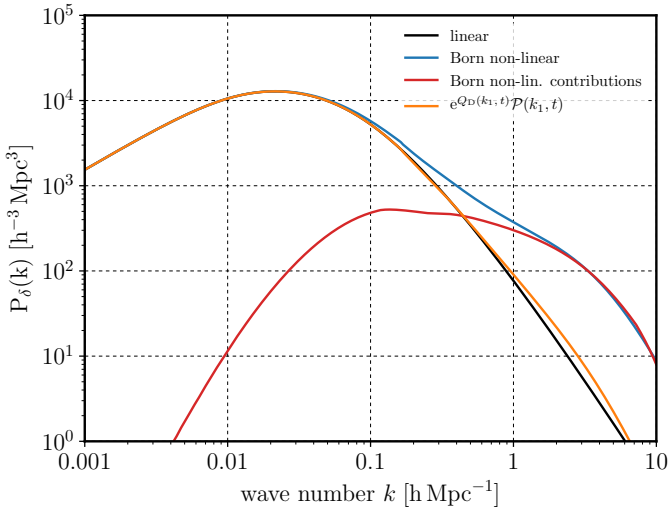

Figure 5.3.: We show the non-linear density-fluctuation power spectrum in (5.12) (blue) together with the linear density-fluctuation power spectrum (black) and the difference thereof, i.e. the non-linear contributions (red). The term $e^{Q_D(k_1,t)}\mathcal{P}(k_1,t)$ which already sets the non-linear shape of the power spectrum (orange).

power spectrum in 5.3 that agrees well with results from numerical simulations.

We will now repeat the analysis discussed in 3.4.2 using Born's approximation. Our aim here is to investigate how the slope of the power spectrum at $k \geq 1\,h\,\mathrm{Mpc}^{-1}$ is affected by the shape of the interaction potential between particles. We will test interaction potentials of the form (5.9) with the respective Fourier transforms given by (5.10).
Let us, at this point, introduce the short hand

$$m := \frac{3-n}{2}\,. \tag{5.13}$$

The smoothing scale ε should be chosen to be much smaller than the smallest scale we are interested in. Otherwise we run the risk of seeing effects caused by the smoothing scale in (5.16) that are not physical. We take ε such that the condition $0 < k\,\varepsilon \ll \sqrt{|m|+1}$ is automatically satisfied, which allows us to approximate the modified Bessel function

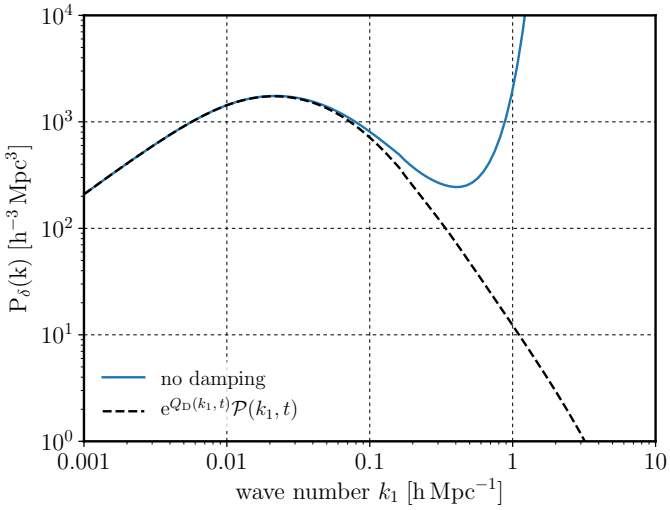

Figure 5.4.: The non-linear density-fluctuation power spectrum from (5.12) is shown here without the damping term $e^{Q_D(k_1,t)}$ (blue). The term $e^{Q_D(k_1,t)}\mathcal{P}(k_1,t)$ is plotted for reference (dashed black).

by its asymptotic form

$$K_{|m|}(k\,\varepsilon) \approx \begin{cases} \frac{\Gamma(|m|)}{2}\left(\frac{2}{k\,\varepsilon}\right)^{|m|}\,, & |m|>0 \\ \\ -\ln\left(\frac{k\,\varepsilon}{2}\right) - \text{const.}\,, & |m|=0 \end{cases} \tag{5.14}$$

up to $k \approx 10^3\,h\,\mathrm{Mpc}^{-1}$ for $\varepsilon \approx 10^{-4}\,h\,\mathrm{Mpc}^{-1}$. Absorbing all factors independent of k into the amplitude $\bar{A}$, we are left with

$$\tilde{v}(k) \approx \bar{A}\,k^{-\alpha} \tag{5.15}$$

for $n \neq 3$ where we have defined $\alpha := m + |m|$. For $n = 3$, (5.14) as well as (5.15) scale logarithmically and not as power laws. We will omit the calculation for this case as there is no new information to be gained from it.

We now need to assess which of the ingredients in (5.12) have to be adjusted to the new particle interaction potential.

The only explicit appearance of the interaction potential in (5.12) is through the integral

$$\mathcal{J} = \int_k \vec{k_1}\cdot\vec{k}\;\tilde{v}(k)\,e^{Q_D(k_1-k,t')}P_\delta(k_1-k,t') \tag{5.16}$$

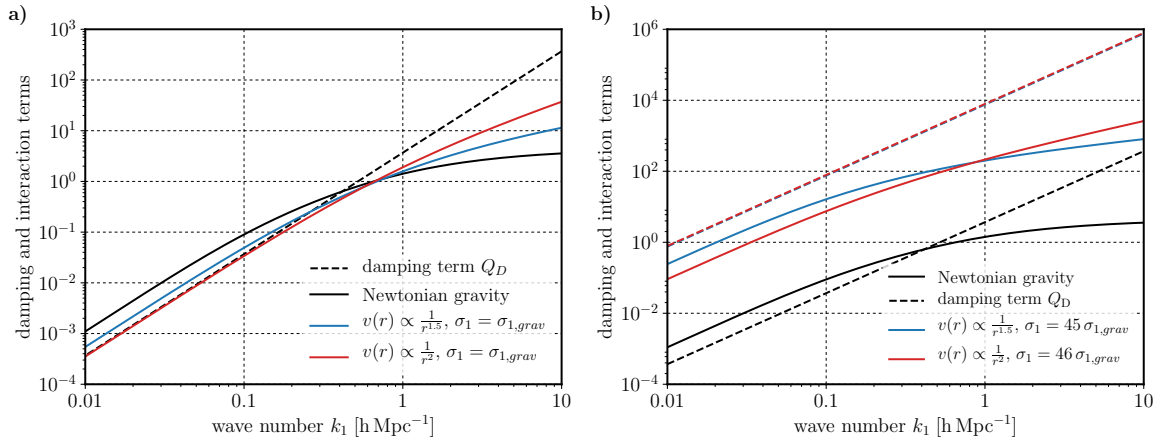

Figure 5.5.: We plot the integral (5.16) for different potentials. In a) we use the same values of σ_1 and the amplitudes of the interaction potential as well as of the initial density power spectrum as for Newtonian gravity. In b) we change these accordingly by using values that we have found in section 3.4.2. The slopes of the damping terms remain the same for any potential. It is clearly visible that at large scales the slopes of the interaction terms also follow k^{-2} for all potentials. The deviations from the Newtonian case become increasingly apparent for $k \geq 0.3\,h\,\mathrm{Mpc}^{-1}$.

in the interaction term

$$\langle \bar{F}(k_1,\, t)\rangle = \int_0^t 2 g_{qp}(t,t') \int_k \vec{k_1}\cdot\vec{k}\;\tilde{v}(k)\,\mathrm{e}^{Q_\mathrm{D}(k_1-k,t')} P_\delta(k_1-k,t')\;. \tag{5.17}$$

with the Fourier transform of the two-particle interaction potential $\tilde{v}(k)$ and the time-evolved density-fluctuation power spectrum $P_\delta(k_1-k,t') = g_{qp}^2(t',0)P_\delta(k_1-k)$. The specific form of the propagator denoted by g_{qp} is of no importance to us here.

Using the interaction potential (5.15) in (5.16) and transforming the integration variable to $\vec{\kappa} := \vec{k_1} - \vec{k}$, introducing $y := \frac{\kappa}{k_1}$ and the angle cosine μ between the vectors $\vec{\kappa}$ and $\vec{k_1}$, yields the integral expression

$$\mathcal{J} = 2\,\pi\,\bar{A}\,k_1^{5-\alpha}\!\int\!\mathrm{d}y\,y^2\int_{-1}^{+1}\!\mathrm{d}\mu\;\frac{(1-y\mu)\;\mathrm{e}^{Q_\mathrm{D}(k_1\,y,t')}P_\delta(k_1\,y,t')}{(1+y^2-2y\mu)^{\alpha/2}}\;. \tag{5.18}$$

This function is shown in Fig. 5.5 a).
In Fig. 5.6 we see that the largest contributions to the integral (5.18) are from scales around $\kappa \approx 0.02\,h\,\mathrm{Mpc}^{-1}$. On scales relevant for the inner halo structure,

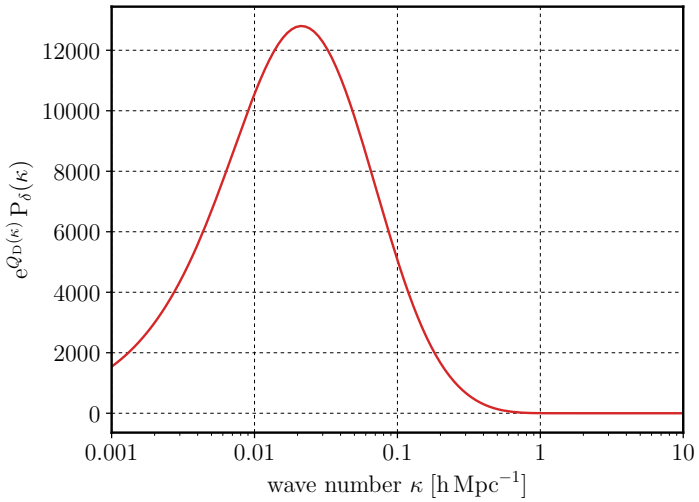

Figure 5.6.: The linear power spectrum with damping factor appearing in (5.16) shows a peak at $\kappa \approx 0.02\,h\,\mathrm{Mpc}^{-1}$. The largest contributions of this factor to the value of the integral (5.16) will therefore be found around these small scales. At larger scales than $\kappa \approx 0.1\,h\,\mathrm{Mpc}^{-1}$, this integration kernel falls off at least exponentially and damps away any contributions to the integral (5.16).

$k_1 > 1\,h\,\mathrm{Mpc}^{-1}$, power contributions from the integration kernel are damped away as shown in Fig. 5.5 a) such that the slope of the integral value remains the same for any interaction potential. The relevant scaling with wave number k_1 is thus,

$$\mathcal{J} \propto k_1^{5-\alpha}\, g(k_1)\ , \tag{5.19}$$

where the function $g(k_1)$ is the value of the integral over $\mathrm{d}\mu$ and $\mathrm{d}y$ in (5.18) as a function of k_1. According to Fig. 5.5, $g(k_1)$ has almost the same slope for any potential on small scales, although its amplitude my change.
For $n = 1$, the integral $\mathcal{J}$ in (5.19) scales as $k_1^3\, g(k_1)$, as we expect for Newtonian gravity. Going from $n = 1$ to $n = 6$, the slope changes from $k_1^3\, g(k_1)$ to $k_1^5\, g(k_1)$.

We consider (5.18) for two cases: In the first case, we set σ_1 in the damping term Q_D for any interaction potential to the same value as for Newtonian gravity. The result is shown in Fig. 5.5 a). In the second case, we apply the same normalisation criterion as in section 3.4.2 for the growth of large scale structures. We use the same amplitudes

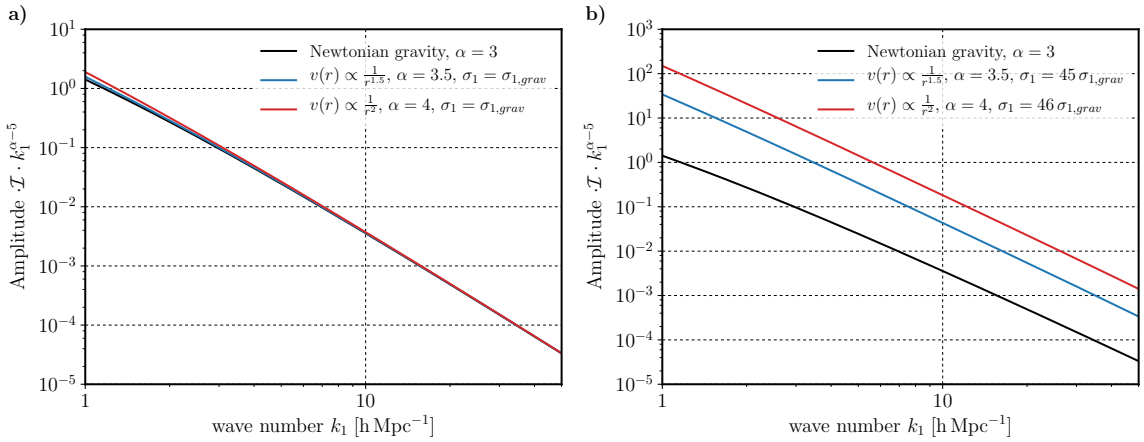

Figure 5.7.: We plot the integral in (5.16) divided by the factor $k_1^{5-\alpha}$. It is clearly visible that the deviations from the Newtonian case of the integral value in (5.16) for different interaction potentials become negligible for increasing wave numbers k_1. This is due to the exponential damping of the integration kernel (see Fig.5.6). In conclusion, only the factor $k_1^{5-\alpha}$ in (5.16) can have any effect on the slope of the interaction term.

for the initial power spectrum and the interaction potential as in 3.4.2. The result is then shown in Fig. 5.5 b). Here we see that the slopes at large scales remain the same for varying interaction potentials, but at small scales, we see a significantly different scaling with k_1 and higher amplitudes. Consequently, this effect will be highly visible in the non-linear density-fluctuation power spectrum, unless the factor $\mathrm{e}^{Q_\mathrm{D}(k_1,t)}\mathcal{P}(k_1,t)$ in (5.12) can counteract the increase in power on small scales.
The same two cases are shown for the function $g(k_1)$ in (5.19) in Fig. 5.5. Interestingly, $g(k_1)$ still has the slope (5.19) b) for any potential on small scales, but the amplitudes become much higher.

To verify that the delicate balance between the damping and the interaction terms in (5.12) is still intact, we plot the difference $\langle \bar{F}(k_1, t)\rangle - Q_\mathrm{D}(k_1, t)$ for interaction potentials with different slopes in Fig. 5.8, again for the two cases as in Fig. 5.5. We see that the balance between the damping and the interaction terms is gradually destroyed with increasing deviation of the potential slope from Newtonian gravity. We see that, apparently, adjusting the amplitudes by applying the same normalisation criterion as in section 3.4.2 for the growth of large scale structures, makes the imbalance even worse.

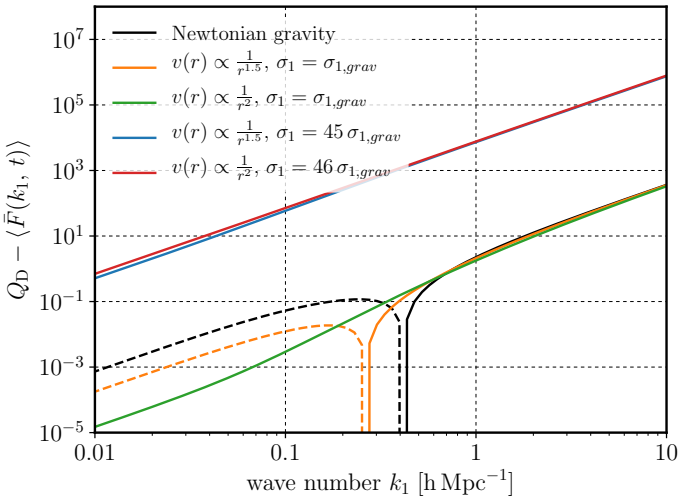

Figure 5.8.: The difference $\langle \bar{F}(k_1, t) \rangle - Q_D(k_1, t)$ for interaction potentials with different slopes in Fig. 5.8 is shown for the same two cases as in Fig. 5.5. The balance between the damping and the interaction term is gradually destroyed with increasing deviation of the potential slope from Newtonian gravity.

As a last step in our analysis, we show (5.12) in Fig. 5.9 for a $\frac{1}{r^2}$-potential for four different cases in an attempt to restore the balance between interaction and damping. In Fig. 5.9 a), we leave all amplitudes at the same value as for Newtonian gravity. We do not believe that this gives the correct non-linear power spectrum for the $\frac{1}{r^2}$-potential, we simply use it as a reference scenario. If we now adjust the amplitudes according to the normalisation criterion as in section 3.4.2 for the growth of large scale structures in (5.12), we end up with Fig. 5.9 c). Although the amplitudes were chosen such that the linear growth on large scales should reproduce the linear growth for Newtonian gravity under the assumption of (5.11), we clearly see that this is not the case. In Fig. 5.9 b), we have adjusted the amplitudes in the interaction term $\langle \bar{F}(k_1, t) \rangle$ only, but have left them at the same value as for Newtonian gravity in the term $e^{Q_D(k_1,t)}\mathcal{P}(k_1, t)$. We now reproduce the same linear growth on large scales as for Newtonian gravity, however the non-linear power spectrum deviates strongly from the Newtonian case at intermediate scales already. Subtracting a purely linear contribution from the non-linear power spectrum in the sense of (5.11) will lead nowhere near the same results for the non-linear contributions that we have computed in section 3.4.2. In all of these cases we have just discussed, we see behaviour similar to that shown in Fig. 5.4 where we

have switched off the damping term for Newtonian gravity.
Finally, in Fig. 5.9 d) we have adjusted the amplitudes everywhere but in $\mathcal{P}(k_1, t)$. Damping is very strong now and wipes away structures starting already at large scales. These examples illustrate that we cannot restore the balance between the attractive force due to the interaction between particle-pairs and the damping term in a simple, heuristic manner.

5.6 Discussion of results

The results can be interpreted in different ways. The question is how well we trust results obtained either from the perturbative ansatz or with the Born approximation. The perturbative ansatz is a very straightforward way to include particle interactions. There is no need for a sophisticated averaging process. Once the inertial trajectories are defined perturbations with respect to these trajectories are performed in orders of the interaction potential. If we believe that the results from the perturbative approach are wrong, then we would expect significant deviations from the first-order approximation for higher order corrections. This would mean that the series would not simply converge. The convergence of the expansion series has not been checked so far.
But even if the series is in fact convergent, there might be another problem with choosing the inertial trajectories: The inertial trajectories which we perturb by means of the interaction potential are the so-called Zel'dovich trajectories or, to be more precise, the *improved* Zel'dovich trajectories. The Zel'dovich approximation is of the form

$$\mathbf{x} = \mathbf{x}^{(\mathrm{i})} + D_+(a)\,\mathbf{u}\,, \tag{5.20}$$

where $\mathbf{x}$ and $\mathbf{x}^{(\mathrm{i})}$ are the final and initial particle coordinates, respectively, $\mathbf{u}$ is the initial velocity field, and $D_+(a)$ is the linear growth factor and in this case a preferred time coordinate. At first glance, nothing seems to speak against using the same Zel'dovich trajectories for all interaction potentials since $D_+(a)$ plays the role of a time coordinate. It is however unclear if this approximation is truly valid for any interaction potential or if it is a good approximation for the Newtonian gravitational potential only, where the growth factor is indeed scale independent and only a function of the scale factor (or time). If this should indeed be the case, then the so produced error is much more pronounced in the interaction term of the Born approximation, where interactions are included in the exponential. This would imply that we cannot fully trust our results from the perturbative ansatz, but the results from the Born approach might be even

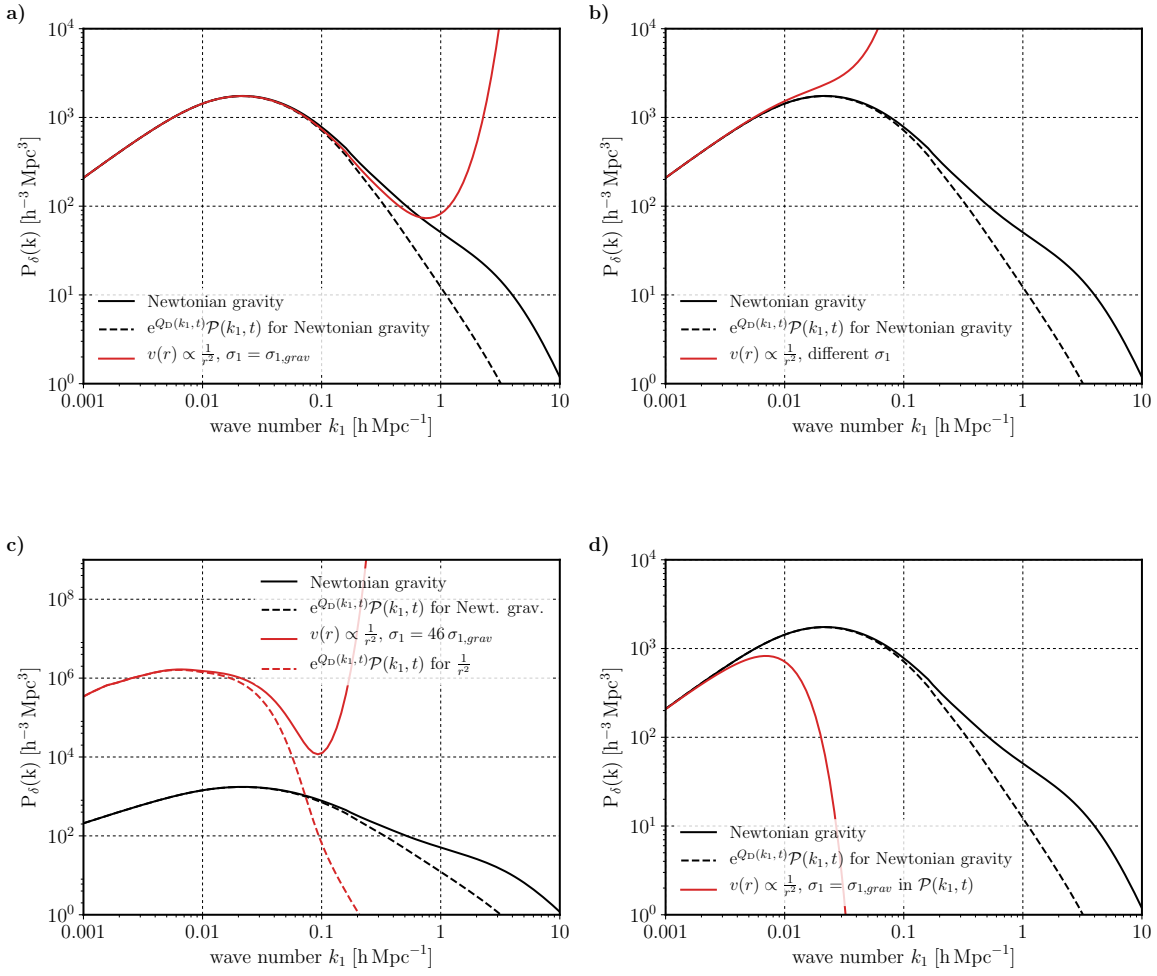

Figure 5.9.: We show (5.12) for a $\frac{1}{r^2}$-potential for four different cases. **a)** We leave all amplitudes at the same value as for Newtonian gravity. **b)** We have adjusted the amplitudes in the interaction term $\langle \bar{F}(k_1, t) \rangle$, but have left them at the same value as for Newtonian gravity in the term $e^{Q_D(k_1,t)}\mathcal{P}(k_1,t)$. **c)** We have adjusted the amplitudes in (5.12) according to the normalisation criterion described in section 3.4.2 for the growth of large scale structures. **d)** We have adjusted the amplitudes everywhere but in $\mathcal{P}(k_1,t)$.

farther away from reality.

But what does this mean for the density profiles of dark matter halos?
At this point we can neither confirm nor exclude that the non-linear density-fluctuation power spectrum is consistent with an NFW profile on scales $k \geq 1\,h\,\mathrm{Mpc}^{-1}$ in the scope of the Born approximation. In the Born approximation, we cannot identify the term that directly corresponds to the one-halo term of the halo model. The non-linear power spectrum in the Born approximation gives us a mixture between the one- and the two-halo terms. Since we expect the mass function $n(m)$ to also change with the potential slope and the halo-terms are convolutions of the mass function with the halo density profile, the non-linear power spectra may well be consistent with the NFW profile. To prove this, it would suffice to obtain the correct mass function for each interaction potential, which does not rely on the spherical collapse model. It can be easily shown that the virial radius, which is needed in order to set up the spherical collapse model, is ill-defined for potentials steeper than $\frac{1}{r^2}$. It is also not clear how to define collapsed structures in the spherical collapse model, since collapse becomes scale-dependent instead of the uniform collapse found for Newtonian gravity.

5.7 Conclusions

The formation of large-scale dark matter structures in our KFT formulation as well as in numerical simulations is governed by only a few physical properties. These are the interaction potential between dark matter particles, the equations of motion governing particles trajectories, the underlying cosmology, i.e. the expansion history of the background universe, and initial density and momentum correlations set, as is most commonly believed, by quantum fluctuations during inflation. It appears that in observations as well as numerical simulations, these physical properties governing large-scale structure formation or their interplay lead to a particular shape of the density profile for dark matter halos that is valid for halos on all scales from dwarf galaxies to massive galaxy clusters.
In [9], the authors have investigated the effects of full initial momentum correlations on the non-linear density-fluctuation power spectrum. We have found that taking into account initial momentum correlations leads to a characteristic deformation of the non-linear power spectrum on scales of the order of $k \approx 0.3\,h\,\mathrm{Mpc}^{-1}$ but not at the larger k that are relevant for the formation of dark matter halos. Furthermore, it can be shown that the full initial density correlations play a role for the shape of the

density-fluctuation power spectrum at early times but can be neglected for late times when $a = 1$.
In this work, we have explored the effects of the particle interaction potential on the small-scale behaviour of the cosmic density-fluctuation power spectrum. We have shown that the purely non-linear fraction of the power spectrum obtained in a perturbative ansatz with KFT is consistent with the one-halo term of the halo model explicitly containing the universal NFW halo-density profile for any interaction potential. We treat these results with caution, since we could not reproduce them using the Born approximation to evaluate particle trajectories. We believe that the perturbative ansatz becomes increasingly incorrect for increasingly steep interaction potentials, because most power is accumulated on increasingly small scales. We have also shown that using the closed expression (5.12) with other interaction potentials than Newtonian gravity yields un-plausible results, because the balance between interaction and damping seems to be broken. This may be due to an increasing deviation of the real particle trajectories for non-Newtonian gravity from Zel'dovich trajectories which are set up for Newtonian gravity in the first place.
With this, we cannot conclusively answer the question as to whether the form of the Newtonian interaction potential or the initial conditions determine the particular form of the density profile or its universal behaviour.

So far our analysis assumes Hamiltonian equations of motion and a ΛCDM cosmological model. While we do not see any justification to vary the first assumption, changing the expansion history may be a worthwhile task. This could give better insights into how the expansion history affects structure formation and which scales are sensitive to this.

Part III.

Classical many-body systems

6

Theoretical background on Rydberg systems

6.1 Rydberg atoms

6.1.1 Interaction between Rydberg atoms

In the past decade Rydberg atoms – atoms excited into a very high principal quantum number n – have gained increasing popularity in theoretical as well as experimental physics. Due to the large separation of the outer electron and the nucleus, Rydberg atoms have a strong dipole moment. Therefore the interaction of atoms in Rydberg states with each other even when they are separated by a microscopic distance is still strong whereas the van der Waals forces between two ground state atoms separated by a macroscopic distance would be negligible. In addition Rydberg atoms have a long lifetime of $\sim 100\,\mu s$. This makes Rydberg atoms excellent candidates for the study of interactions in many-body systems [47, 48].
The two properties of Rydberg atoms that make them such interesting systems for us are their strong interactions and the Rydberg blockade.
Two Rydberg atoms separated by a distance r that is much larger than than the sum of their radii interact via a dipole-dipole coupling. Depending on their distance the atoms will either interact through a dipole potential, if they are very close

$$v_{\mathrm{d}} = \frac{C_3}{r^3} \,, \tag{6.1}$$

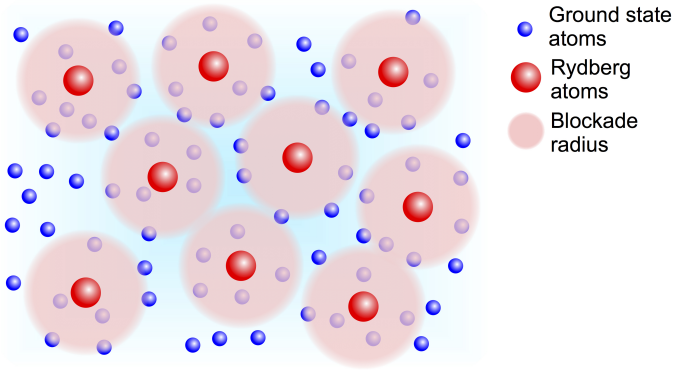

Figure 6.1.: Illustration of the Rydberg blockade in a gas. The ground state atoms (blue) are exited into Rydberg states (red). However, due to the Rydberg blockade, there is a radius R_b (6.3) around each Rydberg atom where no other ground state atom can be excited.

or a van der Waals interaction if they are farther apart

$$v_{\mathrm{vdW}} = \frac{C_6}{r^6} \,. \tag{6.2}$$

Note that the interaction potentials are repulsive.

6.1.2 Rydberg blockade

We consider two atoms separated by a distance r. Individually, each atom is a two-level system with a ground state $|g\rangle$ and a Rydberg state $|r\rangle$. The two states are separated by an energy E. The two-atom system can be in one of the following four states: both atoms are in the ground state denoted by $|gg\rangle$, one of the atoms is in the Rydberg state and the other is in the ground state denoted by $|rg\rangle$ or $|gr\rangle$, both atoms are in the Rydberg state denoted by $|rr\rangle$. Assuming that the separation between the two atoms is large, they are in the van der Waals regime and the energy of the state $|rr\rangle$ is shifted by an amount ΔE_{vdW}. All other states are essentially unshifted, since the atoms only interact strongly when they are both in the Rydberg state. Consequently, a laser tuned on resonance with the excitation of one atom is not resonant with the excitation of the second atom, given that the linewidth of the excitation is smaller than ΔE_{vdW}. Thus, the excitation of one atom prevents the excitation of the second one. This is called the "Rydberg blockade" and is illustrated in Fig. 6.1.
This blockade is confined to a radius R_b which is set by the bandwidth of the excitation.

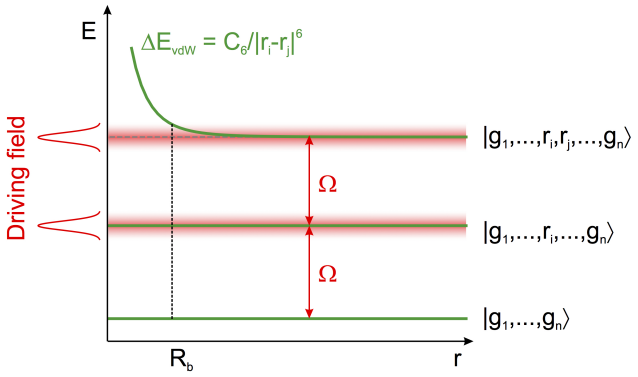

Figure 6.2.: Illustration of energy shift due to the Rydberg blockade. A laser tuned on resonance with the excitation of one atom is not resonant with the excitation of the second atom inside the Rydberg blockade radius, given that the linewidth of the excitation is smaller than ΔE_{vdW}. When in the Rydberg blockade regime, the system undergoes Rabi oscillations between the collective states $|gg...g\rangle$ and $|\psi\rangle$ at a frequency $\sqrt{N}\Omega$ with the single-atom Rabi frequency Ω characterizing the coupling between the ground and Rydberg state of a single atom.

This means, that atoms inside the blockade radius cannot be excited due to the shift in their excitation energy, but atoms outside R_b can well be excited. In the case of the van der Waals interaction the blockade radius is given by

$$\hbar\Omega = \frac{C_6}{R_b^6} \;\Rightarrow\; R_b = \left(\frac{\hbar\Omega}{C_6}\right)^{\frac{1}{6}} , \tag{6.3}$$

with the Rabi-oscillation frequency Ω. The blockade radius is obtained by replacing the Rabi frequency Ω by the line width of the laser $\Delta\nu$.
The Rydberg blockade can be extended to the general case of N atoms which are located within a sphere given by the blockade radius R_b. The N-atom system will oscillate between the collective state $|gg...g\rangle$ and

$$|\psi\rangle = \frac{1}{\sqrt{N}} \sum_{j=1}^{N} |gg...r_j...g\rangle \tag{6.4}$$

where all atoms are in the ground state and only one of the N atoms is excited into the Rydberg state $|r\rangle$. The oscillation frequency is $\sqrt{N}\Omega$ with the Rabi-frequency of a single atom Ω. This behaviour confirms that the N atoms are not independent of each other but form a coupled many-body system.

6.2 Rydberg systems and KFT

The kinetic field theory we have introduced in section 3 can in principle be applied to any classical many-body system. Strictly speaking, a system of Rydberg atoms has to be treated in the scope of quantum mechanics. We, however, will treat Rydberg atoms as classical particles. This is possible because, first of all, we do not describe the excitation of atoms into Rydberg states. In our description, the Rydberg atoms are already in existence and we simply describe their (classical) trajectories. Secondly, we neglect all quantum effects, since we are interested in the classical evolution of the system. Being able to distinguish between quantum and classical correlations in strongly-correlated many-body systems is a central task in this field and may help to understand the nature of correlations due to quantum-mechanical effects.
Rydberg systems are especially suitable for our purposes because of the Rydberg blockade which provides a natural means to set up a correlation function. In case of the Rydberg blockade we have an anti-correlation within the Rydberg-blockade radius R_b, because no two Rydberg atoms can be excited closer together than $2\,R_b$. We will thus apply our KFT to study the dynamics of many-body Rydberg systems. To do so, we will shortly describe how the initial conditions and propagation of particles need to be set up.

6.2.1 Initial conditions

To set up the initial correlation function we imagine the following scenario: N ground-state atoms with a high packing fraction are simultaneously excited into the Rydberg state. Due to the Rydberg blockade no two Rydberg atoms are closer than $2\,R_b$. With this picture in mind, we can well approximate the Rydberg atoms as hard spheres. We assume that the excitation is a Gaussian random process. This, however, is a simplifying assumption. In reality, gaussianity is broken precisely because of the Rydberg blockade effect due to a strong interaction between the atoms. It stands to reason that, although, gaussianity is broken on very small scales around each Rydberg atom, it is again restored on scales outside of the Rydberg blockade, where interactions between atoms are negligible and atoms are excited at random. Since we formulate our initial conditions at the scales of the Rydberg blockade radius and the volume of the Rydberg blockade is very small compared to the scales we are interested in, we can safely assume the excitation to be a Gaussian random process. Thus, the initial distribution of Rydberg atoms will be given by a multivariate Gaussian with a correlation matrix determined by anti-correlations due to the Rydberg blockade. The initial correlations

can thus be formulated just as in section 3.3.1.

We will consider systems of N Rydberg atoms where the particle positions are initially correlated due to the Rydberg blockade. There will, however, be no correlation of momenta for different particles. We will merely have a momentum dispersion due to a physical temperature that will be set externally. We will also assume, as in the cosmological case, that averaged over sufficiently large scales the system is homogeneous and isotropic.

6.2.2 Propagator

Since we are treating Rydberg atoms as classical particles, their trajectories will be subject to Hamilton's equations of motion. However, we will no longer be able to capture as much of the non-linear structure with a simple perturbative approach to first order or the Born approximation as in our cosmological application. The reason for this is that we will no longer be able to use the Zel'dovich trajectories as our inertial trajectories. As described in 4.4.2, the Zel'dovich trajectories capture part of the effect of the Newtonian interaction potential on particle trajectories and which consequently take us already quite far into the non-linear regime.
Thus, if we simply use the Hamiltonian equations of motion to determine the free motion of particles and set up a perturbation series in the interaction potential which we truncate at low order, we will end up with small corrections to the free evolution of particles which might not even be enough to capture the full linear evolution of the structures.
Since we are considering correlations in particle positions only, it can be shown explicitly that to first order in perturbation theory we will not be able to capture non-linear effects due to the homogeneity of the system. It has been shown in [49] that for a two-point correlations function to first order in the particle interactions, all appearing terms are linear in the initial power spectrum. During its evolution non-linear structures will, of course, be built up, but can thus not be captured by the first order perturbation theory [50].
At the same time, we know that in the scope of a simple perturbative ansatz as used in [1] we will not get the full linear evolution of structures either. Instead, we will employ a resummation scheme developed in [51] [paper in preparation]. This allows us to include all terms linear in the interaction potential already at the lowest order in this resummed perturbative approach. In this way, we will at least be able to account for all linear effects. The first results were presented in [52].

7

Structure formation in a Rydberg gas

7.1 Density-fluctuation power spectrum

As explained in the previous chapter, we employ the resummation scheme introduced in [51] to compute the density-fluctuation power spectrum with linear effects. The resummation scheme is built upon replacing the microscopic by macroscopic fields and reformulating the path integral in terms of those macroscopic fields. This allows to set up a new perturbative approach to KFT following the standard procedure in quantum and statistical field theory, i. e. in terms of propagators and vertices. Since the development of this scheme is the subject of [51], we mill merely briefly review the procedure and give the result.

7.1.1 Resummed propagator

Macroscopic fields $\psi \coloneqq (\rho, \beta)$ are introduced, with the auxiliary field β being conjugate to the number density ρ in the same way as χ_a to φ_a in (3.8). The partition function can then be reformulated in terms of the macroscopic fields. The macroscopic generating functional Z_ψ can be defined by introducing a source field $M = \big(M_\rho, M_\beta\big)$ conjugate to ψ into the partition function,

$$Z_\psi[M] \coloneqq \int \mathcal{D}\psi \; \mathrm{e}^{\mathrm{i}S_\psi[\psi]+\mathrm{i}M\cdot\psi} \,, \tag{7.1}$$

with the macroscopic action that contains the inverse macroscopic propagator Δ^{-1} and the macroscopic $(n_\beta + n_\rho)$-point vertices $\mathcal{V}_{\beta\cdots\beta\rho\cdots\rho}$.

Within this approach, the interacting 2-point density cumulant $G_{\rho\rho}$, for example, is again obtained analogously to the microscopic formulation via

$$G_{\rho\rho}(1,2) = \frac{\delta}{\mathrm{i}\delta M_\rho(1)} \frac{\delta}{\mathrm{i}\delta M_\rho(2)} \ln Z_\psi[M]\Big|_{M=0} \tag{7.2}$$

$$= \Delta_{\rho\rho}(1,2) + \text{terms involving vertices}\,. \tag{7.3}$$

The inverse macroscopic propagator Δ^{-1} can be identified as

$$\Delta^{-1}(1,2) = \begin{pmatrix} (\Delta^{-1})_{\rho\rho} & (\Delta^{-1})_{\rho\beta} \\ (\Delta^{-1})_{\beta\rho} & (\Delta^{-1})_{\beta\beta} \end{pmatrix}(1,2) \tag{7.4}$$

$$= \begin{pmatrix} \sigma_{\rho B}\cdot G^{(0)}_{BB}\cdot\sigma_{B\rho} & \mathrm{i}\mathcal{I} + \sigma_{\rho B}\cdot G^{(0)}_{B\rho} \\ \mathrm{i}\mathcal{I} + G^{(0)}_{\rho B}\cdot\sigma_{B\rho} & G^{(0)}_{\rho\rho} \end{pmatrix}(1,2)\,, \tag{7.5}$$

where $\mathcal{I}$ denotes the unit 2-point function,

$$\mathcal{I}(1,2) \coloneqq (2\pi)^3\,\delta_\mathrm{D}\big(\vec{k}_1+\vec{k}_2\big)\;\delta_\mathrm{D}(t_1-t_2)\,. \tag{7.6}$$

It is also possible to give an expression for the vertices $\mathcal{V}_{\beta\cdots\beta\rho\cdots\rho}$, but we will omit it here, as we are interested in the tree-level propagator only.
The propagator Δ is obtained by a combined matrix and functional inversion of Δ^{-1}, defined via the matrix integral equation

$$\int \mathrm{d}\bar{1}\;\Delta(1,-\bar{1})\;\Delta^{-1}(\bar{1},2) \stackrel{!}{=} \mathcal{I}(1,2)\;\mathcal{I}_2\,, \tag{7.7}$$

with the 2×2 unit matrix $\mathcal{I}_2$. The matrix part of the inversion can be performed immediately and yields

$$\Delta(1,2) = \begin{pmatrix} \Delta_{\rho\rho} & \Delta_{\rho\beta} \\ \Delta_{\beta\rho} & \Delta_{\beta\beta} \end{pmatrix}(1,2) = \begin{pmatrix} \Delta_\mathrm{R}\cdot G^{(0)}_{\rho\rho}\cdot\Delta_\mathrm{A} & -\mathrm{i}\Delta_\mathrm{R} \\ -\mathrm{i}\Delta_\mathrm{A} & 0 \end{pmatrix}(1,2)\,. \tag{7.8}$$

The remaining functional inverses

$$\Delta_\mathrm{R}(1,2) = \Delta_\mathrm{A}(2,1) \coloneqq \Big(\mathcal{I} - \mathrm{i}G^{(0)}_{\rho B}\cdot\sigma_{B\rho}\Big)^{-1}(1,2) \tag{7.9}$$

can generally only be computed numerically.

7.1.2 Analytical result

For a static space-time, no initial momentum correlations and zero temperature, however, there is an analytical solution,

$$\Delta_\mathrm{R}(1,2) = \mathcal{I}(1,2) - (2\pi)^3\,\delta_\mathrm{D}\big(\vec{k}_1+\vec{k}_2\big)\sqrt{\frac{k_1^2\,v(k_1)\bar{\rho}}{m}}\;\sin\left(\sqrt{\frac{k_1^2\,v(k_1)\bar{\rho}}{m}}\,(t_1-t_2)\right)\,, \tag{7.10}$$

with the single particle potential v, the particle mass m and the mean number density $\bar{\rho}$. The $\rho\rho$-component of the propagator then reads

$$\Delta_{\rho\rho}(1,2) = (2\pi)^3\,\delta_{\mathrm{D}}\big(\vec{k}_1+\vec{k}_2\big)\,\bar{\rho}^2\,\cos\left(\sqrt{\frac{k_1^2\,v(k_1)\bar{\rho}}{m}}\,t_1\right)\,\cos\left(\sqrt{\frac{k_1^2\,v(k_1)\bar{\rho}}{m}}\,t_2\right)\,P_\delta^{(\mathrm{i})}(k_1)\,, \tag{7.11}$$

resulting in the density-fluctuation power spectrum

$$P_\delta(k,t) = \cos^2\left(\sqrt{\frac{k^2\,v(k)\bar{\rho}}{m}}\,t\right)\,P_\delta^{(\mathrm{i})}(k)\,. \tag{7.12}$$

The result of this resummation scheme has been applied to cosmic structure formation for dark matter and for baryonic matter. In both cases, the description has yielded plausible results. Expanding the resummation to include one-loop corrections to the propagator, [53] was able to show that the obtained power spectra for cosmic structure formation match known results from other perturbative schemes based on Eulerian perturbation theory. Due to this consistency, we can be confident that the above proposed resummation approach is a viable description of structure formation.

7.2 Numerical reference model

7.2.1 Molecular dynamics simulation

The ultimate goal of our endeavour is, of course, the comparison of structures in a system of Rydberg atoms predicted by KFT with the structures found in the experiment. However, until the theory is ready to be put to the test for real systems, we need a means to assess the quality of predictions made by KFT. We have therefore set up a simplistic molecular dynamics (MD) simulation as a reference model[1]. Unlike cosmological N-body simulations where one has to deal with the long-ranged Newtonian interaction potential, the interactions in a Rydberg gas are comparably short-ranged, i.e. van der Waals or dipole interactions. The computational cost is therefore greatly reduced.

Essentially, the simulation propagates $N = 32000$ particles in a box of volume $V = (200\,\mu\mathrm{m})^3$ with periodic boundary conditions under the influence of Hamiltonian dynamics.
The excitation of Rydberg states and the anti-correlation effect due to the Rydberg

[1] The credit goes to Martin Pauly and Robert Lilow.

blockade are realised by assigning particles to positions at random. Regions with blockade radius R_b around each already present Rydberg atom are excluded when a new particle is assigned a position. We perform several realisations of the system and then average over those to obtain statistics on the system and thus make it comparable to our KFT results.
We do not simulate the presence of ground state atoms. All particles in our simulation are Rydberg atoms. The time scales on which we observe the dynamics of the system are well within the life-time of a Rydberg state.

7.2.2 Shot noise

In [1] it was argued that shot-noise terms that arise because the density field is composed of discrete particles can be neglected for our cosmological application in the thermodynamic limit of $N \to \infty$ particles. In our MD simulation, however, we have a finite number of particles in a finite-sized box. We can therefore not simply assume that shot noise is negligible. In fact, we will see that we need to take shot noise into account during the time evolution in our KFT computations to make them comparable with the MD simulation.
We therefore have to include shot noise in the computation of the power spectrum from KFT. The analytical expression (7.12) then reads

$$P_\delta(k,t) = \cos^2\left(\sqrt{\frac{k^2\, v(k)\bar{\rho}}{m}}\, t\right)\left(\bar{\rho}^{-1} + P_\delta^{(\mathrm{i})}(k)\right) - \bar{\rho}^{-1}\,. \tag{7.13}$$

where we subtract the shot noise $\bar{\rho}^{-1}$ again after having evolved the system forward in time. The same is done in the MD simulation: after the system has evolved including shot noise, only contributions from distinct particle-pairs are included in the pair-correlation function. We subtract the shot-noise term, i.e. the one-point contribution, to obtain the two-point correlations only.

7.2.3 Initial power spectrum

The initial correlation function is set by the Rydberg blockade radius, i.e. two particles cannot be closer than $2\,R_b$ at the initial time, thus providing an anti-correlation. The Rydberg blockade around each particle can be approximated by a hard sphere. The initial correlation function is directly sampled from the MD simulations and shown in Fig. 7.1. Note that we always plot the radial distribution function (RDF) which is directly connected to the two-point correlation function $\xi(r)$,

$$\mathrm{RDF}(r) = \xi(r) + 1\,. \tag{7.14}$$

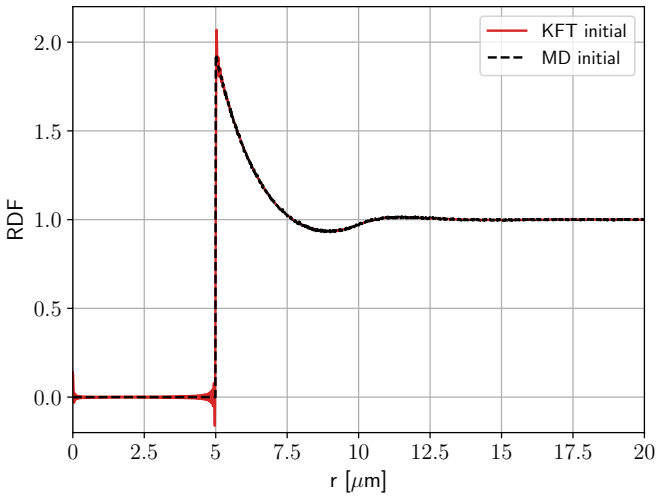

Figure 7.1.: We show the initial radial distribution function (7.14). The black (dashed) line shows the initial RDF which is sampled directly from a set of MD simulations. In red (solid) we show the same quantity that has been run through two Fourier transforms: the initial RDF from MD simulations (black dashed line) has been Fourier transformed to give the initial power spectrum used for KFT computations. The initial power spectrum was then again Fourier transformed to give the initial RDF. We show this to illustrate the stability of the Fourier transformations involved.

Thus, by construction, the RDF is a positive semi-definite function.
For our KFT computations we require the power spectrum instead of the correlation function. We therefore Fourier transform the correlation function $\xi(r)$, which is sampled from the MD simulation, to an initial power spectrum $P_\delta^{(\mathrm{i})}(k)$. We then use the formalism discussed in section 7.1.1 to compute the evolved density-fluctuation power spectrum.

7.3 Results

Before we turn to the results, let us introduce a time scale in terms of which we will present the evolution of the Rydberg system.

Parameters	free evolution	Gauss	van der Waals
Box volume V [μm^3]	$8 \cdot 10^6$	$8 \cdot 10^6$	$8 \cdot 10^6$
Particle mass m [kg]	$1.443161 \cdot 10^{-25}$	$1.443161 \cdot 10^{-25}$	$1.443161 \cdot 10^{-25}$
Particle number n	32000	32000	32000
Rydberg radius R_b [μm]	5	5	5
Potential amplitude [J]	$A = 0.0$	$A = 1.47585 \cdot 10^{-26}$	$C_6 = 5 \cdot 10^{-58}$
Potential width/ smoothing [μm]	0.0	$\sigma = \{0.5, 5, 10\}$	$\varepsilon = 5$

Table 7.1.: Overview of the parameter values used for the MD simulations and the KFT computations.

With the mean particle distance

$$\bar{d} = \left(\frac{V}{n}\right)^{\frac{1}{3}} \tag{7.15}$$

where V is the volume of the system and n the number of particles, and the thermal velocity

$$v_{\text{th}} = \sqrt{\frac{k_{\text{B}}\, T}{m}} \tag{7.16}$$

with temperature T, particle mass m and Boltzmann constant k_{B}, we define a collision time-scale

$$t_c = \frac{\bar{d}}{v_{\text{th}}}\,. \tag{7.17}$$

The collision time-scale t_c contains information on the average number of particle encounters and can give an estimate on how strongly particles interact with each other. If the collision time-scale is short, a particle will interact strongly with many other particles and we can thus expect, that non-linear effects will become important for the evolution of structure and thus the actual trajectories of particles will deviate strongly from their inertial trajectories.
For our parameters (see table 7.1) the collision time-scale is $t_c \approx 64\,\mu s$.

7.3.1 Free evolution

As a first test we compare the free evolution, i.e. no interaction potential between particles, of the system. The result is shown in Fig. 7.2 for parameters given in table 7.1. We show the result in terms of the RDF for both the MD simulation and the

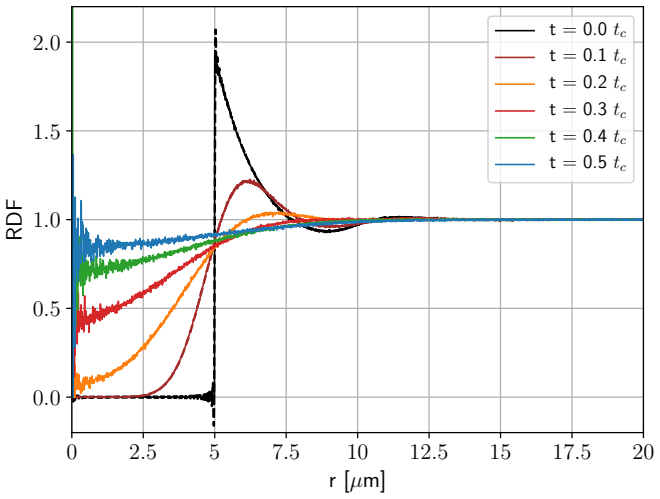

Figure 7.2.: We show the comparison between predictions from KFT (**dashed**) and MD simulations (**solid**) for the free evolution, i.e. no interaction potential between particles, of a system of initially anti-correlated Rydberg atoms. The parameters we used are summarised in table 7.1.

KFT computation. The RDF can be directly sampled from the MD simulation, but for KFT, we need to Fourier transform the evolved density-fluctuation power spectrum first to obtain the RDF.
We see very good agreement between the predictions from simulations and KFT for the free evolution of particles on all scales. The interpretation is simple: The initial structures due to the Rydberg blockade are gradually washed out by thermal motion.

7.3.2 Evolution with Gaussian potential

To quantify the influence of the interaction potential on the evolution of structure in the Rydberg gas, we found it useful to start with a repulsive Gaussian interaction potential of the form

$$v_{\mathrm{G}}(r) = A\,\mathrm{e}^{-\frac{r^2}{2\,\sigma^2}}\ , \tag{7.18}$$

with the Fourier transform

$$\tilde{v}_{\mathrm{G}}(k) = A\,(2\,\pi\sigma^2)^{\frac{3}{2}}\mathrm{e}^{-\frac{k^2}{2\,\sigma^2}}\ . \tag{7.19}$$

With the width of the Gaussian σ we can easily control the range of the interaction potential.

The results are shown in Fig. 7.3 where we have kept the interaction amplitude constant at $A = 1.47585 \cdot 10^{-26}\,\mathrm{J}$ while varying the potential width σ (see table 7.1). We show three cases in 7.3: in the first row the potential width has been set to the same value as the Rydberg blockade radius $\sigma = R_b$, in the second row we chose $\sigma = 0.1\,R_b$ and in the third row $\sigma = 2\,R_b$.

Comparing the left and right columns of Fig. 7.3, we see that shot noise is indeed relevant for this system. Including shot noise brings the KFT predictions very close to the simulation results. However, we also observe, that when we do include shot noise in our KFT calculations we get negative values for the RDF at small radii. By definition, this should never happen. We have not been able to identify the source of this issue yet. It might be due to an error when including the shot noise or it might be an artefact from the Fourier transformation of the initial RDF to an initial power spectrum. Although, we have not been able to find such an error. We will thus ignore the un-physical occurrence of negative values of the RDF in KFT and focus on the comparison of the KFT and MD results on scales where the RDF behaves properly.
For all three values of σ we see that structures are wiped out due to thermal damping and that during the evolution of particle trajectories the particles cross the Rydberg blockade radius. We also show the evolution due to the interaction potential only in Fig. 7.4, where we have switched off thermal motion by setting the temperature to zero. The left column shows the results for KFT and the right for the MD simulation. We again set σ to three different values as in Fig. 7.3. In the KFT panels we see that either no evolution is visible ($\sigma = 10\,\mu$m) or the behaviour becomes un-physical ($\sigma = 5\,\mu$m and $\sigma = 0.5\,\mu$m). For the MD simulation, on the other hand, we observe perfectly plausible behaviour in all three cases: For the smallest potential width $\sigma = 0.5\,\mu$m particles do not feel each other's interaction potential and there is no evolution. For a wider potential with $\sigma = 5\,\mu$m we see that particles feel each other's repulsive potentials and thus drift apart. The same can be seen for $\sigma = 10\,\mu$m, although, we would expect the drift to be stronger as the potential is wider. However, as a common procedure for MD simulations, we have introduced a potential cut-off so that the calculations of the forces between particles can be accomplished in a reasonable amount of time. The cut-off must be chosen to be much smaller than the box size we consider. This criterion is, however, poorly fulfilled for $\sigma = 10\,\mu$m. Since it is so wide-ranged, the cut-off radius is about one fifth of the box size. Thus, we believe we do not capture the full effect of the potential interaction. It may also be, that due to the wide range of the interaction potential the particles do not feel a strong force, because the forces from different particles average out due to the overlap of interaction potentials.

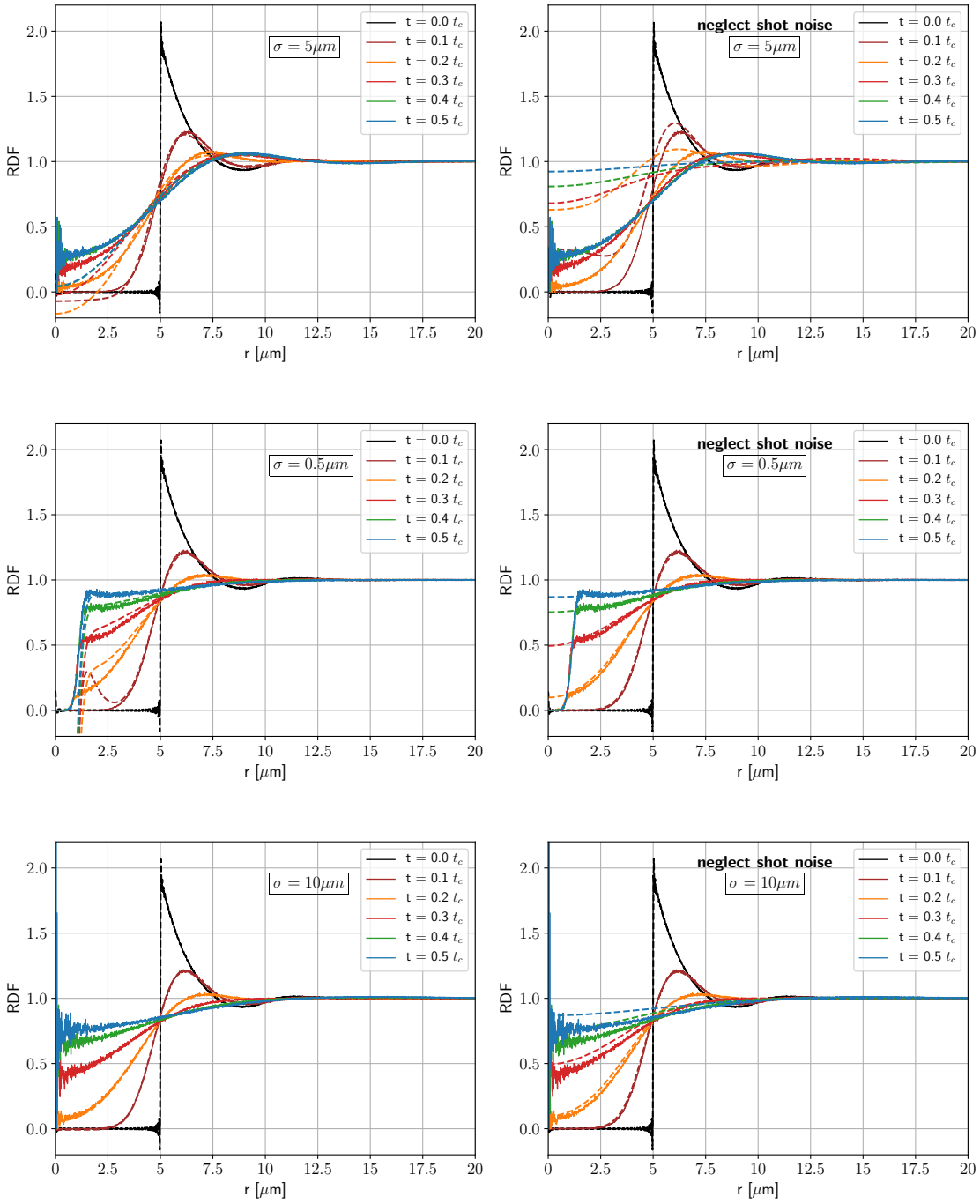

Figure 7.3.: Comparison between predictions from KFT (**dashed**) and MD simulations (**solid**) for the evolution of a system of initially anti-correlated Rydberg atoms with a Gaussian particle interaction potential (7.18) at $T = 100\,\mu$K for three different values of the potential width σ. *Left:* Shot noise effects are included in the KFT description. *Right:* Shot noise effects are neglected in the KFT description. For parameters used see table 7.1.

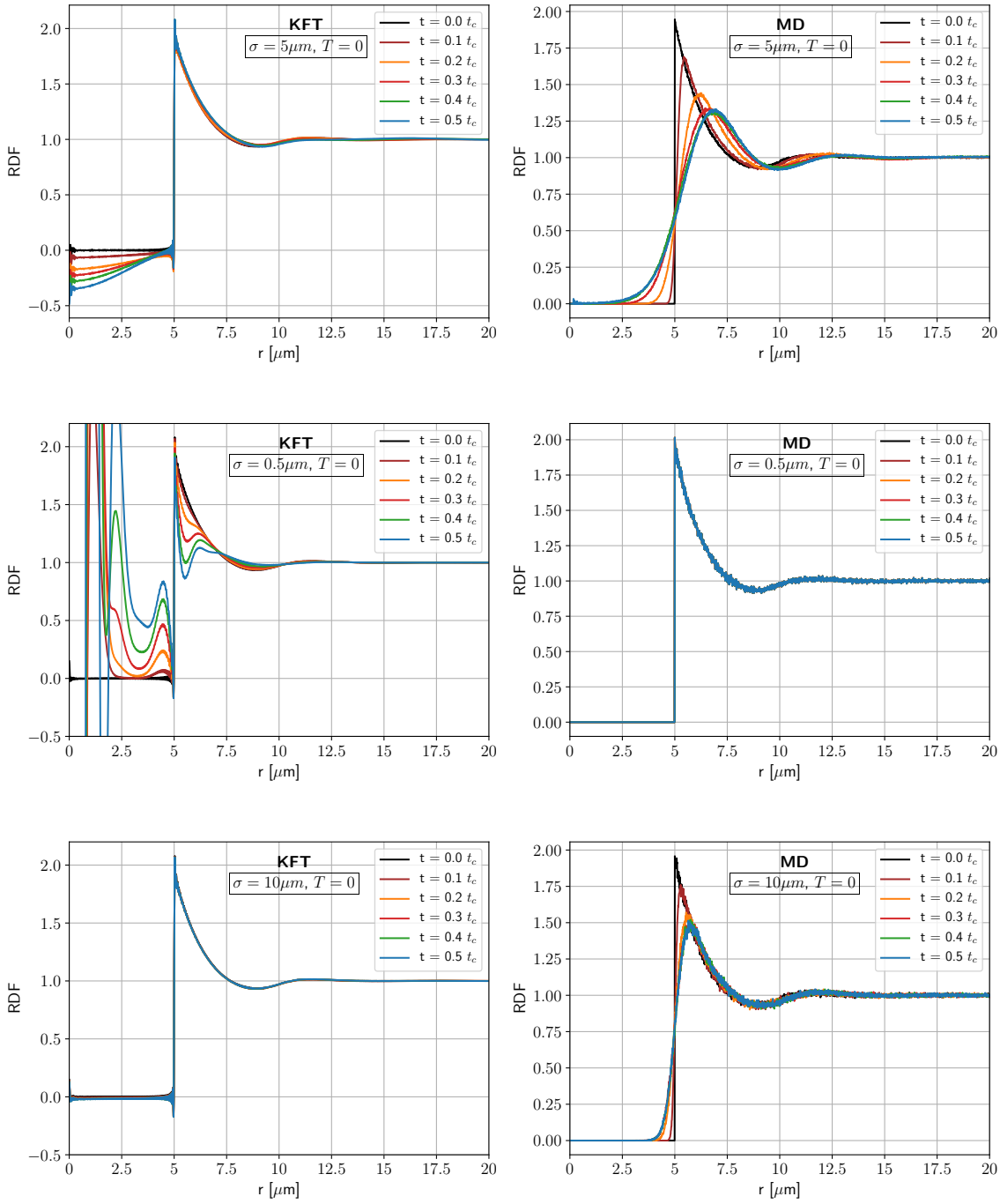

Figure 7.4.: Comparison between predictions from KFT (**left column**) and MD simulations (**right column**) for the evolution of a system of initially anti-correlated Rydberg atoms with a Gaussian particle interaction potential (7.18) at $T = 0\,\mu$K for three different values of the potential width σ. For parameters used see table 7.1.

If we compare the evolution in Fig. 7.4 to the evolution in Fig. 7.3, we see that thermal effects dominate in all cases. For $\sigma = 0.5\,\mu$m we see that the particles undergo a purely thermal evolution at first, and then encounter the steep potential barrier at radius $r \approx 0.5\,\mu$m. However, their kinetic energy is insufficient to cross it.
It is, therefore, due to the dominant effect of thermal motion even at small temperatures of $T = 100\,\mu$K, that we still see good agreement between the KFT and MD predictions, although the results for a purely interacting system without temperature do not match at all. This suggests to study the behaviour in the limit of $T \to 0$, but keeping the temperature finite.

7.3.3 Evolution with van der Waals potential

In the last step of our analysis we equip the particles with a van der Waals interaction potential of the form

$$v_{\mathrm{W}}(r) = \frac{C_6}{\sqrt{r^2 + \varepsilon^2}^6} \tag{7.20}$$

where we have to introduce a smoothing scale ϵ in order to perform the Fourier transform which is given by

$$\tilde{v}_{\mathrm{W}}(k) = C_6 \frac{\pi^2}{4} \frac{(1 + k\,\varepsilon)}{\varepsilon^3} \mathrm{e}^{-k\,\varepsilon}\ . \tag{7.21}$$

Once again, the parameters for KFT and MD for this case can be read off table 7.1. Unfortunately, replacing the Gaussian interaction potential with the van der Waals potential does not remedy the issues we have seen in 7.3.2. In Fig. 7.5 we show the results for a van der Waals potential with the smoothing scale set to $\varepsilon = 5\,\mu$m which corresponds to the Rydberg blockade radius.
The RDF obtained from KFT becomes negative for small radii as before for the Gaussian potential. However, for the van der Waals potential the KFT results disagree with the MD results on scales around $r \approx 5\,\mu$m which are most interesting for us with regard to the evolution of structure. The deviation of KFT predictions from the simulation results occurs for early times already. Varying the smoothing scale, unfortunately, brings no improvement. On large scales, though, KFT and MD results agree well.

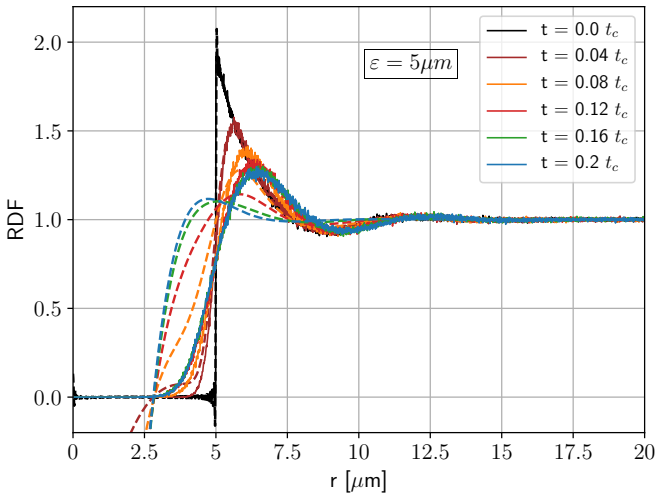

Figure 7.5.: Comparison between predictions from KFT (**dashed**) and MD simulations (**solid**) for the evolution of a system of initially anti-correlated Rydberg atoms with a van der Waals particle interaction potential (7.20) at $T = 100\,\mu$K for a smoothing scale $\varepsilon = 5\,\mu$m. For all parameters used see table 7.1.

7.4 Conclusions

We have shown how to apply the kinetic field theory formalism to non-cosmological systems. We have discussed that the best way to treat systems that lack initial momentum correlations and are initially correlated in particle positions only, is by a resummation scheme. We have then used the KFT resummation scheme proposed by [51] to compute the full linear evolution of a system of Rydberg atoms, treating them as classical particles, which are initially anti-correlated due to the Rydberg blockade. On the one hand, we have shown that the KFT predictions agree well with results from molecular dynamics simulations for a Gaussian interaction potential. It appears that even at very small temperatures, i.e. $T = 100\,\mu$K, structure evolution is dominated by thermal effects. On the other hand, we have observed that if temperature is neglected completely, i.e. $T = 0\,\mu$K, so that only the evolution due to particle interaction can play a role, KFT either shows no structure evolution or produces un-physical effects. Seeing no evolution of structures in KFT when an evolution is observed in MD simulations may indicate that these effects are purely non-linear and hence cannot be captured

by the resummed propagator at tree-level. The un-physical behaviour, like negative RDFs, that KFT produces is an issue that has yet to be resolved.
Furthermore, we have made predictions for a system with a van der Waals particle interaction potential which is a more realistic description of Rydberg gases and brings us closer to experiments. However, we observed the same issues as with a Gaussian potential. What is more, we see that KFT predictions deviate from MD results at very early times already. This may have to do with an earlier onset of non-linear effects than for a Gaussian potential. At this point, however, this is just speculation and has yet to be analysed.

8

Extension of the KFT formalism to spin systems

8.1 Motivation

The kinetic field theory formalism does not necessarily need to describe the dynamics of particles in terms of their positions and momenta. The formalism can be used to describe the dynamics of more abstract properties for any (classical) Hamiltonian system like, for example, the dynamics of classical spins. In this chapter, we will develop a toy model of initially correlated, interacting spins on a lattice and demonstrate how their many-body spin dynamics can easily be described by the KFT formalism and how to compute equal-time n-point correlation functions at some later time t.

Interacting spin systems are of fundamental relevance in the study of quantum many-body systems and thus are the subject of active research in theoretical physics as well as in experimental physics. In the last couple of years, controlled observations of non-equilibrium spin dynamics has become experimentally possible [54–56]. Large systems with long-range interactions, i.e. van der Waals interaction potentials, have been realised with Rydberg atoms [57, 58]. This development calls for adequate theoretical descriptions of such systems, but it appears that current techniques are not suitable to describe quantum dynamics of large spin systems. Current approaches using perturbative techniques as well as kinetic theories (usually based on the Langevin equation) and phase-space models are valid in near-equilibrium situations or on short time scales only [59, 60]. New numerical techniques are being developed to overcome

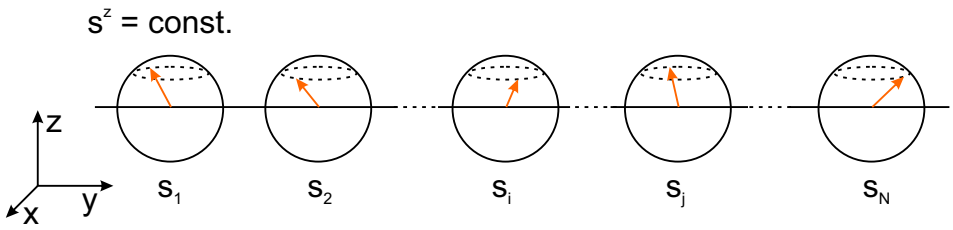

Figure 8.1.: Illustration of a $1D$ classical spin lattice. As in our later calculations s^z is the same for all spins and $\dot{s}^z = 0$. The spins are precessing in the x-y-plane.

these limitations [61].

Coming from the field of cosmology, our expertise is not in the field of correlated spin-systems and we cannot yet assess how well KFT is suited for their description or if we will be able to properly incorporate quantum effects in our approach.
In the long run, our aim is to find out if our method is suitable to give a sufficiently accurate description of correlated classical many-body spin systems such that our classical description may help to understand which effects are the result of the quantum nature of spin systems and which effects are due to classical dynamics.
The research presented in this thesis is the very first step towards this goal. In this chapter, we will present how to set up such a spin-lattice system in the scope of KFT and show simple results which are intended as a proof of concept. This research has been carried out together with Marie Teich under our direct supervision. Thus, the results discussed here can also be found in her Bachelor's Thesis [62].

8.2 Many-body spin systems in KFT

The main idea is very simple:
We consider $N \gg 1$ classical rotors, i.e. classical spins, on a (one-dimensional) lattice with sites i. The spin components of each spin at site i will be given by (s_i^x, s_i^y, s_i^z). For the description of this spin-system we return to (3.31). We name our source field $\mathbf{Q}$ to avoid confusion with the spin coupling later, and replace particle coordinates by spin components. The generating functional then reads

$$Z[\mathbf{Q}] = \int \mathrm{d}\mathbf{s}^0 P\left(\mathbf{s}^0\right) \exp\left(\mathrm{i}\int_0^\infty \mathrm{d}t' \langle \mathbf{Q}(t'), \mathbf{s}(t')\rangle\right) \tag{8.1}$$

where the trajectories of spin-components as well as the source field are bundled into the tensorial structure,

$$\vec{s}_j \coloneqq \begin{pmatrix} s_j^x \\ s_j^y \\ s_j^z \end{pmatrix} , \quad \vec{Q}_j \coloneqq \begin{pmatrix} Q_j^x \\ Q_j^y \\ Q_j^z \end{pmatrix} , \tag{8.2}$$

$$\mathbf{s} \coloneqq \vec{s}_j \otimes \vec{e}_j , \quad \mathbf{Q} \coloneqq \vec{Q}_j \otimes \vec{e}_j , \tag{8.3}$$

and a summation over the position on the lattice j is implied in $\langle \cdot, \cdot \rangle$. The initial probability distribution for correlated spin-components $P\left(\mathbf{s}^0\right)$ as well as the solution to the equations $\mathbf{s}(t')$ will have to be specified later.

Correlation functions can now be computed analogously to 3.2.2, by applying functional derivatives to (8.1) with respect to the source field $\mathbf{Q}$ and setting it to zero afterwards. We can compute correlations between the same spin-components at different lattice sites as well as correlations between different spin-components.

8.3 Hamiltonian of the spin-system

The classical Hamilton function for individual spins in the usual phase-space representation of quantum dynamics is given by

$$H = \frac{1}{2} \sum_{i \neq j} \left[\frac{J_{ij}^{\perp}}{2} \left(s_i^x s_j^x + s_i^y s_j^y \right) + J_{ij}^z s_i^z s_j^z \right] + \Omega \sum_i s_j^x , \tag{8.4}$$

with the interaction couplings

$$J_{ij}^{\perp/z} \equiv \frac{J}{|\vec{r}_{ij}|^n} , \tag{8.5}$$

where $\vec{r}_{ij}$ is the vector connecting spins on sites i and j and J denotes the amplitude. In addition to interactions between spins we could, in principle, also have an external transverse field with strength Ω.
The equations of motion for spin-components can be obtained from the Hamiltonian via

$$\dot{s}_i^{\alpha} = \{ s_i^{\alpha}, H \} = 2 \sum_{\beta} \varepsilon_{\alpha\beta\gamma} s_i^{\gamma} \frac{\partial H}{\partial s_i^{\beta}} \tag{8.6}$$

where $\{\cdot, \cdot\}$ denotes the Poisson bracket and $\varepsilon_{\alpha\beta\gamma}$ is the fully antisymmetric Levi-Civita tensor in three dimensions.
There is no exact solution for the set of equations of motion obtained from the full

Hamiltonian (8.4), but we can easily give an exact solution to the equations of motion for the Ising part of this Hamiltonian,

$$H_{\text{Ising}} = \frac{1}{2}\sum_{i,j} J^z_{ij} s^z_i s^z_j \ , \tag{8.7}$$

with $J^z_{ij} = J^z_{ji}$ and $J^z_{ii} = 0$. The equations of motion for (8.7) are given by the set of coupled differential equations

$$\begin{aligned} \dot{s}^x_i &= -2\, s^y_i \sum_j J^z_{i,j} s^z_j = -2\, s^y_i \beta^z_i \ , \\ \dot{s}^y_i &= 2\, s^x_i \sum_j J^z_{i,j} s^z_j = 2\, s^x_i \beta^z_i \ , \\ \dot{s}^z_i &= 0 \ . \end{aligned} \tag{8.8}$$

Taking the second time derivative, we can decouple the equations and write

$$\begin{aligned} \ddot{s}^x_i &= -2\, \dot{s}^y_i \beta^z_i \\ &= -4\, s^x_i \left(\beta^z_i\right)^2 \ . \end{aligned} \tag{8.9}$$

With the usual ansatz, we solve the equations of motion with suitable initial conditions. The solutions are then given by

$$\begin{aligned} s^x_i(t) &= s^{x,0}_i \cos\left(2\,\beta^z_i t\right) - s^{y,0}_i \sin\left(2\,\beta^z_i t\right) \ , \\ s^y_i(t) &= s^{x,0}_i \sin\left(2\,\beta^z_i t\right) + s^{y,0}_i \cos\left(2\,\beta^z_i t\right) \ , \\ s^z_i(t) &= s^{z,0}_i = \text{const.} \ , \end{aligned} \tag{8.10}$$

with the initial condition $s^x_i(t=0) = s^{x,0}_i$ and $s^y_i(t=0) = s^{y,0}_i$.

8.4 Initial conditions and correlation functions

We assume that the initial conditions for correlated spin-components are given by a multivariate Gaussian distribution of the form

$$P\left(\mathbf{s}^0\right) = \frac{1}{\sqrt{(2\pi)^{3N}\det C}} \exp\left(-\frac{1}{2}{\mathbf{s}^0}^\top C^{-1}\mathbf{s}^0\right) \ , \tag{8.11}$$

as we have done for all our applications so far. We further assume for simplicity, that initially the z-components of all spins are aligned. Thus, we will only be interested in the dynamics in the x-y-plane and $s^{z,0}_i \equiv s^{z,0}$ is the same at each lattice site. We can therefore neglect the integration over the initial conditions of the z-component.

In order to rid ourselves of the functional determinant in (8.11), we re-write the generating functional (8.1) in the following way

$$Z[\mathbf{Q}] = \int \mathrm{d}\mathbf{s}^0 \frac{1}{\sqrt{(2\pi)^{3N}\det C}} \exp\left(-\frac{1}{2}{\mathbf{s}^0}^\top C^{-1}\mathbf{s}^0\right) \mathrm{e}^{\mathrm{i}\langle \mathbf{s}^0, \bar{\mathbf{Q}}\rangle} \tag{8.12}$$

with

$$\bar{\mathbf{Q}} := \begin{pmatrix} \int_0^\infty \mathrm{d}t' \left[Q_i^x(t')\cos\left(2\,\beta_i^z t'\right) + Q_i^y(t')\sin\left(2\,\beta_i^z t'\right)\right] \\ \int_0^\infty \mathrm{d}t' \left[Q_i^y(t')\cos\left(2\,\beta_i^z t'\right) - Q_i^y(t')\sin\left(2\,\beta_i^z t'\right)\right] \end{pmatrix} . \tag{8.13}$$

Integrating over the initial conditions then gives the simple result

$$Z[\mathbf{Q}] = \mathrm{e}^{-\frac{1}{2}\mathbf{Q}^\top C\,\mathbf{Q}} , \tag{8.14}$$

with the correlation matrix

$$C = \begin{pmatrix} C_{s_i^x s_j^x} & C_{s_i^x s_j^y} \\ C_{s_i^y s_j^x} & C_{s_i^y s_j^y} \end{pmatrix} . \tag{8.15}$$

By taking functional derivatives, we can now compute the general expression for the 2-point correlation function from (8.14)

$$\left\langle s_i^\alpha(t) s_j^\beta(t)\right\rangle = \frac{\delta}{\delta Q_i^\alpha(t)} \frac{\delta}{\delta Q_j^\beta(t)} Z[\mathbf{Q}]\Big|_{Q=0} , \tag{8.16}$$

where the upper indices indicate spin components and the lower indices denote the lattice site. The resulting correlation functions are oscillatory. Here, we give an example of their form,

$$\begin{aligned}\left\langle s_i^x(t) s_j^y(t)\right\rangle = {} & C_{s_i^y s_j^x} \sin\left(2\,\beta_i^z t\right) \sin\left(2\,\beta_j^z t\right) + C_{s_i^x s_j^y} \sin\left(2\,\beta_i^z t\right) \cos\left(2\,\beta_j^z t\right) \\ & - C_{s_i^x s_j^x} \cos\left(2\,\beta_i^z t\right) \sin\left(2\,\beta_j^z t\right) - C_{s_i^y s_j^y} \cos\left(2\,\beta_i^z t\right) \cos\left(2\,\beta_j^z t\right) .\end{aligned} \tag{8.17}$$

The computation of the correlation function was the main subject of [62] and we will not repeat all the lengthy expressions here.

As a last step we specify the form of the initial correlation functions in the correlation matrix C. Once again, we adopt a very simple form of the correlation function: a power law. We assume

$$C_{s_i^x s_j^x} = C_{s_j^y s_i^y} = \frac{A_0}{|i-j|^\gamma} , \quad C_{s_i^y s_j^x} = C_{s_j^y s_i^x} = \frac{B_0}{|i-j|^\rho} \tag{8.18}$$

and set the auto-correlations to unity. To simplify matters further, we can assume an infinitely ranged interaction force, setting the coupling $J_{i,j}$ in (8.10) to the same

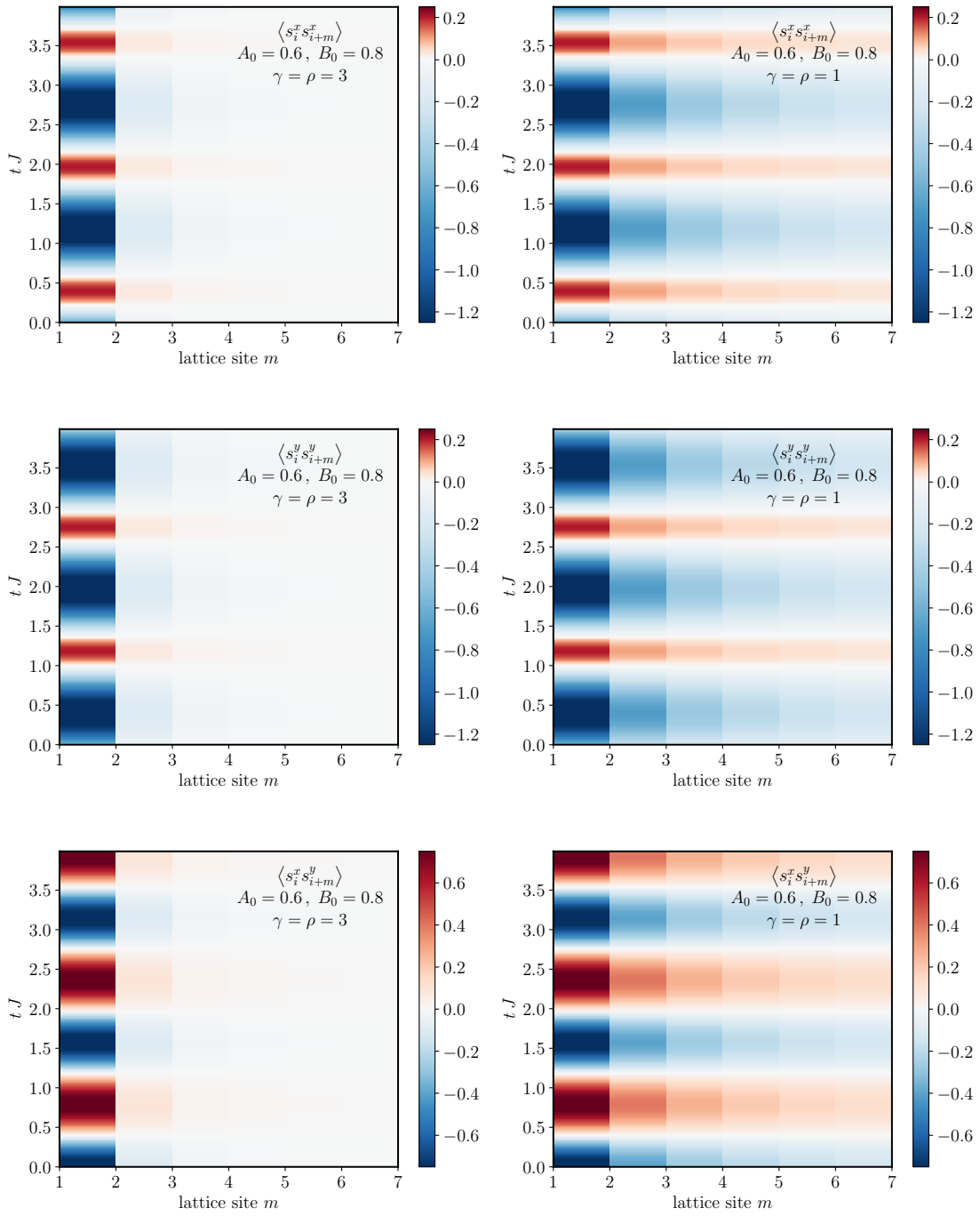

Figure 8.2.: We show the 2-point correlation functions from (8.19) of spins separated by by m lattice sites. *Left column:* The initial correlations are short ranged with powers $\gamma = \rho = 3$, quickly decaying with increasing distance. *Right column:* Here, the initial correlations are long ranged with powers $\gamma = \rho = 1$.

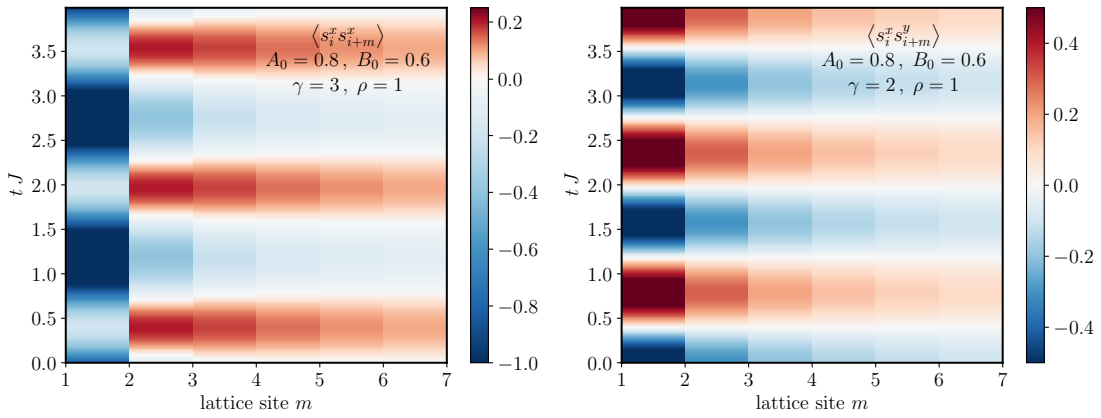

Figure 8.3.: The 2-point correlation function of the x-components (*left*) and correlations between x- and y-components (*right*) of spins separated by by m lattice sites are shown. We have chosen different powers and amplitudes for the initial correlation functions for the initial correlations of same-spin components $\langle s_i^\alpha(t) s_{i+m}^\alpha(t) \rangle$ and different-spin components $\left\langle s_i^\alpha(t) s_{i+m}^\beta(t) \right\rangle$ with $\alpha \neq \beta$. We see in the left plot that correlations are largest at lattice site $m = 2$ due to the xy-correlation and then decrease again with increasing distance.

value for all i and j. Since we have chosen the z-components to be aligned initially and therefore remain so due to $\dot{s}_z = 0$, the oscillation frequency β_j^z will be the same at every lattice site, too, which we will simply denote by β. We quote the results from [62],

$$\begin{aligned}
\langle s_i^x(t) s_{i+m}^x(t) \rangle &= -\frac{A_0}{|m|^\gamma} + 2\frac{B_0}{|m|^\rho} \cos(2\,\beta t) \sin(2\,\beta t)\ , \\
\langle s_i^y(t) s_{i+m}^y(t) \rangle &= -\frac{A_0}{|m|^\gamma} - 2\frac{B_0}{|m|^\rho} \cos(2\,\beta t) \sin(2\,\beta t)\ , \\
\langle s_i^x(t) s_{i+m}^y(t) \rangle &= \frac{B_0}{|m|^\rho} \left(2 \sin^2(2\,\beta t) - 1\right)\ . \qquad (8.19)
\end{aligned}$$

We show (8.19) in Fig. 8.2 and Fig. 8.3 for different values of the correlation amplitudes A_0, B_0 and powers γ, ρ. In Fig. 8.2 we simply see the qualitative difference between long and short range correlations. Correlations simply decay with increasing distance. In addition, we show a mix of long range correlation between different spin-components and short range correlations between same spin-components in 8.3 with different amplitudes. If we switched to short range correlation between different spin-components and long range correlations between same spin-components the picture

would look much the same. For the $\left\langle s_i^x(t) s_{i+m}^x(t) \right\rangle$ correlation in Fig. 8.3 we can observe that the second term in (8.19) representing initial x-y-component correlations becomes dominant at $m = 2$ because, compared to the x-x-correlations, it is long-ranged.
All in all, we see that correlations decay with distance, and over time a periodic behaviour of the correlations is manifest. This, of course, is no surprise for a simplistic setup like that.

8.5 Conclusions and outlook

We have illustrated in this chapter how the kinetic field theory formalism can be extended to describe the non-equilibrium dynamics of classical many-body spin-systems. Based on simplifying assumptions about initial correlations and spin interactions, we have computed the first results for such a system. The simplifications we have made have allowed us to keep computations very simple, but on the other hand have deprived us of reproducing any of the more interesting features of the correlation function.
We have chosen here the Ising-Hamiltonian not only because calculations become manageable for the KFT formalism, but also because exact analytical solutions exist for this case [63–65] which turns it into an excellent benchmark. These solutions, however, describe more complex systems than the one we have presented here. Therefore, we would like to continue to study the non-equilibrium dynamics of the Ising model while gradually extending the complexity of the system. As a next step, we propose to study how finite ranged interactions (8.5), i.e. $n \neq 0$, will affect particle correlations. We would then suggest to allow an initial distribution of the z-component of the spins instead of aligning s_i^z at all lattice points i. This would make the integration over initial conditions in (8.12) more difficult, but is well in the scope of the KFT formalism.

In the long run, however, we would like to extend the description to the full Hamiltonian 8.4. The challenge is, of course, that in this case we cannot solve the equations of motion exactly. A possible way to address this issue might be through an expansion scheme similar to the one discussed in section 3.4.2. The inertial trajectories then could be given by the Ising-trajectories (8.10) and the XY interaction in (8.4) could be understood as an additional force causing deviations from the inertial Ising-trajectories.

So far, we have been solely focusing on classical systems. Going beyond the classical description of non-equilibrium dynamics of correlated systems will require the incorporation of quantum effects, like Heisenberg's uncertainty principle, in our theory.

It is however possible that under these conditions KFT will simply morph into the truncated Wigner approximation. This remains yet to be seen.

9

Conclusions

In this chapter, we give a summary of the conclusions from the cosmological as well as from the classical laboratory many-body systems.
We have demonstrated how KFT can be adapted to describe n-point correlation functions of classical spin-systems. The results we presented are for a simple toy model so far, but can be extended to describe more realistic systems in the future. We are, however, unsure yet how far into the non-linear regime we can get for this kind of systems.
In a second application, we have shown how an initially correlated Rydberg gas can be treated in the framework of KFT. Although the Rydberg atoms and their trajectories were treated classically, the Rydberg blockade which is a feature of their quantum nature, was taken into account through initial spacial correlations in the initial conditions in our KFT approach. More work still needs to be done to resolve the issues we have encountered with badly-behaved radial distribution functions.
The power of the KFT approach, though, lies in its immense flexibility. It is therefore our long-term goal to combine particle dynamics with spin-dynamics to provide a more complete description of systems probed by experiments, since spins usually do not grow on lattices, but are a property of particles that can follow their own dynamics.

In the field of cosmology, which is far more familiar to us, we have used the KFT approach to investigate the influence of the interaction potential on structure formation on scales $k \geq 1\,h\,\mathrm{Mpc}^{-1}$. Since these are scales where contributions from the inner structures of dark matter halos to the non-linear density-fluctuation power spectrum

become dominant, we were hoping to learn about the influence of the interaction potential between particles on the density profiles of said halos. From perturbation theory with KFT it seems that the density profiles are insensitive to the shape of the interaction potential. Recent developments of the KFT approach using the Born approximation for particle trajectories, however, have shed some doubt on this finding. Instead, we have learned that a deviation from Newtonian gravity destroys the delicate balance between a damping due to momentum-diffusion and the attractive particle interaction.

We are curious to learn why this balance exists for Newtonian gravity in the first place and whether it can be restored for other power-law potentials as well. Our hope is that the resummation scheme developed for KFT [51, 53] will be able to provide insight into a consistent scheme for balancing interactions and damping.

10

Acknowledgements

Now, dropping the scientific "we", I would like to acknowledge a few people explicitly for their support during the last three years that eventually lead to this thesis.

First, I would like to thank Matthias Bartelmann for being a great boss and mentor. For allowing me to learn from him and work in the amazing environment that he has created in our group. For giving me the freedom to pursue my own ideas and for providing help when it was needed.
Second, I would like to thank Björn Malte Schäfer, who has been somewhat of a scientific "godfather" to me. For answering questions, for many discussions and for all the hoots.
I would very much like to thank Matthias Weidemüller for his guidance and advice regarding the work on Rydberg gases and spin-systems. Without this collaboration, a large part of my work would not have been possible.

I would like to thank Prof. Manfred Salmhofer for agreeing to be the referee for this thesis despite the slightly odd combination of topics of my thesis.
I would like to thank the members of my thesis committee, Professors Matthias Bartelmann, Manfred Salmhofer, Markus Oberthaler and Björn Malte Schäfer, for taking the time to examine this work.

I would also like to thank the coadvisors of my HGSFP thesis committee Prof. Matthias Weidemüller and Prof. Volker Springel.

I am especially grateful to Robert Lilow, Felix Fabis and Christian Angrick for the many discussions we had, that certainly helped advance the work done in this thesis. I especially thank Robert Lilow for helping me with my coding and the time we spent debugging.
I would also like to thank Andre Salzinger for providing a bridge between our theory and experiment and for many inspiring discussions, which among other things, led to the consideration of spin systems.
I would like to thank the, then, Bachelor students Alexander Schuckert, Martin Pauly and Marie Teich. It was a pleasure to work with them on the classical many-body systems. Many of the results would not have been possible without their hard work.

I would like to thank Carsten Littek, Celia Viermann, Robert Reischke, Sara Konrad and everyone who also worked on the KFT formalism with me, for the valuable input they provided during the past years.

During the last three years I was very lucky to be a member of the Heidelberg Graduate School for Fundamental Physics. I would like to thank the HGSFP and especially Prof. Sandra Klevansky for the generous support; especially for the opportunity and financial aid to organise the three "Schöntal Workshops".

A very personal and special thank you goes to Veit Stooß. For going with me through thick and thin.

I am incredibly grateful to my parents who have left behind everything they had, so that I could have all of this.

11

Publications

This is a list of publications the author of this thesis was involved in.

Results from the following publications were used in this thesis

Matthias Bartelmann, Felix Fabis, Daniel Berg, Elena Kozlikin, Robert Lilow, and Celia Viermann. A microscopic, non-equilibrium, statistical field theory for cosmic structure formation. New Journal of Physics, 18(4):043020, 2016.

Matthias Bartelmann, Felix Fabis, Elena Kozlikin, Robert Lilow, Johannes Dombrowski, and Julius Mildenberger. Kinetic field theory: effects of momentum correlations on the cosmic density-fluctuation power spectrum. New Journal of Physics, 19(8):083001, 2017.

M. Bartelmann, F. Fabis, S. Konrad, E. Kozlikin, R. Lilow, C. Littek, and J. Dombrowski. Analytic calculation of the non-linear cosmic density-fluctuation power spectrum in the Born approximation. ArXiv e-prints, October 2017.

F. Fabis, E. Kozlikin, R. Lilow, and M. Bartelmann. Kinetic Field Theory: Exact free evolution of Gaussian phase-space correlations. ArXiv e-prints, accepted for publication in JSTAT, October 2017.

Results from the following publications do not (directly) appear in this thesis

C. Viermann, F. Fabis, E. Kozlikin, R. Lilow, and M. Bartelmann. Nonequilibrium statistical field theory for classical particles: Basic kinetic theory. Phys. Rev. E, 91(6):062120, June 2015. doi: 10.1103/PhysRevE.91.062120.

E. Kozlikin, F. Fabis, R. Lilow, C. Viermann, and M. Bartelmann. Non-equilibrium statistical field theory for classical particles: Impact of correlated initial conditions on non-ideal gases. ArXiv e-prints, December 2014.

F. Fabis, D. Berg, E. Kozlikin, and M. Bartelmann. Non-equilibrium statistical field theory for classical particles: Initially correlated grand canonical ensembles. ArXiv e-prints, December 2014.

Bibliography

[1] Matthias Bartelmann, Felix Fabis, Daniel Berg, Elena Kozlikin, Robert Lilow, and Celia Viermann. A microscopic, non-equilibrium, statistical field theory for cosmic structure formation. *New Journal of Physics*, 18(4):043020, 2016. URL `http://stacks.iop.org/1367-2630/18/i=4/a=043020`.

[2] M.E. Peskin and D.V. Schroeder. *An Introduction to Quantum Field Theory*. Advanced book classics. Addison-Wesley Publishing Company, 1995. ISBN 9780201503975. URL `http://books.google.de/books?id=i35LALN0GosC`.

[3] P. C. Martin, E. D. Siggia, and H. A. Rose. Statistical Dynamics of Classical Systems. *Phys. Rev. A*, 8:423–437, July 1973. doi: 10.1103/PhysRevA.8.423.

[4] G. F. Mazenko. Smoluchowski dynamics and the ergodic-nonergodic transition. *Phys. Rev. E*, 83(4):041125, April 2011. doi: 10.1103/PhysRevE.83.041125.

[5] G. F. Mazenko. Fundamental theory of statistical particle dynamics. *Phys. Rev. E*, 81(6):061102, June 2010. doi: 10.1103/PhysRevE.81.061102.

[6] S. P. Das and G. F. Mazenko. Newtonian Kinetic Theory and the Ergodic-Nonergodic Transition. *Journal of Statistical Physics*, 152:159–194, July 2013. doi: 10.1007/s10955-013-0755-3.

[7] S. P. Das and G. F. Mazenko. Field Theoretic Formulation of Kinetic Theory: Basic Development. *Journal of Statistical Physics*, 149:643–675, November 2012. doi: 10.1007/s10955-012-0610-y.

[8] E. Gozzi, M. Reuter, and W. D. Thacker. Hidden brs invariance in classical mechanics. ii. *Phys. Rev. D*, 40:3363–3377, Nov 1989. doi: 10.1103/PhysRevD.40.3363. URL `https://link.aps.org/doi/10.1103/PhysRevD.40.3363`.

[9] Matthias Bartelmann, Felix Fabis, Elena Kozlikin, Robert Lilow, Johannes Dombrowski, and Julius Mildenberger. Kinetic field theory: effects of momentum correlations on the cosmic density-fluctuation power spectrum. *New Journal of Physics*, 19(8):083001, 2017. URL `http://stacks.iop.org/1367-2630/19/i=8/a=083001`.

[10] M. Bartelmann, F. Fabis, S. Konrad, E. Kozlikin, R. Lilow, C. Littek, and J. Dombrowski. Analytic calculation of the non-linear cosmic density-fluctuation power spectrum in the Born approximation. *ArXiv e-prints*, October 2017.

[11] J. F. Navarro, C. S. Frenk, and S. D. M. White. The Structure of Cold Dark Matter Halos. *Astrophysical Journal*, 462:563, May 1996. doi: 10.1086/177173.

[12] J. F. Navarro, C. S. Frenk, and S. D. M. White. A Universal Density Profile from Hierarchical Clustering. *Astrophysical Journal*, 490:493–508, December 1997. doi: 10.1086/304888.

[13] S. M. Carroll, W. H. Press, and E. L. Turner. The cosmological constant. *Annu. Rev. Astron. Astrophys.*, 30:499–542, 1992. doi: 10.1146/annurev.aa.30.090192.002435.

[14] F. Bernardeau, S. Colombi, E. Gaztañaga, and R. Scoccimarro. Large-scale structure of the Universe and cosmological perturbation theory. *Phys. Rep.*, 367:1–248, September 2002. doi: 10.1016/S0370-1573(02)00135-7.

[15] P. J. E. Peebles. *The large-scale structure of the universe*. Princeton University Press, 1980.

[16] T. Buchert. Lagrangian theory of gravitational instability of Friedman-Lemaitre cosmologies and the 'Zel'dovich approximation'. *MNRAS*, 254:729–737, February 1992.

[17] T. Buchert and J. Ehlers. Lagrangian theory of gravitational instability of Friedman-Lemaitre cosmologies – second-order approach: an improved model for non-linear clustering. *MNRAS*, 264:375–387, September 1993.

[18] T. Buchert. Lagrangian Theory of Gravitational Instability of Friedman-Lemaitre Cosmologies - a Generic Third-Order Model for Nonlinear Clustering. *MNRAS*, 267:811, April 1994.

[19] F. R. Bouchet, S. Colombi, E. Hivon, and R. Juszkiewicz. Perturbative Lagrangian approach to gravitational instability. *A&A*, 296:575, April 1995.

[20] C.-P. Ma and E. Bertschinger. Cosmological Perturbation Theory in the Synchronous and Conformal Newtonian Gauges. *Astrophysical Journal*, 455:7, December 1995. doi: 10.1086/176550.

[21] J. Ehlers and T. Buchert. Newtonian Cosmology in Lagrangian Formulation: Foundations and Perturbation Theory. *General Relativity and Gravitation*, 29: 733–764, June 1997. doi: 10.1023/A:1018885922682.

[22] U. Seljak. Analytic model for galaxy and dark matter clustering. *MNRAS*, 318: 203–213, October 2000. doi: 10.1046/j.1365-8711.2000.03715.x.

[23] P. Valageas. Dynamics of gravitational clustering. I. Building perturbative expansions. *A&A*, 379:8–20, November 2001. doi: 10.1051/0004-6361:20011309.

[24] A. Cooray and R. Sheth. Halo models of large scale structure. *Phys. Rep.*, 372: 1–129, December 2002. doi: 10.1016/S0370-1573(02)00276-4.

[25] P. Valageas. A new approach to gravitational clustering: A path-integral formalism and large-N expansions. *A&A*, 421:23–40, July 2004. doi: 10.1051/0004-6361: 20040125.

[26] P. Valageas and D. Munshi. Evolution of the cosmological density distribution function: new analytical model. *MNRAS*, 354:1146–1158, November 2004. doi: 10.1111/j.1365-2966.2004.08325.x.

[27] C.-P. Ma and E. Bertschinger. A Cosmological Kinetic Theory for the Evolution of Cold Dark Matter Halos with Substructure: Quasi-Linear Theory. *Astrophysical Journal*, 612:28–49, September 2004. doi: 10.1086/421766.

[28] F. Bernardeau and P. Valageas. Propagators in Lagrangian space. *Phys. Rev. D*, 78(8):083503, October 2008. doi: 10.1103/PhysRevD.78.083503.

[29] M. Pietroni. Flowing with time: a new approach to non-linear cosmological perturbations. *JCAP*, 10:036, October 2008. doi: 10.1088/1475-7516/2008/10/036.

[30] S. Anselmi, S. Matarrese, and M. Pietroni. Next-to-leading resummations in cosmological perturbation theory. *JCAP*, 6:015, June 2011. doi: 10.1088/1475-7516/2011/06/015.

[31] M. Pietroni, G. Mangano, N. Saviano, and M. Viel. Coarse-grained cosmological perturbation theory. *JCAP*, 1:019, January 2012. doi: 10.1088/1475-7516/2012/01/019.

[32] J. J. M. Carrasco, M. P. Hertzberg, and L. Senatore. The effective field theory of cosmological large scale structures. *Journal of High Energy Physics*, 9:82, September 2012. doi: 10.1007/JHEP09(2012)082.

[33] S. Anselmi and M. Pietroni. Nonlinear power spectrum from resummed perturbation theory: a leap beyond the BAO scale. *JCAP*, 12:013, December 2012. doi: 10.1088/1475-7516/2012/12/013.

[34] P. Valageas, T. Nishimichi, and A. Taruya. Matter power spectrum from a Lagrangian-space regularization of perturbation theory. *Phys. Rev. D*, 87(8): 083522, April 2013. doi: 10.1103/PhysRevD.87.083522.

[35] R. A. Porto, L. Senatore, and M. Zaldarriaga. The Lagrangian-space Effective Field Theory of large scale structures. *JCAP*, 5:022, May 2014. doi: 10.1088/1475-7516/2014/05/022.

[36] J. J. M. Carrasco, S. Foreman, D. Green, and L. Senatore. The Effective Field Theory of Large Scale Structures at two loops. *JCAP*, 7:057, July 2014. doi: 10.1088/1475-7516/2014/07/057.

[37] Asantha Cooray and Ravi Sheth. Halo models of large scale structure. *Physics Reports*, 372(1):1 – 129, 2002. ISSN 0370-1573. doi: https://doi.org/10.1016/S0370-1573(02)00276-4. URL `http://www.sciencedirect.com/science/article/pii/S0370157302002764`.

[38] W. H. Press and P. Schechter. Formation of Galaxies and Clusters of Galaxies by Self-Similar Gravitational Condensation. *Astrophysical Journal*, 187:425–438, February 1974. doi: 10.1086/152650.

[39] Carlo Giocoli, Matthias Bartelmann, Ravi K. Sheth, and Marcello Cacciato. Halo model description of the non-linear dark matter power spectrum at $k \gg 1$ Mpc^{-1}. *Mon. Not. Roy. Astron. Soc.*, 408:300, 2010. doi: 10.1111/j.1365-2966.2010.17108.x.

[40] K. Heitmann, M. White, C. Wagner, S. Habib, and D. Higdon. The Coyote Universe. I. Precision Determination of the Nonlinear Matter Power Spectrum. *Astrophysical Journal*, 715:104–121, May 2010. doi: 10.1088/0004-637X/715/1/104.

[41] K. Heitmann, D. Higdon, M. White, S. Habib, B. J. Williams, E. Lawrence, and C. Wagner. The Coyote Universe. II. Cosmological Models and Precision Emulation of the Nonlinear Matter Power Spectrum. *Astrophysical Journal*, 705: 156–174, November 2009. doi: 10.1088/0004-637X/705/1/156.

[42] E. Lawrence, K. Heitmann, M. White, D. Higdon, C. Wagner, S. Habib, and B. Williams. The Coyote Universe. III. Simulation Suite and Precision Emulator for the Nonlinear Matter Power Spectrum. *Astrophysical Journal*, 713:1322–1331, April 2010. doi: 10.1088/0004-637X/713/2/1322.

[43] K. Heitmann, E. Lawrence, J. Kwan, S. Habib, and D. Higdon. The Coyote Universe Extended: Precision Emulation of the Matter Power Spectrum. *Astrophysical Journal*, 780:111, January 2014. doi: 10.1088/0004-637X/780/1/111.

[44] J. M. Comerford and P. Natarajan. The observed concentration-mass relation for galaxy clusters. *MNRAS*, 379:190–200, July 2007. doi: 10.1111/j.1365-2966.2007.11934.x.

[45] Shinji Sato, Fumie Akimoto, Akihiro Furuzawa, Yuzuru Tawara, Manabu Watanabe, and Yasuki Kumai. The observed mass profiles of dark halos and the formation epoch of galaxies. *The Astrophysical Journal Letters*, 537(2):L73, 2000. URL `http://stacks.iop.org/1538-4357/537/i=2/a=L73`.

[46] J. Merten, M. Meneghetti, M. Postman, K. Umetsu, A. Zitrin, E. Medezinski, M. Nonino, A. Koekemoer, P. Melchior, D. Gruen, L. A. Moustakas, M. Bartelmann, O. Host, M. Donahue, D. Coe, A. Molino, S. Jouvel, A. Monna, S. Seitz, N. Czakon, D. Lemze, J. Sayers, I. Balestra, P. Rosati, N. Benítez, A. Biviano, R. Bouwens, L. Bradley, T. Broadhurst, M. Carrasco, H. Ford, C. Grillo, L. Infante, D. Kelson, O. Lahav, R. Massey, J. Moustakas, E. Rasia, J. Rhodes, J. Vega, and W. Zheng. CLASH: The Concentration-Mass Relation of Galaxy Clusters. *Astrophysical Journal*, 806:4, June 2015. doi: 10.1088/0004-637X/806/1/4.

[47] Matthias Weidemüller. There can be only one. *Nature Physics*, 5:91 EP –, 02 2009. URL `http://dx.doi.org/10.1038/nphys1193`.

[48] Antoine Browaeys and Thierry Lahaye. *Interacting Cold Rydberg Atoms: A Toy Many-Body System*. Progress in Mathematical Physics. 04 2016. ISBN 978-3-319-14315-6.

[49] Alexander Schuckert. Collective dynamics of correlated rydberg atoms in non-equilibrium statistical field theory for classical particles. Bachelor thesis, Ruperto-Carola University of Heidelberg, 2015.

[50] F. Fabis, E. Kozlikin, R. Lilow, and M. Bartelmann. Kinetic Field Theory: Exact free evolution of Gaussian phase-space correlations. *ArXiv e-prints, accepted for publication in JSTAT*, October 2017.

[51] Robert Lilow. Developing a macroscopic reformulation of statistical field theory for classical particles to investigate cosmic structure formation. Master thesis, Ruperto-Carola University of Heidelberg, 2015.

[52] Martin Pauly. Dynamics of correlations in rydberg atoms in a statistical field theory for classical particles. Bachelor thesis, Ruperto-Carola University of Heidelberg, 2015.

[53] *PhD Thesis*. PhD thesis, Ruperto-Carola University of Heidelberg, 2018. In preparation.

[54] Immanuel Bloch, Jean Dalibard, and Sylvain Nascimbène. Quantum simulations with ultracold quantum gases. *Nature Physics*, 8:267 EP –, 04 2012. URL `http://dx.doi.org/10.1038/nphys2259`.

[55] R. Blatt and C. F. Roos. Quantum simulations with trapped ions. *Nature Physics*, 8:277 EP –, 04 2012. URL `http://dx.doi.org/10.1038/nphys2252`.

[56] Alán Aspuru-Guzik and Philip Walther. Photonic quantum simulators. *Nature Physics*, 8:285 EP –, 04 2012. URL `http://dx.doi.org/10.1038/nphys2253`.

[57] Robert Löw, Hendrik Weimer, Johannes Nipper, Jonathan B Balewski, Björn Butscher, Hans Peter Büchler, and Tilman Pfau. An experimental and theoretical guide to strongly interacting rydberg gases. *Journal of Physics B: Atomic, Molecular and Optical Physics*, 45(11):113001, 2012. URL `http://stacks.iop.org/0953-4075/45/i=11/a=113001`.

[58] Peter Schauß, Marc Cheneau, Manuel Endres, Takeshi Fukuhara, Sebastian Hild, Ahmed Omran, Thomas Pohl, Christian Gross, Stefan Kuhr, and Immanuel Bloch. Observation of spatially ordered structures in a two-dimensional rydberg gas. *Nature*, 491:87 EP –, 10 2012. URL `http://dx.doi.org/10.1038/nature11596`.

[59] A. Kamenev. Many-body theory of non-equilibrium systems. *eprint arXiv:cond-mat/0412296*, December 2004.

[60] Anatoli Polkovnikov. Phase space representation of quantum dynamics. *Annals of Physics*, 325(8):1790 – 1852, 2010. ISSN 0003-4916. doi: https://doi.org/10.1016/j.aop.2010.02.006. URL http://www.sciencedirect.com/science/article/pii/S0003491610000382.

[61] J. Schachenmayer, A. Pikovski, and A. M. Rey. Many-body quantum spin dynamics with monte carlo trajectories on a discrete phase space. *Phys. Rev. X*, 5:011022, Feb 2015. doi: 10.1103/PhysRevX.5.011022. URL https://link.aps.org/doi/10.1103/PhysRevX.5.011022.

[62] Marie Teich. Spin correlation in kinetic field theory. Bachelor thesis, Ruperto-Carola University of Heidelberg, 2018.

[63] Michael Foss-Feig, Kaden R. A. Hazzard, John J. Bollinger, and Ana Maria Rey. Nonequilibrium dynamics of arbitrary-range ising models with decoherence: An exact analytic solution. *Phys. Rev. A*, 87:042101, Apr 2013. doi: 10.1103/PhysRevA.87.042101. URL https://link.aps.org/doi/10.1103/PhysRevA.87.042101.

[64] I. J. Lowe and R. E. Norberg. Free-induction decays in solids. *Phys. Rev.*, 107:46–61, Jul 1957. doi: 10.1103/PhysRev.107.46. URL https://link.aps.org/doi/10.1103/PhysRev.107.46.

[65] Mauritz van den Worm, Brian C Sawyer, John J Bollinger, and Michael Kastner. Relaxation timescales and decay of correlations in a long-range interacting quantum simulator. *New Journal of Physics*, 15(8):083007, 2013. URL http://stacks.iop.org/1367-2630/15/i=8/a=083007.